Soil organic matter decomposition in permafrost-affected soils and sediments

Dissertation zur Erlangung des Doktorgrades an der
Fakultät für Mathematik, Informatik und Naturwissenschaften,
Fachbereich Geowissenschaften der Universität Hamburg

vorgelegt von
Josefine Walz
aus
Berlin

Hamburg
2017

Tag der Disputation: 10.07.2017

Folgende Gutachter empfehlen die Annahme der Dissertation:
Prof. Dr. Eva-Maria Pfeiffer
Dr. Christian Knoblauch

Parts of this dissertation have been published previously:

Walz J, Knoblauch C (2015) Böden und Landschaft der Großen Ljachow-Insel. In: Böden im Wandel (eds Knoblauch C, Fiencke C, Berger K). Hamburger Bodenkundliche Arbeiten, Band 77: 61-75.

Walz J, Knoblauch C, Böhme L, Pfeiffer E-M (2017) Regulation of soil organic matter decomposition in permafrost-affected Siberian tundra soils - Impact of oxygen availability, freezing and thawing, temperature, and labile organic matter. *Soil Biology and Biochemistry*, **110**, 34–43. doi:10.1016/j.soilbio.2017.03.001

Table of contents

List of figures

List of tables

List of symbols and abbreviations

Ae	aerobic
AL	active layer
An	anaerobic
ANOVA	analysis of variance
asl	above sea level
bAL	bottom active layer
bs	below surface
C	carbon
$C_6H_{12}O_6$	glucose
$CH_3COO^-H^+$	acetate
CH_4	methane
CO_2	carbon dioxide
DOC	dissolved organic carbon
FT	freeze-thaw
GHG	greenhouse gas
H_2	hydrogen
H_2O	water
IC	ice complex
IW	ice-wedge
IRSL	infrared stimulated luminescence
ka BP	thousand years before present
LGM	Last Glacial Maximum
LGT-MIS1	late glacial-early Holocene transition
MIS	marine isotope stage
N	nitrogen
n	sample size
NE	northeast
O_2	oxygen
OC	organic carbon
OM	organic matter
P	precipitation
p	probability
Pf	permafrost
Pr	priming
Q_{10}	temperature sensitivity coefficient
r	(Pearson's) correlation coefficient
RCF	relative climate forcing
sAL	surface active layer
SOC	soil organic carbon
SOM	soil organic matter
T	temperature
Th	thorium
TZ	transition zone
U	uranium
vol%	volume percent
VPBD	Vienna Pee Dee Belemnite
wt%	weight percent

Abstract

Permafrost regions play an important role in the global climate system. For millennia, atmospheric carbon (C) has been sequestered in permafrost-affected soils and sediments. Thus, the soil organic carbon (SOC) pool of the permafrost region has grown to ~1 300 Pg, of which ~800 Pg are perennially frozen and are therefore not part of the active C-cycle. However, there is increasing concern about warming-induced environmental changes in the Arctic, which will result in enhanced microbial decomposition of soil organic matter (SOM) and subsequent release of greenhouse gases (GHG) like carbon dioxide (CO_2) and methane (CH_4). The regulating factors of SOM decomposition in the seasonally thawed active layer and perennially frozen permafrost, however, are insufficiently understood to confidently predict the feedback of thawing permafrost to global warming. The objective of this work was therefore to quantify CO_2 and CH_4 production potentials in different soil and sediment layers and identify environmental drivers of SOM decomposition in permafrost-affected landscapes in northeastern (NE) Siberia through laboratory incubations.

The focus was two-fold: First, the influence of oxygen availability, freezing and thawing, temperature, and substrate availability on CO_2 and CH_4 production in the active layer and upper (<1 m) permafrost soils from the Lena River Delta was quantified. Generally, production under aerobic and anaerobic conditions was highest in the surface layers (0–10 cm). Under anaerobic conditions, 2–4 times less SOC was decomposed. Methanogenesis was only observed after a lag phase of several weeks (active layer) to months (permafrost). The contribution of CH_4-C to the cumulative anaerobic C production gradually increased over the incubation period, indicating that in the long-term, anaerobic decomposition processes and methanogenesis could play a more dominant role in the C-cycle of tundra soils than previously assumed. A freeze-thaw cycle caused a short-lived pulse of CO_2 production directly after re-thawing in the active layer, suggesting that higher substrate availability after re-thawing, e.g. from break down of dead cell membranes (lysis) and physical breakdown of soil aggregates, can enhance CO_2 production, while permafrost SOM as well as CH_4 production was unaffected. To assess the temperature sensitivity of SOM decomposition, Q_{10} values were calculated via the equal-C method. This method compares the time needed to decompose the same amount of SOM with a 10 °C temperature difference. The advantage of this method compared to the traditional Q_{10} method (equal-time, SOM decomposition at different temperatures over the same time) is, that temperature-induced differential depletion of fast and slow decomposing SOC pools are excluded. Q_{10} values in the current work ranged between 2.1–7.8, with higher Q_{10} values observed for slower decomposing SOC pools. The addition of labile plant-derived organic matter (*Carex aquatilis*, a dominant plant species at the study site) generally increased aerobic CO_2 production in all soil layers. Most of the additional CO_2, however, came from the amendment. A real priming effect, i.e. a change in the autochthonous SOM-derived CO_2 production, was only observed in permafrost. SOM

decomposition in permafrost samples from Samoylov increased (positive priming effect) while the SOM decomposition in permafrost samples from Kurungnakh decreased (negative priming effect).

The second focus was on the decomposability of several deep permafrost deposits, which accumulated under different climatic regimes. The investigated deposits from Muostakh Island and the Buor Khaya Peninsula in the central Laptev Sea and Bol'shoy Lyakhovsky in the eastern Laptev Sea cover two glacial-interglacial cycles between the marine isotope stages (MIS) MIS7–MIS1. Generally, Weichselian deposits from the Late Pleistocene (MIS4–MIS2) Yedoma Ice Complex (IC) contained more labile SOC than Holocene and thermokarst deposits. Especially deposits from the MIS3 interstadial (Kargin) showed higher CO_2 production potentials. However, strong regional differences in the decomposability of SOM from the same stratigraphic unit contort estimations of GHG production potentials. It is therefore unlikely, that SOM decomposability can be generalized solely on the stratigraphic classification. CO_2 production in Yedoma IC deposits in the central Laptev Sea were nearly three times higher than in the eastern Laptev Sea region, which may be explained by regional climatic differences. Also, local depositional environments and post-freezing processes can play a role. Methanogenesis was only sporadically observed in Yedoma IC deposits, despite appropriate substrate, suggesting a microbial limitation. Under *in situ* thaw conditions, CH_4 production from these deposits may occur after the reproduction of ancient or migration of recent methanogenic communities into newly thawed soils and sediments. Methanogenesis was observed in Eemian lacustrine sediments from Bol'shoy Lyakhovsky, but several orders of magnitude smaller than CO_2 production. The anaerobic lake environment favored the preservation of a viable methanogenic community. These sediments could therefore give new insights into the long-term development of thermokarst-lake deposits and their role in the arctic C-cycle.

Zusammenfassung

Permafrostregionen spielen eine zentrale Rolle im globalen Klimasystem. Atmosphärischer Kohlenstoff (C) wurde über Jahrtausende in permafrostbeeinflussten Böden und Sedimenten eingelagert. Der Gesamtvorrat an organischem Kohlenstoff (*eng. soil organic carbon*) wuchs daher auf bis zu 1 300 Pg an, von denen aber ~800 Pg dauerhaft gefroren und daher nicht Teil des aktiven C-Kreislaufes sind. Durch Umweltveränderungen im Zuge steigender Temperaturen können große Mengen der im Permafrost gespeicherten organischen Bodensubstanz (*eng. soil organic matter*) biologisch verfügbar und mikrobiell zu Treibhausgasen wie Kohlenstoffdioxid (CO_2) und Methan (CH_4) umgewandelt und wieder an die Atmosphäre abgeben werden. Die Steuerungsfaktoren der Gasproduktion in der saisonalen Auftauschicht (*eng. active layer*) und des dauerhaft gefrorenen Permafrostes sind jedoch unzureichend bekannt, um die Wechselwirkungen zwischen tauendem Permafrost und globaler Klimaerwärmung verlässlich zu prognostizieren. Das Ziel dieser Arbeit war es daher, die potentielle CO_2- und CH_4-Produktion in verschiedenen Boden- und Sedimentschichten zu bestimmen und die Umweltparameter, die den Abbau der organischen Bodensubstanz in permafrostbeinflussten Landschaften in Nordostsibirien steuern, mittels Laborinkubationen zu identifizieren.

Der Fokus war zweifältig: Zuerst wurde der Einfluss von Sauerstoffverfügbarkeit, Gefrier-Tau-Prozessen, Temperatur und Substratverfügbarkeit auf die CO_2- und CH_4-Produktion in der saisonalen Auftauschicht und im oberflächennahen (<1 m) Permafrostboden in Böden des Lena Deltas bestimmt. Sowohl die aerobe als auch die anaerobe Produktion war am höchsten im Oberboden (0–10 cm). Unter anaeroben Bedingungen wurde 2–4-mal weniger organische Substanz umgesetzt als unter aeroben Bedingungen. Methanogenese wurde erst nach einer Verzögerung von mehreren Wochen (Auftauschicht) bis Monaten (Permafrost) beobachtet. Der Anteil von CH_4-C am anaeroben Gesamtumsatz stieg mit der Inkubationsdauer. Anaerober Kohlenstoffabbau und Methanogenese könnten daher eine bedeutendere Rolle im C-Kreislauf einiger Tundraböden spielen, als bisher angenommen. In der saisonalen Auftauschicht führte ein Gefrier-Tau-Zyklus zu einem kurzlebigen CO_2-Puls direkt nach dem Wiederauftauen. Die erhöhte Substratverfügbarkeit nach dem Tauen, z.B. durch Auflösung toter Zellmembranen (Lyse) und mechanisches Aufbrechen von Bodenaggregaten, kann die CO_2-Produktion steigern. Die organische Substanz im Permafrost und die CH_4-Produktion waren nicht betroffen. Um die Temperaturabhängigkeit aerober Abbauprozesse zu bestimmen, wurden Q_{10}-Werte mittels der *equal-C*-Methode berechnet. Diese Methode vergleicht die Dauer bis die gleiche Menge organischer Substanz bei einem Temperaturunterschied von 10 °C abgebaut worden ist. Der Vorteil gegenüber der traditionellen Methode (*equal-time*, verschiedene Kohlenstoffmenge über die gleiche Zeit) ist, dass so temperaturbedingte Unterschiede zwischen schnell und langsam abbaubarer Kohlenstoffreservoire ausgeschlossen werden können. Q_{10}-Werte in der vorliegenden Arbeit bewegten sich zwischen 2.1–7.8. Langsam abbaubarer Kohlensoff zeigte

meistens höhere Q_{10}-Werte als schnell abbaubarer Kohlenstoff. Die Zugabe von frischer Pflanzenmaterie (*Carex aquatilis*, eine weitverbreitete Pflanze im Untersuchungsgebiet) führte zu einer Steigerung der aeroben CO_2-Produktion in allen Bodenschichten. Das zusätzliche CO_2 stammte jedoch vorwiegend aus dem Abbau des zugesetzten Materials. Ein realer Priming-Effekt, d.h. eine Veränderung des Abbaus der bodeneigenen Substanz, wurde nur im Permafrost festgestellt. Der Abbau in Permafrostproben der Insel Samoylov stieg (positiver Priming-Effekt), während der Abbau in Proben der Insel Kurungnakh zurückging (negativer Priming-Effekt).

Das zweite Augenmerk lag auf der Abbaubarkeit organischer Substanz in tiefen Permafrostsedimenten, welche unter unterschiedlichen Klimabedingungen abgelagert wurden. Die untersuchten Ablagerungen der Insel Muostakh und der Buor Khaya-Halbinsel in der zentralen Laptewsee und der Großen Ljachow-Insel in der östlichen Laptewsee beinhalten Ablagerungen zweier glazial-interglaziale Zyklen zwischen den Sauerstoff-Isotopenstufen (*engl. marine isotope stage, MIS)* MIS7–MIS1. Im Allgemeinen lagerten spät-pleistozäne (MIS2–MIS4) Yedoma-Ablagerungen mehr labilen Kohlenstoff ein als holozäne und Thermokarstablagerungen. Insbesondere Ablagerungen des MIS3-Interstadials (Kargin) zeigten vergleichsweise hohe CO_2-Produktionspotentiale. Große regionale Unterschiede in der Abbaubarkeit der organischen Substanz innerhalb derselben stratigraphischen Einheit verzerren jedoch die Vorhersagbarkeit der Treibhausgasproduktion in tauendem eisreichen Permafrost. Es ist daher unwahrscheinlich, dass eine Vorhersage der Abbaubarkeit auf Grundlage der stratigraphischen Position getroffen werden kann. Die CO_2-Produktion in Yedoma-Ablagerungen in der westlichen Laptewsee war fast dreimal höher als in der östlichen Laptewsee, was auf regionale Klimaunterschiede zurückzuführen ist. Auch lokale Bedingungen während und nach dem Einfrieren spielen eine Rolle. So wurde in Yedoma-Ablagerungen nur vereinzelt CH_4-Produktion gemessen, obwohl geeignetes Substrat vorhanden war, was auf eine mikrobielle Limitierung hindeutet. Unter *in situ* Bedingungen ist eine Methanproduktion in diesen Sedimenten vorstellbar, wenn sich ehemalige methanogene Mikroorganismen vermehren oder rezente Gemeinschaften in neu getaute Bereiche migrieren. Methanogenese wurde in Seesedimenten der Eem-Warmzeit von der Großen Ljachow-Insel festgestellt, wenn auch mehrere Größenordnungen kleiner als die CO_2-Produktion. Das anaerobe Ablagerungsmilieu begünstigte das Einfrieren einer methanogenen Gemeinschaft. Diese Ablagerungen könnten daher Aufschluss über die Langzeitentwicklung von Thermokarstseen und ihrer Bedeutung im arktischen C-Kreislauf geben.

1 Introduction and objectives

Permafrost, i.e. ground that remains below 0 °C for at least two consecutive years (van Everdingen, 2005) underlies 24% of the exposed landmass in the northern hemisphere (Zhang *et al.*, 2008). Permafrost regions play an important role in the global climate system and acted as a stable sink for atmospheric carbon (C) for millennia. Soils and sediments in these regions have accumulated ~1 300 Pg of soil organic carbon (SOC), of which about 800 Pg are perennially frozen (Hugelius *et al.*, 2014) and are therefore not part of the active C-cycle. Only in the seasonally thawed active layer do soil microorganisms actively decompose soil organic matter (SOM) to greenhouse gases (GHG) such as carbon dioxide (CO_2) and methane (CH_4), which may be released back to the atmosphere.

Permafrost regions are particular sensitive to environmental changes and increasing global temperatures. Air temperatures in the Arctic are rising twice as fast as the global average (Serreze *et al.*, 2000). As a result, currently frozen SOM may become microbially available, which in turn results in higher SOM decomposition and GHG release. In a warmer Arctic, an additional 250–450 Pg of SOC could thaw until 2100 (Harden *et al.*, 2012), of which 37–174 Pg could be released back to the atmosphere (Schuur *et al.*, 2015). Although it is expected that warming-induced environmental changes will result in higher GHG fluxes between soils and the atmosphere (Schneider von Deimling *et al.*, 2012), the regulating factors of SOM decomposition in permafrost-affected soils and sediments are insufficiently understood to confidently predict the feedback of thawing permafrost to global warming.

A current gap in the scientific literature is the limited number of studies that investigated differences in seasonally and perennially frozen soil layers. Environmental conditions in the seasonally thawed active layer and perennially frozen permafrost are substantially different and SOM decomposition may therefore respond differently to warming-induced environmental changes (Gillespie *et al.*, 2014). While microbial activity in the active layer is affected by labile organic matter (OM) from the recent vegetation, annual freeze-thaw cycles, above freezing temperatures, and often changing oxygen (O_2) availability, conditions in permafrost are substantially more stable. Permafrost thaw dramatically alters environmental conditions in the formerly frozen soil layers, but the consequences, which permafrost thaw will have on SOM decomposition and GHG production remain unclear.

Further, while there is a wide scientific consensus that near-surface permafrost (<3 m) will be subject to widespread thaw during the 21st century (Anisimov & Nelson, 1997; Zimov *et al.*, 2006), there is also growing concern of thawing of deep permafrost. During the Middle and Late Pleistocene, ice-rich permafrost, so called ice complex (IC) deposits, in Siberia, northwestern Canada, and Alaska have grown to several tens of meters in height (Schirrmeister *et al.*, 2013). Due to the high ice content of up to 80 vol% (Schirrmeister *et al.*, 2011), these deposits are particularly susceptible to thermal ice melt and ground subsistence (thermokarst) or thermal melt

combined with mechanical forces (thermo-erosion, van Everdingen, 2005). However, while there is increasing awareness of the vulnerability of deep permafrost SOM to thaw and subsequent microbial decomposition (Schneider von Deimling *et al.*, 2015), few studies have measured GHG production in these deposits directly, either under *in situ* conditions (Vonk *et al.*, 2012) or in laboratory incubations (Dutta *et al.*, 2006; Lee *et al.*, 2012; Knoblauch *et al.*, 2013).

The general objectives of this work were to quantify CO_2 and CH_4 production and to identify drivers of SOM decomposition in permafrost-affected soils and sediments in northeastern (NE) Siberia through laboratory incubations. It focused on the two following research questions:

1. *What factors regulate SOM decomposition in near-surface soil layers?*
2. *How decomposable are deep permafrost SOM pools with respect to surface soils?*

To address the first question, several active layer and shallow (<1 m) permafrost samples were investigated and the impact of O_2 availability, freezing and thawing, temperature, and labile OM additions on GHG production were studied. The main hypothesis was:

H1 *SOM decomposition in seasonally and perennially frozen soil layers responds differently to environmental drivers.*

It was further hypothesized that:

H1.1 *SOM in the active layer is decomposed more quickly than SOM in thawed permafrost.*

H1.2 *The absence of O_2 reduces the production of GHGs.*

H1.3 *Freeze-thaw cycles increase the microbial decomposition of SOM.*

H1.4 *Slow decomposing permafrost SOM has a higher temperature sensitivity than faster decomposing active layer SOM.*

H1.5 *The addition of labile OM increases the decomposition of autochthonous SOM in the whole soil profile.*

The obtained data can be used to inform and validate process-based models and improve projections of GHG production and release from thawing permafrost landscapes.

To address the second question, several deep permafrost deposits were investigated. Samples were recovered from three different locations in the Laptev Sea region and cover two glacial-interglacial cycles, including the Holocene and Eemian interglacial and the Weichselian and Saalian glacial periods. The main hypothesis was:

H2 *Climatic and environmental conditions during OM deposition affect SOM characteristics and thus future GHG production potentials.*

It was further hypothesized that:

H2.1 OM deposited in glacial periods experienced little pre-freezing decomposition and thus provides a better substrate for future microbial decomposition post-thawing.

On the one hand, the obtained data can be used to better constrain GHG production potentials from thawing permafrost deposits based on their stratigraphic position. On the other hand, the data can be used to reconstruct past C dynamics and infer possible future permafrost degradation and SOM decomposition scenarios.

2 State of the Art

2.1 Organic carbon pools in permafrost regions: Quantity and quality

In the northern hemisphere, 17.8×10^6 km^2 of the terrestrial area (without exposed bedrock, glaciers, ice-sheets, and water bodies) are underlain by perennially frozen permafrost (Hugelius *et al.*, 2014). Soils and sediments in these regions represent a major C pool. Impermeable permafrost in the ground impedes water drainage, creating large wetland ecosystems (Lehner & Döll, 2004). Anaerobic conditions and low temperatures inhibit SOM decomposition (Gorham, 1991). As a result, OM inputs from plants, which grow during the relatively short summer months when the surface soil layer thaws (active layer) are higher than SOM decomposition by heterotrophic soil microorganisms. Permafrost aggradation eventually freezes the SOM and protects it from further decomposition. Thus, the SOC pool increases with time. Today, permafrost-affected soils and sediments are estimated to contain 1 307 ± 170 Pg of SOC, of which. nearly 80% (1035 Pg) are stored within the top 3 m (Hugelius *et al.*, 2014). Cryoturbation, i.e. churning of the soil matrix due to repeated freeze-thaw cycles (van Everdingen, 2005) is an important pedogenetic process in permafrost-affected soils, which further protects SOM from decomposition (Bockheim, 2007; Kaiser *et al.*, 2007). Cryoturbated soils (Turbic Cryosols, IUSS Working Group WRB, 2014) are widespread in northern ecosystems and contain a higher proportion of SOC in permafrost-affected soils (476 Pg) than non-cryoturbated Cryosols (251 Pg) or other non-Cryosols (307 Pg, Hugelius *et al.*, 2014). Repeated freeze-thaw cycles, however, can also cause short bursts of GHG after thaw (Matzner & Borken, 2008) and contribute to GHG fluxes from soils.

Of the 1 307 Pg of SOC in permafrost regions, 272 Pg are stored in deep (>3 m) deposits, of which 91 Pg are stored in deltaic deposits and 181 Pg in Yedoma IC and associated thermokarst deposits (Hugelius *et al.*, 2014). Thus, Yedoma IC deposits represent an important fossil SOC pool. They are of polygenetic origin, including alluvial, deltaic, aeolian, and nival processes (Schirrmeister *et al.*, 2011) and cover an area of 1.4×10^6 km^2 (~ 8% of the permafrost region, Strauss *et al.*, 2013) in Siberia (Grosse *et al.*, 2013), Alaska (Kanevskiy *et al.*, 2011), and Canada (Froese *et al.*, 2008). During the last glacial period, large parts of western Beringia remained unglaciated and the cold and arid conditions during the Late Pleistocene favored the accumulation of fine-grained, organic-rich deposits on predominantly flat, poorly drained plains between 60–12 ka BP (Schirrmeister *et al.*, 2013). Syngenetic (concurrently grown) ice-wedges dissect the deposits and amount for up to 60% by volume (Ulrich *et al.*, 2014). Repeated frost cracking in winter, infiltration with snowmelt water in spring, and refreezing enabled ice-wedges to grow in size over millennia. The total ice content of these deposits can thus reach more than 80 vol% (Schirrmeister *et al.*, 2011), which makes IC deposits particular susceptible to warming-induced environmental changes, erosion, and subsidence following permafrost thaw (Morgenstern *et al.*, 2011, 2013; Schneider von Deimling *et al.*, 2015). The Yedoma IC is the most prominent IC, but

in some areas, older Middle Pleistocene IC deposits are also preserved (Schirrmeister *et al.*, 2002a; Wetterich *et al.*, 2016).

In addition to the quantity, the SOM quality, here defined as a measure of microbial decomposability and GHG production potentials after thaw, will influence how much of SOC within permafrost-affected soils and sediments can actually be decomposed and released as GHG when thawed (MacDougall & Knutti, 2016). Permafrost formation plays hereby an important role (Waldrop *et al.*, 2010; Harden *et al.*, 2012). In epigenetic permafrost, that is permafrost aggradation through intermittent freezing, SOM has already undergone some level of transformation before it was frozen (Hugelius *et al.*, 2012) and easily decomposable, labile organic carbon (OC) compounds are decomposed and lost to the atmosphere prior to incorporation into permafrost (Schädel *et al.*, 2014). In contrast, SOM in syngenetic permafrost, i.e. concurrently formed permafrost, had little time to be transformed prior to freezing. Much of the Yedoma IC deposits were frozen quickly after deposition (Schirrmeister *et al.*, 2011) and may thus contain high amounts of labile SOM, which may be quickly decomposed to GHG after thaw. In this case, the quantity and quality of the fossil SOM is controlled by the OM source, i.e. predominantly vegetation, which in turn will depend on climatic conditions (Andreev *et al.*, 2011).

2.2 Controls of soil organic matter decomposition

SOM decomposition in permafrost-affected soils is governed by a complex interplay between several environmental parameters such as temperature, moisture, O_2 and nutrient availability, and other soil forming factors, e.g. parent material, SOM quality, and cryoturbation (Hobbie *et al.*, 2000). Heterotrophic soil microorganisms cover their energy demands by transferring electrons from electron donors to electron acceptors (Megonigal *et al.*, 2004). A selection of the main SOM decomposition processes in soils is given in Table 1 and described in more detail below.

In aerated soil layers, aerobic soil microorganisms can oxidize OC compounds such as glucose ($C_6H_{12}O_6$, electron donor) with O_2 (electron acceptor) to CO_2. Anaerobic decomposition processes are more complex than aerobic decomposition. In the absence of O_2, different groups of anaerobic soil microorganisms compete for alternative electron acceptors (Stams *et al.*, 2006), e.g. CO_2. Anaerobic decomposition processes can therefore be both a source as well as a sink for CO_2. Fermentative intermediate products of anaerobic decomposition processes also include hydrogen (H_2) and acetate (CH_3COOH). Methanogenic soil microorganisms can then use these products in the terminal step of anaerobic SOM decomposition and reduce CO_2 with H_2 to CH_4 (hydrogenotrophic methanogenesis) or cleave CH_3COOH in CH_4 and CO_2 (acetoclastic methanogenesis). Anaerobic decomposition processes yield considerably less energy than aerobic decomposition and thus occurs generally at lower rates (Megonigal *et al.*, 2004). Due to the 28–34 times higher warming potential of CH_4 than CO_2 on a century timescale (Myhre *et al.*, 2013), methanogenesis may principally constitute an important source of GHG. However, the

majority of currently available laboratory incubation studies suggest that GHG production in permafrost-affected soils is dominated by CO_2 (Treat *et al.*, 2015; Schädel *et al.*, 2016). Further, not all of the *in situ* produced CH_4 is released back to the atmosphere. As anaerobically produced CH_4 migrates through aerobic soil layers, it may be partially oxidized to CO_2. For high-latitude wetland ecosystems, estimates of CH_4 oxidation efficiencies range between 30% (Reeburgh *et al.*, 1993) and 50% (Whalen & Reeburgh, 2000; Preuss *et al.*, 2013). For a polygon pond with submerged mosses, Knoblauch *et al.* (2015) reported that up to 99% of the produced CH_4 can be oxidized to CO_2 before it is released to the atmosphere. Anaerobic CH_4 oxidation has also received more attention in recent years and could constrain CH_4 emission from northern peatlands further, depending on electron acceptor (nitrate, sulfate, ferric iron) availability (Gupta *et al.*, 2013).

Table 1: Soil organic matter decomposition processes in soils under aerobic and anaerobic conditions (compiled after Luo & Zhou, 2006).

Process	Oxygen availability	Reaction
Glucose oxidation	Aerobic	$C_6H_{12}O_6 + 6\ O_2 \rightarrow 6\ CO_2 + 6\ H_2O$
Methane oxidation	Aerobic	$CH_4 + 2\ O_2 \rightarrow CO_2 + 2\ H_2O$
Glucose fermentation	Anaerobic	$C_6H_{12}O_6 \rightarrow 2\ CO_2 + 2\ C_2H_5OH$
Hydrogenotrophic methanogenesis	Anaerobic	$CO_2 + 4\ H_2 \rightarrow CH_4 + 2\ H_2O$
Acetoclastic methanogenesis	Anaerobic	$CH_3COOH \rightarrow CH_4 + CO_2$

Temperature is a main driver of biological processes. In permafrost regions, higher temperatures affect C-cycling in three ways. First, higher temperatures can lead to permafrost thaw and active layer deepening and remobilize previously frozen SOM (Oechel *et al.*, 1993). Second, higher temperatures lead to higher microbial decomposition rates (Davidson & Janssens, 2006). Third, higher temperatures result in a shift in vegetation composition and above-ground uptake of CO_2 (Ainsworth & Long, 2004) with contrasting effects on below-ground C dynamics. Additionally, the increased likelihood of fire could result in large GHG fluxes to the atmosphere and accelerate permafrost degradation further (Allison & Treseder, 2011). However, projections of future net annual C fluxes between permafrost-affected soils and sediments and the atmosphere vary both in magnitude and direction (Hobbie *et al.*, 2000).

Active layer deepening, thermokarst activity, talik formation, and erosion of coastal permafrost have been identified as the main mechanisms resulting in substantial release of GHG from soils to the atmosphere (Schuur *et al.*, 2008), thereby initiating a positive feedback and amplifying the warming trend (MacDougall *et al.*, 2012; Schaefer *et al.*, 2014; Schuur *et al.*, 2015). During the last 40 years, average air temperatures in the Arctic have risen at twice the global rate and air temperatures in the Arctic have increased by up to 3 °C since the 1980s (Serreze *et al.*, 2000). Temperature effects are most pronounced near the surface, but increased permafrost temperatures have been detected down to 50 m (Osterkamp & Romanovsky, 1999). Many studies project therefore a reduction in the total extent of permafrost and a deepening of the active layer

(Shaver *et al.*, 1992; Lawrence & Slater, 2005; Delisle, 2007; Schaefer *et al.*, 2011). By the end of the 21st century, active layer depths could increase by tens of centimeters (Koven *et al.*, 2011) and remobilize previously frozen SOM (Dorrepaal *et al.*, 2009; Harden *et al.*, 2012). Especially the decomposability of SOM stored in ice-rich deep inland permafrost, which are primarily affected by thermokarst and talik development, is uncertain (Dutta *et al.*, 2006; Schuur *et al.*, 2009). Viable microorganisms have been detected in several deep NE Siberian permafrost deposits (Gilichinsky & Wagener, 1995; Rivkina *et al.*, 1998; Vishnivetskaya *et al.*, 2000) and could decompose SOM after thaw. Today, intact remnants of Yedoma IC deposits cover an area of ~416 000 km^2 and store an estimated amount of 83 Pg of SOC (Strauss *et al.*, 2013). At the end of the last glacial period, Yedoma IC deposits may have covered an area >10^6 km^2 (Zimov *et al.*, 2006). But extensive permafrost degradation, which affected 70% of the original Yedoma area, led to widespread thermokarst and thaw lake formation (Strauss *et al.*, 2013). Taliks formed underneath these lakes due to the higher heat capacity of liquid water compared to ice, which prevented the deposits underneath lakes to refreeze in winter. These thermokarst and talik deposits may have been a substantial source of GHG during the early Holocene (Walter *et al.*, 2006, 2007; Tesi *et al.*, 2016), which was ~4 °C warmer than today (Andreev *et al.*, 2002a). Refrozen talik deposits after lake drainage are referred to as taberal deposits. Permafrost SOM can further be remobilized by erosion of permafrost exposed along coastal bluffs (Jones *et al.*, 2009; Vonk *et al.*, 2012). Along the 7 500 km long coastline in the Laptev Sea region, coastal erosion is estimated to thaw 88 to 800 t SOC km^{-1} a^{-1} (Günther *et al.*, 2013) which could be microbially decomposed before redeposition (Rachold *et al.*, 2000) and burial (Vonk *et al.*, 2012) in the Arctic shelf oceans.

Higher temperature are expected to increase microbial activity and SOM decomposition (Davidson & Janssens, 2006). The most common measure of temperature sensitivity is the Q_{10} approach, which is a measure of the rate change in decomposition rates with a 10 °C temperature change. Comparing *in situ* eddy covariance measurements of terrestrial ecosystem respiration in different biomes, Mahecha *et al.* (2010) report that at the ecosystem level, Q_{10} values converge around 1.4. In many laboratory studies, however, Q_{10} values are often much higher (>2), with strong difference between biomes. Temperature sensitivity of SOM decomposition in cold climates are generally higher than in temperate regions (Kirschbaum, 1995; Hamdi *et al.*, 2013). Further, many studies report a negative relationship between temperature sensitivity and SOM quality. Low quality SOM incorporated in permafrost could therefore be particularly sensitive to temperature changes (Knorr *et al.*, 2005).

Temperature may also indirectly influence C dynamics. Shifts in plant community structures, higher air temperatures, and rising atmospheric CO_2 concentrations can lead to higher plant net primary production and above-ground uptake of CO_2 (Ainsworth & Long, 2004). Part of this additional C will be transferred into soils, e.g. as plant litter or root exudates (Jastrow *et al.*, 2005). In addition, higher temperatures and associated increases in active layer depths will lead to larger

rooting depths and higher C inputs (Jorgenson *et al.*, 2010). However, it remains unclear, whether a higher allocation of below-ground C increases (Kong *et al.*, 2005) or decreases the SOC pool (Fontaine *et al.*, 2004). The higher availability of relatively labile OC compounds from plants and roots may affect the decomposition of SOM through a process called priming (Bingeman *et al.*, 1953, Figure 1). Priming effects can be positive, i.e. a stimulation of low quality SOM decomposition after the addition of easily decomposable OC compounds (e.g. glucose, cellulose, proteins, amino acids), or negative, i.e. a retardation of SOM decomposition after substrate addition (Kuzyakov, 2010).

Higher temperatures are likely to result in higher decomposition rates of SOM in permafrost-affected soils. However, this does not necessarily result in a decrease of the permafrost SOC pool and higher net ecosystem exchange. Higher temperatures and a longer growing season (Euskirchen *et al.*, 2006) increase the uptake of atmospheric CO_2 through photosynthesis (Ainsworth & Long, 2004). Shrub encroachment (Myers-Smith *et al.*, 2011) and shifts in the tree line (Kruse *et al.*, 2016) increase C-fixation in biomass further. However, a recent expert assessment (Abbott *et al.*, 2016), suggested, that increase C-fixation will not offset increased C release through SOM decomposition, fire, and runoff, suggesting that the permafrost region could eventually switch from a sink to a source for atmospheric C (Schaefer *et al.*, 2011).

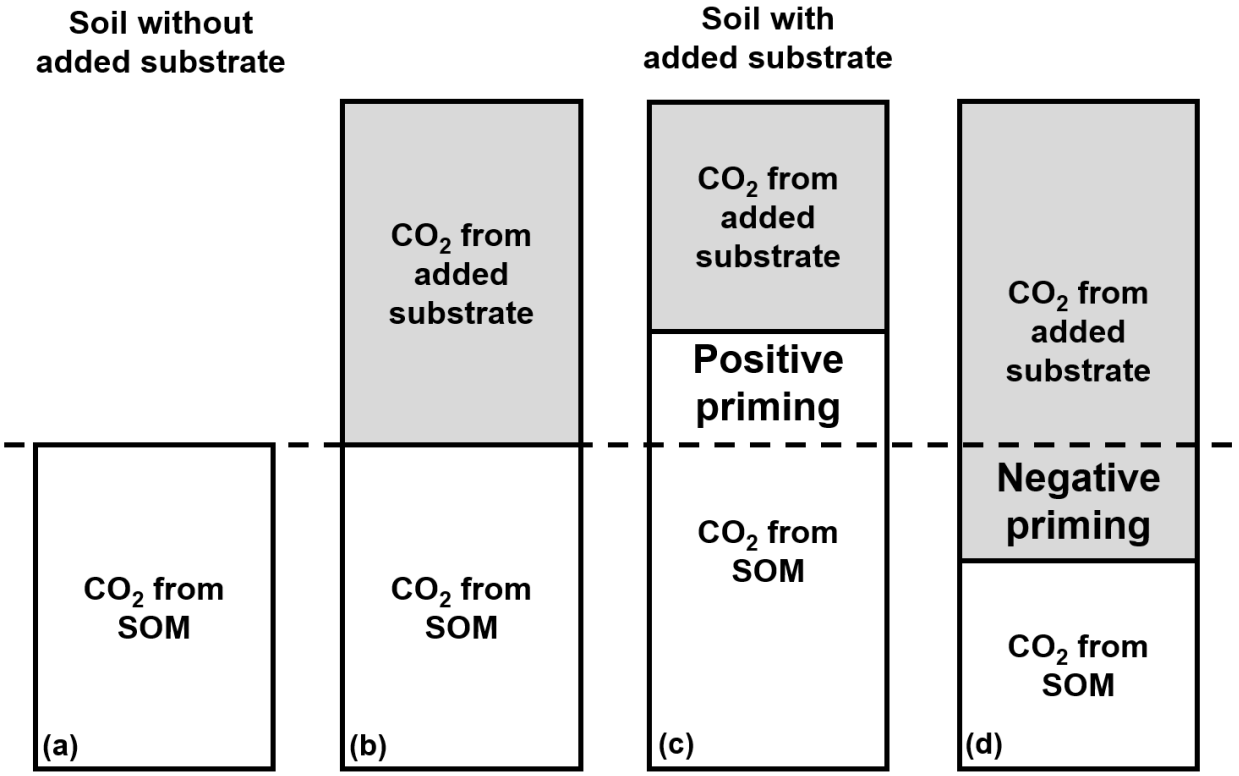

Figure 1: Priming effects in soils (modified after Kuzyakov *et al.*, 2000). Substrate addition (b–d) results in higher CO_2 production than in a control soil, without substrate addition (a). Partitioning the CO_2 flux into CO_2 from the added substrate and from soil organic matter (SOM) reveals no priming effect if the SOM-derived fraction did not change compared to the control (b), a positive priming effect, if the SOM-derived fraction increased (c), or a negative priming effect, if the SOM-derived fraction decreased (d).

2.3 Chronostratigraphy of permafrost deposits in NE Siberia

The Laptev Sea region in NE Siberia (Figure 2) is underlain by continuous permafrost reaching depths of 450–650 m onshore and 200–600 m offshore (Romanovskii *et al.*, 2004) with ground temperatures of -11 °C for terrestrial permafrost (Drozdov *et al.*, 2005) and -1 °C for submarine permafrost (Overduin *et al.*, 2015). Permafrost deposits are an excellent paleo-environmental archive, which preserved ground ice, sediments, and organic remains from past plant and animal communities. The sedimentary record in NE Siberia includes at least two glacial-interglacial cycles and thus serve as a basis to reconstruct past climate and environmental dynamics. However, not all periods are uniformly well preserved at different locations. Also, no supra-regional definition of the periods and the assigned strata names exists (Shkatova, 2011 cited in Wetterich *et al.*, 2014). An updated chronostratigraphy of the Quaternary deposits of the Dmitriy Laptev Strait and other coastal lowlands in Northern Yakutia has been proposed by Tumskoy (2012). It was adapted by the international scientific community and is also used in this work. An overview of the chronostratigraphy of permafrost deposits in NE Siberia is given below and the regional vegetation and climate conditions are summarized in Table 2.

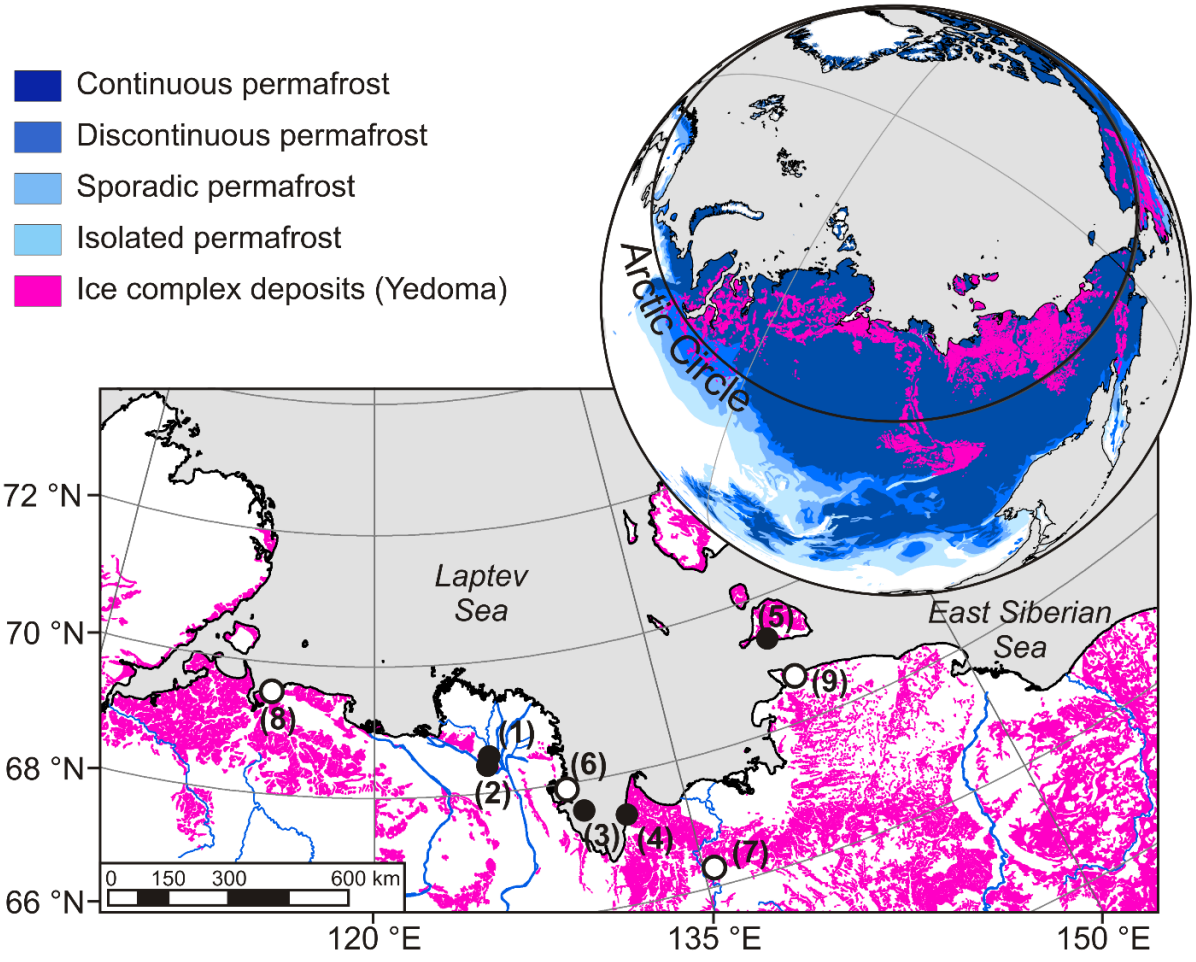

Figure 2: Overview map of the Laptev Sea region with circumpolar permafrost extent (Brown *et al.*, 1998) and distribution of (Yedoma) ice complex deposits (Strauss *et al.*, 2016). Closed and open circles represent sites investigated in this work and reference locations, respectively: (1) Samoylov; (2) Kurungnakh; (3) Muostakh Island; (4) Buor Khaya Peninsula; (5) Bol'shoy Lyakhovsky; (6) Bykovsky Peninsula; (7) lower Yana River; (8) Cape Mamontov Klyk; (9) Oyogos Yar.

Table 2: Compilation of the regional chronostratigraphy used in this work with climate and vegetation history (based on an overview by Andreev *et al.*, 2011) and references therein as well as revised ages based on new dating studies (Wetterich *et al.*, 2011, 2014, 2016; Tumskoy, 2012; Opel *et al.*, 2017; Schirrmeister *et al.*, 2017).

Age ka BP	Period	Regional chronostrati-graphy	Marine isotope stage (MIS)	Regional climate and vegetation
ca 200–190	Late Saalian glacial (interstadial)	Taz	MIS7	Severe winter, but relatively warm and wet summer conditions; wet grass-sedge tundra vegetation
ca 190–130	Late Saalian glacial (stadial)	Keremesitsko	MIS6	Considerably colder and drier than during the previous interstadial; sparse grass-sedge vegetation, increase in coniferous and reworked pollen
ca 130–80	Eemian interglacial	Kazantsevo	MIS5	Generally warmer (up to 10 °C) than today; grass-sedge dominated tundra vegetation, tundra steppe vegetation during the Middle Eemian climate optimum
ca 80–55	Early Weichselian glacial (stadial)	Zyryan	MIS4	Colder and drier than present; sparse grass-sedge vegetation
ca 55–30	Middle Weichselian glacial (interstadial)	Kargin	MIS3	Climate amelioration compared to previous stadial with relatively warm and wet summers; tundra-steppe vegetation, open larch forest
ca 30–13	Late Weichselian glacial (stadial)	Sartan	MIS2	Cold and dry summer conditions, winter colder than today; open steppe-like and herb tundra communities
ca 13–10.3	Late glacial-early Holocene transition			Climate amelioration after the Last Glacial Maximum; transition to shrubby tundra vegetation
<10.3	Holocene	Holocene	MIS1	Climate amelioration during the early Holocene; shrub-tundra vegetation gradually disappeared ca 7.6 ka BP

The Yukagir IC on the southern coast of Bol'shoy Lyakhovsky (site 5 in Figure 2) contains Saalian (MIS7/MIS6, ca 200–130 ka BP) IC complex deposits (Andreev *et al.*, 2004). Peat deposits overlying the Yukagir IC have been dated by uranium-thorium (^{230}Th/U) radioisotope disequilibria to ~200 ka BP (Schirrmeister *et al.*, 2002b). Stable hydrogen and oxygen isotopes (δ^2H and δ^{18}O) analysis of ice-wedges indicate that this period was characterized by severe winter conditions (Meyer *et al.*, 2002a; Wetterich *et al.*, 2016; Opel *et al.*, 2017). For the Saalian interstadial period between 200–190 ka BP, pollen spectra (Andreev *et al.*, 2004) indicate a wet grass-sedge tundra vegetation with high concentrations of Poaceae and Cyperaceae, comparable to modern Siberian tundra ecosystems. In contrast, the pollen concentrations decreased sharply during the stadial period between 190–130 ka BP. The sparser vegetation was still dominated by grasses and sedges, but also a comparatively high abundance of *Equisetum*, *Riccia*, and *Encalypta* spores. The pollen assemblage also contained high concentrations of reworked pollen, indicative of erosional processes during cold periods.

Eemian interglacial (MIS5, ca 130–80 ka) sediments are only preserved sporadically in the study region. Thermo-erosion at the beginning of the Eemian interglacial period melted the Saalian ice-wedges and refilled the ice-wedge casts (Figure 3), with younger lacustrine sediments (Andreev *et al.*, 2004). Age-diverse sediments may therefore coexist laterally. In NE Siberia, deposits from the MIS5 are exposed in the Krest Yuryakh Suite and the Buchchagy IC on the southern coast of Bol'shoy Lyakhovsky and the Oyogos Yar coast (site 9 in Figure 2, Wetterich *et al.*, 2009). Thermoluminescence dating of the lacustrine sediments of the Krest Yuryakh Suite on Bol'shoy Lyakhovsky yielded ages of ~136 ka BP (Andreev *et al.*, 2004). Newer infrared stimulated luminescence (IRSL) ages of the corresponding unit on the Oyogos Yar coast of ~102 ka BP, however, suggest that this unit is considerably younger (Opel *et al.*, 2017). The stratigraphic position of the Bychchagy IC is still debated, but recent ^{230}Th/U radioisotope disequilibria dating of peaty layers date the Bychchagy IC to 126–89 ka BP (Wetterich *et al.*, 2016). Pollen data indicate a continental inland climate with open tundra steppe and high abundance of *Alnus fruticosa*, *Salix*, and *Betula nana* (Andreev *et al.*, 2004), similar to modern vegetation in southern Yakutia (Kienast *et al.*, 2008). During the middle Eemian climate optimum, the tree line was likely located near the Oyogos Yar coast, whose sediments contain a relative high abundance of *Larix* pollen, which are absent in the corresponding sediments on Bol'shoy Lyakhovsky, 60 km north (Wetterich *et al.*, 2009). Summer conditions during the MIS5 were warmer and probably wetter than present (Andreev *et al.*, 2004, 2011; Wetterich *et al.*, 2009), with mean July temperatures up to 13 °C (Kienast *et al.*, 2008, 2011), which is ~10 °C higher than today. However, climatic instability of the Eemian interglacial period limits its potential use as a Holocene analog. The pronounced warm periods during the MIS5 with associated permafrost degradation through thermokarst activity alternated with cold periods, which favored permafrost aggradation and IC formation (Wetterich *et al.*, 2016). Additionally, MIS5 sediments are preserved in submarine permafrost deposits from Cape Mamontov Klyk (site 8 in Figure 2). These sediments were IRSL dated to 111 ka BP and the pore-water chemistry and sediment properties indicate an aquatic depositional environment, possibly a coastal lagoon (Winterfeld *et al.*, 2011).

Yedoma IC sediments, deposited during the Weichselian glacial period (MIS4–MIS2) are widespread in Siberia, Alaska, and Canada (Froese *et al.*, 2008; Kanevskiy *et al.*, 2011; Grosse *et al.*, 2013). There is, however, a long sedimentation hiatus of 60 ka (Andreev *et al.*, 2004) to 150 ka (Meyer *et al.*, 2002a) between Weichselian and older deposits. During the early Weichselian period (MIS4, ca 80–60 ka BP), also referred to as the Zyryan stadial in the regional stratigraphy, environmental conditions deteriorated considerably compared to the previous interglacial and were comparable to the MIS7 (Andreev *et al.*, 2004). Pollen analysis from MIS4 deposits exposed in the Kuchchugui Suite on Bol'shoy Lyakhovsky indicate sparse grass and sedge communities (Andreev *et al.*, 2009). However, the stratigraphic position of the Kuchchugui Suite is still debated and may not contain MIS4 deposits, but rather deposits from the MIS7

(Wetterich *et al.*, 2016), which was also characterized by sparse vegetation and cold and arid conditions (Meyer *et al.*, 2002a; Andreev *et al.*, 2004). MIS4 deposits are also preserved on Kurungnakh in the Lena River Delta (site 2 in Figure 2, Schirrmeister *et al.*, 2003; Wetterich *et al.*, 2008), but pollen were rarely preserved in the floodplain deposits of the meandering paleo-Lena River. A comprehensive Weichselian permafrost record, including deposits from the MIS4, is preserved on the Bykovsky Peninsula (site 6 in Figure 2, Schirrmeister *et al.*, 2002b; Siegert *et al.*, 2002). δ^2H and δ^{18}O analysis of ice-wedges indicate that the MIS4 was characterized by severe winter conditions (Meyer *et al.*, 2002b), while large concentrations of reworked pollen suggest widespread denudation of deposits covered only in sparse grass-sedge tundra vegetation at times of low summer temperatures and precipitation (Andreev *et al.*, 2002b).

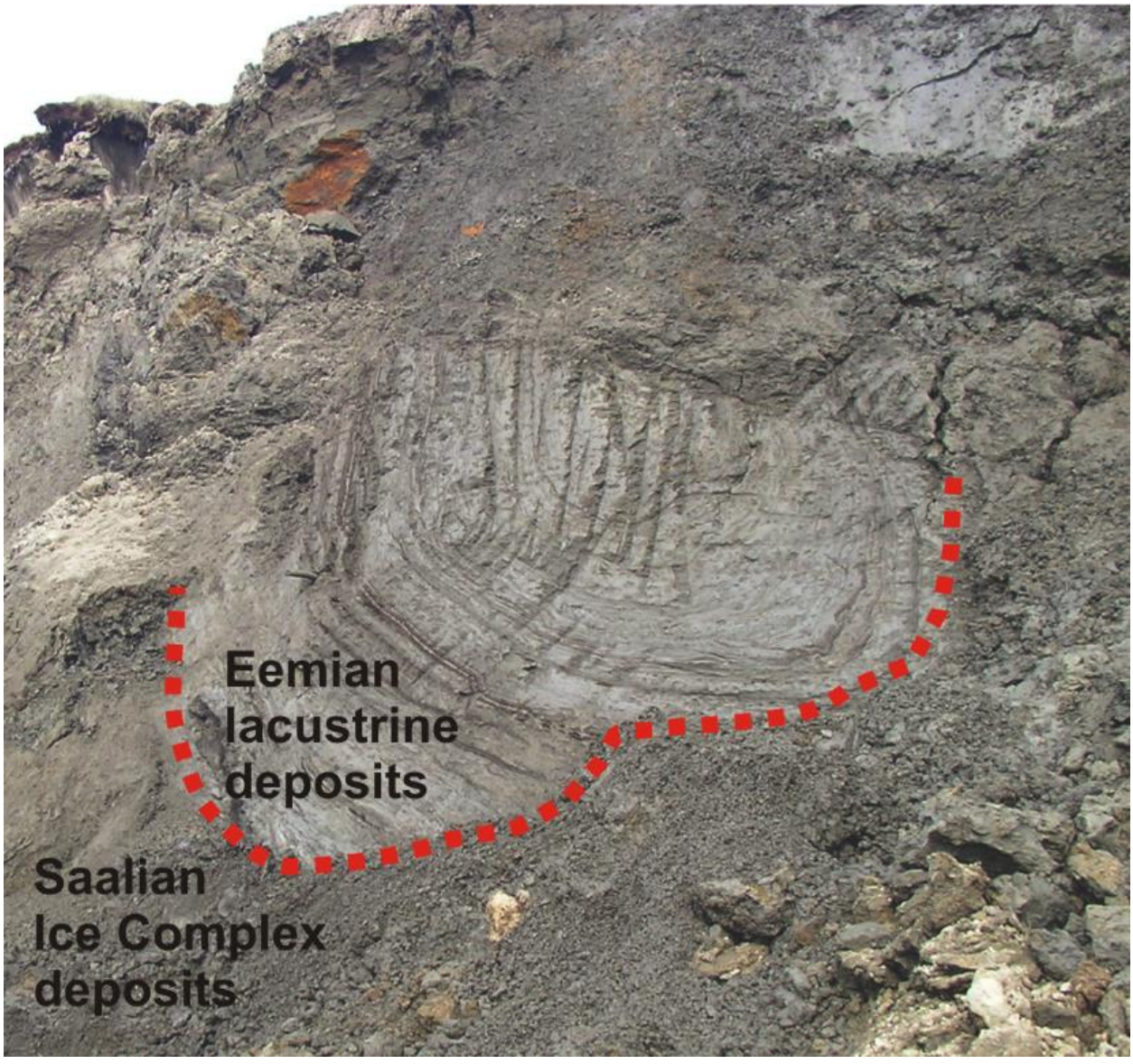

Figure 3: Ice-wedge pseudomorph. The ice-wedge of the Saalian glacial ice complex melted at the beginning the Eemian interglacial. The formed ice-wedge cast was then refilled with lacustrine sediments.

Climate conditions ameliorated during the following middle Weichselian interstadial (MIS3, 55–30 ka BP), also known as the Kargin interstadial, with warmer and wetter summer conditions than during the MIS4 (Andreev *et al.*, 2009). Deposits from this period are well preserved in NE Siberia and are characterized by fast continuous deposition of fine-grained sediments with many organic inclusions and extensive ice-wedge growth (Figure 4, Grosse *et al.*, 2013; Schirrmeister *et al.*, 2011). Multi-proxi paleo-environmental reconstructions from MIS3 deposits of the Molotkov horizon from Bol'shoy Lyakhovsky (Andreev *et al.*, 2002b; Wetterich *et al.*, 2014), the Mamontovy Khayata section on the Bykovsky Peninsula (Andreev *et al.*, 2002a; Sher *et al.*, 2005), the Buor Khaya Peninsula (Schirrmeister *et al.*, 2017; Zimmermann *et al.*, 2017), and Kurungnakh (Schirrmeister *et al.*, 2003; Wetterich *et al.*, 2008) indicate relatively warm and wet summer conditions.

Figure 4: Exposed Yedoma Ice Complex on the southern coast of Bol'shoy Lyakhovsky. View from the thermo-terrace (compare with Figure 8).

Deposits from the late Weichselian stadial period (MIS2, 30–13 ka BP), also referred to as the Sartan stadial, are sparsely preserved in NE Siberian permafrost deposits and have been presumably eroded by thermokarst processes at the beginning of the Holocene (Wetterich *et al.*, 2008, 2011). Nevertheless, remnants of the Sartan IC are partly preserved on Muostakh Island (Meyer *et al.*, in prep), Kurungnakh (Schirrmeister *et al.*, 2003; Wetterich *et al.*, 2008; Knoblauch *et al.*, 2013), Bol'shoy Lyakhovsky (Wetterich *et al.*, 2011), the Bykovsky Peninsula (Schirrmeister *et al.*, 2002a; Grosse *et al.*, 2007), Cape Mamontov Klyk (Schirrmeister *et al.*, 2008), and the lower Yana River (site 7 in Figure 2; Pitul'ko *et al.*, 2007). A shift in IC formation is indicated by a change in the accumulation areas between MIS3 and MIS2 (Wetterich *et al.*, 2011). On Bol'shoy Lyakhovsky for example, MIS2 deposits accumulated in an erosional valley, carved by intensified fluvial erosion, while the previous MIS3 deposits accumulated on flat plains. The MIS2 Sartan and MIS3 Molotkov horizon are therefore found at the same altitude (Figure 13). Pollen data indicate an open steppe-tundra, dominated by grassed and only few sedges (Andreev *et al.*, 2002a, 2002b; Schirrmeister *et al.*, 2008; Wetterich *et al.*, 2011) with relatively cold and dry summer conditions during this stadial. δ^2H and δ^{18}O analyses of ice-wedges also indicated severe winter conditions (Meyer *et al.*, 2002a, 2002b; Wetterich *et al.*, 2011). The coldest conditions where reached during the Last Glacial Maximum (LGM) between 26–15 ka BP, but there are some

regional differences in the timing and intensity of the LGM. Generally, the coldest and driest conditions were reached in the eastern Laptev Sea region between 26–20 ka BP. In contrast, LGM conditions in the western and central Laptev manifested <20 ka BP and were less severe than in the eastern Laptev Sea region (Wetterich *et al.*, 2011).

The late glacial-early Holocene transition (LGT-MIS1, 13–10.3 ka BP) was characterized by rapid marine transgression (Bauch *et al.*, 2001) and increasing seasonality. Winters were still relatively cold and dry, but summer temperatures increased by several °C compared to the LGM. Overall, pollen concentrations were low but indicate a slow transition to shrub tundra (Andreev *et al.*, 2009; Zimmermann *et al.*, 2017). The onset of the Holocene (MIS1, <13.5 ka BP) occurred rapidly in NE Siberia. It is estimated that 70% of the original Yedoma IC area (>10^6 km^2) was eroded by thermokarst during the early Holocene (Strauss *et al.*, 2013), which was ~4 °C warmer than today (Andreev *et al.*, 2002a, 2002b, 2009). The pollen records from Holocene cover and thermokarst deposits show that shrubs (*Alnus fruticosa, Betula nana, Salix*) dominated during the climate optimum (10–7.6 ka BP) but then gradually disappeared (Naidina & Bauch, 2001). But while global summer temperatures decreased after the climate optimum (Sundqvist *et al.*, 2014), winter temperatures in NE Siberia gradually increased over the last 7 000 years (Meyer *et al.*, 2015a). Today, modern tundra vegetation is dominated by moss and sedge wetland vegetation in the Lena River Delta and shrub, sedge, and moss tundra in Yedoma regions (CAVM Team, 2003).

2.4 Incubation studies

One way to assess the potential decomposability of SOM are laboratory incubation experiments. The advantage of incubation studies is the external control of conditions, which in turn allows a closer investigation of different environmental controls on SOM decomposition, such as O_2 availability, temperature, moisture, or nutrient availability. Incubation studies have been widely used in permafrost research, as well as in soil science in general. Recent summaries of different incubation studies from permafrost-affected soils and sediments from tundra, boreal forest, Arctic peatlands in Alaska, Greenland, Canada, Siberia are given by Schädel *et al.* (2016, 2014) and Treat *et al.* (2015). Some of the main findings of these syntheses were: (1) the labile SOC pool of permafrost-affected soils and sediments is generally <5% of SOC, but does not differ between organic, shallow (<1 m) and deep (>1 m) mineral soils (Schädel *et al.*, 2014), (2) under aerobic conditions 3.4 times more SOC is decomposed than under anaerobic conditions, independent of the biome as well as incubation temperature (Schädel *et al.*, 2016), and (3) methanogenesis plays a minor role (Schädel *et al.*, 2016) and is only initiated after a long lag phase of several months to years (Treat *et al.*, 2015).

Some of the remaining knowledge gaps are addressed in this work. In particular, the differences between active layer and near-surface permafrost soils, since most studies focused on either one or the other, but mostly the active layer. Further, most studies focused on one or two environmental drivers (mostly O_2 availability and temperature) but not on the interconnection between different drivers. Further, the length of the incubation studies varies greatly from a few days (Whalen & Reeburgh, 2000; Treat *et al.*, 2014) to several years (Elberling *et al.*, 2013; Knoblauch *et al.*, 2013). Long-term incubation studies are helpful to project long-term GHG production potentials and assess the decomposability of stable SOC pools. Finally, yet importantly, the decomposability of deep SOC pools is poorly constrained and the number of incubation studies limited.

3 Study regions

Samples were collected at five different locations in the continuous permafrost zone of NE Siberia (Figure 2): (1) Samoylov and (2) Kurungnakh in the Lena River Delta, (3) Muostakh Island and (4) the Buor Khaya Peninsula in central Laptev Sea region, and (5) Bol'shoy Lyakhovsky in the eastern Laptev Sea. The different locations are described in more detail below.

3.1 Lena River Delta

Two islands, Samoylov (72°22' N, 126°30' E), and Kurungnakh (72°19' N, 126°12' E), were sampled in the Lena River Delta, which is the largest Arctic delta (Walker, 1998). It consists of three main geomorphological units (terraces) and the active floodplains (Grigoriev, 1993 cited in Schwamborn *et al.*, 2002). Samoylov is part of the youngest first terrace, which developed during the Holocene (Bolshiyanov *et al.*, 2015). The elevated river terrace is characterized by ice-wedge polygons with low-lying polygon centers and elevated polygon rims, while the active floodplain shows little to no surface morphology. Modern vegetation is characterized by sedge, moss, dwarf-shrub wetland vegetation (CAVM Team, 2003). The dominating vascular plant species is *Carex aquatilis*, with a total coverage of 25% in polygon centers on the river terrace (Kutzbach *et al.*, 2004). Below ground, *C. aquatilis* forms as dense mat of coarse perennial roots and fine roots can be found down to the permafrost table (Kutzbach *et al.*, 2004). The main soil types (IUSS Working Group WRB, 2014) include Histic Cryosols in polygon centers and Turbic Glacic Cryosols in elevated polygon rims on the river terrace and Cryosols (Fluvic) on the floodplain (Pfeiffer *et al.*, 2002; Zubrzycki *et al.*, 2014). The main climate, permafrost, and land cover characteristics (1998–2011) were summarized by Boike *et al.* (2013). Briefly, the mean annual temperature is -12.5 °C. The warmest month is usually July with a mean temperature of 10.1 °C. The mean summer precipitation is 125 mm, with strong inter-annual variability. The ground remains completely frozen from November until June. The mean duration of thaw on Samoylov is about 130 days with a mean thaw depth of ~49 cm.

Kurungnakh is part of the third and oldest terrace and represents remnants of the Late Pleistocene Yedoma IC (Grigoriev, 1993 cited in Schwamborn *et al.*, 2002) which accumulated between 100–17 ka BP (Schirrmeister *et al.*, 2003; Wetterich *et al.*, 2008). Thermo-erosion has shrunk the area of Kurungnakh by nearly 100 km^2 (~25%) since the end of the last glacial period and 50% of the remaining area are affected by thermokarst (Romanovskii *et al.*, 2000; Morgenstern *et al.*, 2011). Several thermokarst depressions, so called alasses, characterize the surface morphology. Some of these alasses are filled, or partly filled, by thermokarst lakes. One of the largest alas (7.5 km^2, >20 m deep) formed during the early Holocene (13–12 ka BP, Morgenstern *et al.*, 2013). Today, the alas is filled with three small lakes, after the initial lake drained abruptly 5.7 ka BP (Morgenstern *et al.*, 2013). In the alas, wetland vegetation dominates, but tussock tundra and willow shrubs also occur in drier areas.

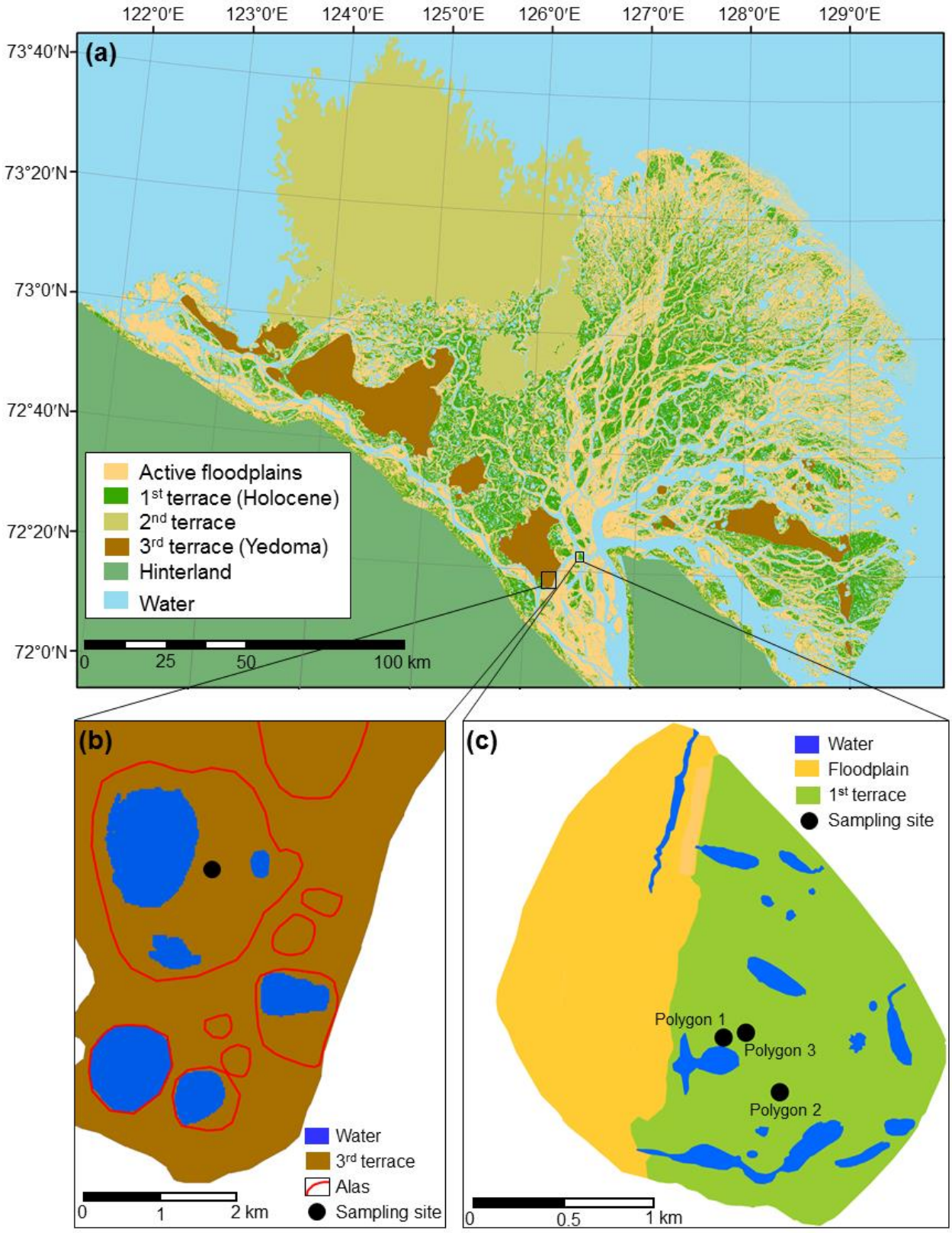

Figure 5: Overview map of the Lena River Delta. The different geomorphological units and active floodplains (Grigoriev, 1993, Schwamborn *et al.*, 2002) are shown in panel (a). The sampling locations in an alas (Morgenstern *et al.*, 2017) of Kurungnakh and on the river terrace of Samoylov (Zubrzycki *et al*., 2013) are shown in panels (b) and (c), respectively.

3.2 Buor Khaya Bay area

The Buor Khaya Bay is located in the central Laptev Sea region (Figure 6). The closest climate station (WMO index 21824) is located in Tiksi. The mean annual (1981–2010) temperature is -12.7 °C and mean annual precipitation is 317 mm (Figure 9a, Bulygina and Razuvaev, 2012). Modern vegetation is dominated by erect dwarf-shrub and in places by sedge, moss, low-shrub wetland vegetation or tussock-sedge, dwarf-shrub, moss tundra vegetation (CAVM Team, 2003).

Two terrestrial permafrost sites were sampled in the Buor Khaya Bay area. The first sampling location (MUO12) is on Muostakh Island (70°35' N, 130°0' E), a small island in the middle of the Buor Khaya Bay; 40 km east of Tiksi. The Yedoma IC deposits of Muostakh Island are thought to be of the same origin as on the Bykovsky Peninsula (Grosse *et al.*, 2007), which formed continuously between about 58–12 ka BP (Schirrmeister *et al.*, 2002a). However, Muostakh Island is subject to intensive permafrost thaw subsidence. Between 1951–2013, the area and volume of Muostakh decreased by 24% and 40%, respectively (Günther *et al.*, 2015).

The second sampling location (BK8) is on the Buor Khaya Peninsula (72°25' N, 132°6' E), ~120 km east of Tiksi. The IC deposits on the Buor Khaya Peninsula mainly accumulated between 54.1–30.1 ka BP, but deposition continued until 14.7 ka BP (Schirrmeister *et al.*, 2017). The deposits reach thicknesses of up to 40 m, but 85% of the region is affected by thermokarst, which resulted in permafrost thaw subsidence of more than 20 m (Morgenstern *et al.*, 2017). Additionally, the coastal permafrost deposits are subjected to high erosion rates (1 m a^{-1}, Günther *et al.*, 2013).

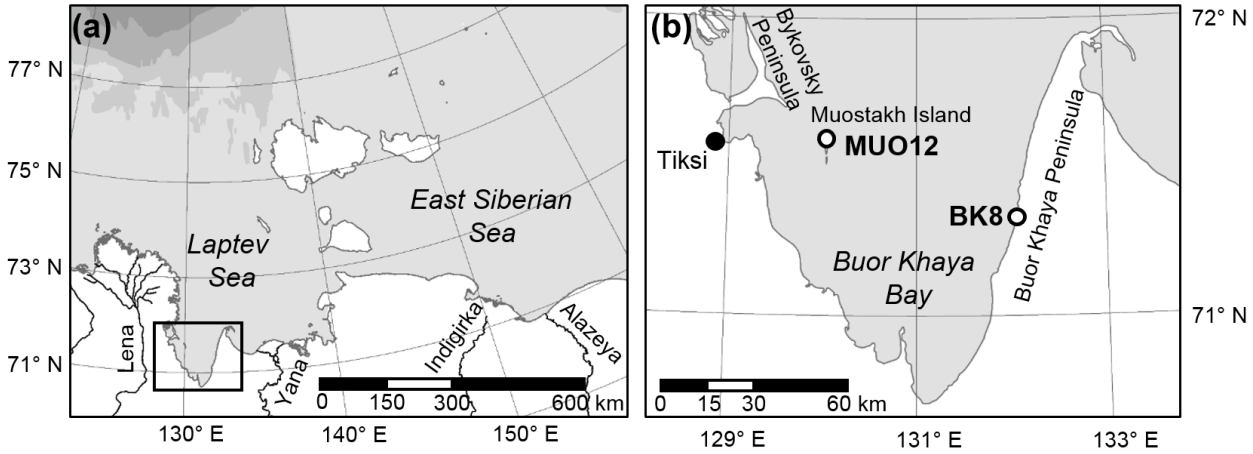

Figure 6: Overview map of central Laptev Sea region. The Buor Khaya Bay area is framed by the black box in panel (a). The sampling locations on Muostakh Island (MUO12) and the Buor Khaya Peninsula (BK8) and the location of the closest climate station in Tiksi WMO (index 21647) is shown in panel (b).

3.3 Bol'shoy Lyakhovsky

Bol'shoy Lyakhovsky is the southernmost island of the New Siberian Island archipelago, ~450 km east of Tiksi. The 60 km wide Dmitry Laptev Strait separates Bol'shoy Lyakhovsky from the Oyogos Yar coast on the Siberian mainland (Figure 7). The work on Bol'shoy Lyakhovsky concentrated on the southern coast (73°19' N, 141°20' E), where several permafrost outcrops are accessible. The ice-rich permafrost deposits, however, are subject to widespread thaw and thermo-erosion. Parts of the exposed IC deposits have already been eroded and formed several thermo-erosional cirques (thermo-terraces), which extent >100 m inland. Thaw mounds, so called baydzherakhs, characterize the surface morphology of the thermo-terraces as well as the Yedoma surface. A schematic cross section of the southern coast of Bol'shoy Lyakhovsky is shown in Figure 8.

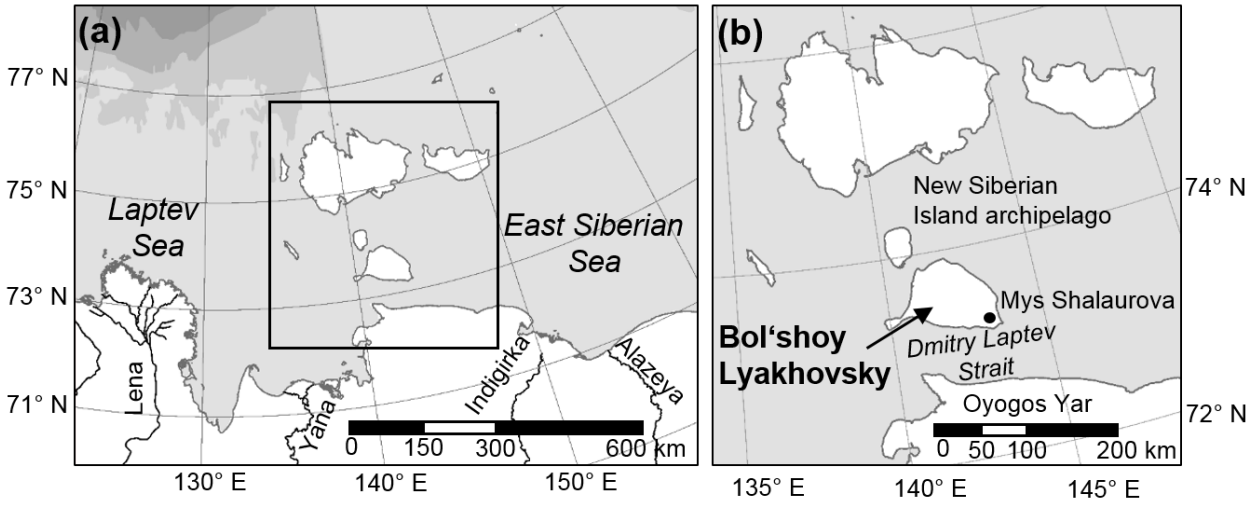

Figure 7: Overview map of eastern Laptev Sea region. The New Siberian Island archipelago is framed by the black box in panel (a). The location of the closest climate station (WMO index 21647) at Mys Shalaurova on Bol'shoy Lyakhovsky is shown in panel (b).

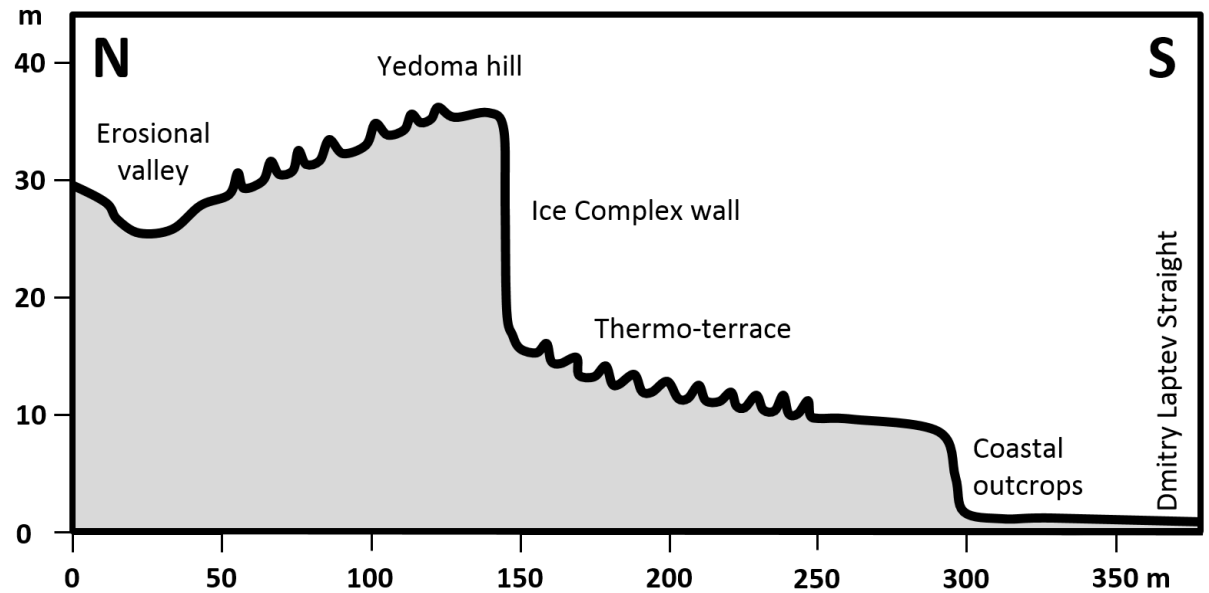

Figure 8: Schematic cross section of the southern coast of Bol'shoy Lyakhovsky (modified after Kunitsky *et al.*, 2000). A frontal view of the exposed ice complex wall is shown in Figure 4.

The climate of Bol'shoy Lyakhovsky is characterized by long cold winter, short cool summers, and low to moderate precipitation. The closest climate station (Mys Shalaurova, WMO index 21647) is located on the southeastern coast of Bol'shoy Lyakhovsky (~60 km from the sampling sites, Figure 7b). The station was closed down in 2000. The mean annual (1971-2000) temperature and precipitation are with -14.9 °C and 145 mm (Figure 9b, Bulygina and Razuvaev, 2012) considerably lower than in the Buor Khaya Bay area over the same period (-13.3 °C, 266 mm). The highest temperatures are observed in July and August, but are also low (~2 °C), Modern vegetation is dominated by rush/grass, forb, cryptogam tundra (CAVM Team, 2003).

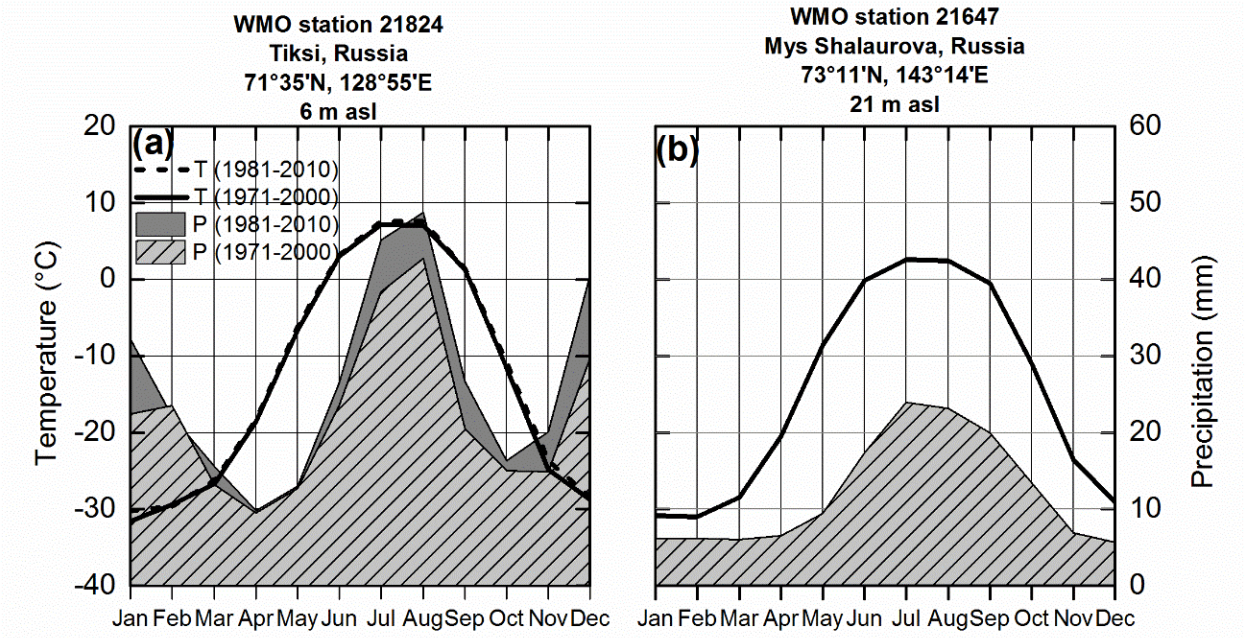

Figure 9: Climate diagrams for Tiksi (a) and Mys Shalaurova (b) with temperature (T) and precipitation (P). Data from Bulygina & Razuvaev (2012). The station at Mys Shalaurova was closed in 2000. For better comparison between the two locations, data for Tiksi are shown for the 1971–2000 as well as 1981–2010 period.

4 Material and methods

4.1 Soil sampling

4.1.1 Lena River Delta

Three different low-centered polygons (Figure 5c) were sampled on the river terrace of Samoylov. Soil cores were obtained using a portable SIPRE-corer (Jon's Machine Shop, Fairbanks, AK, USA) with a STIHL BT 121 engine (STIHL, Waiblingen, Germany). Coring was conducted in April 2011 (Polygons 1 and 2) and May 2013 (Polygon 3) while the entire soil profile was still frozen (Zubrzycki, 2012). Cores were recovered to depths of 82 cm, 86 cm, and 92 cm. A fourth core was drilled in an alas on Kurungnakh Island in April 2013. Core recovery was 96 cm (Figure 5b).

4.1.2 Bol'shoy Lyakhovsky

On Bol'shoy Lyakhovsky, four landscape units were sampled in August 2014 (Figure 10): (1) Yedoma Ice Complex (Y), (2) thermo-terrace (TT), (3) thermo-erosional valley (EY), and (4) alas (A). Soil pits were dug to the frost table and profiles described (FAO, 2006). Diagnostic horizons and properties were identified in the field and additional soil properties were analyzed in the laboratory.

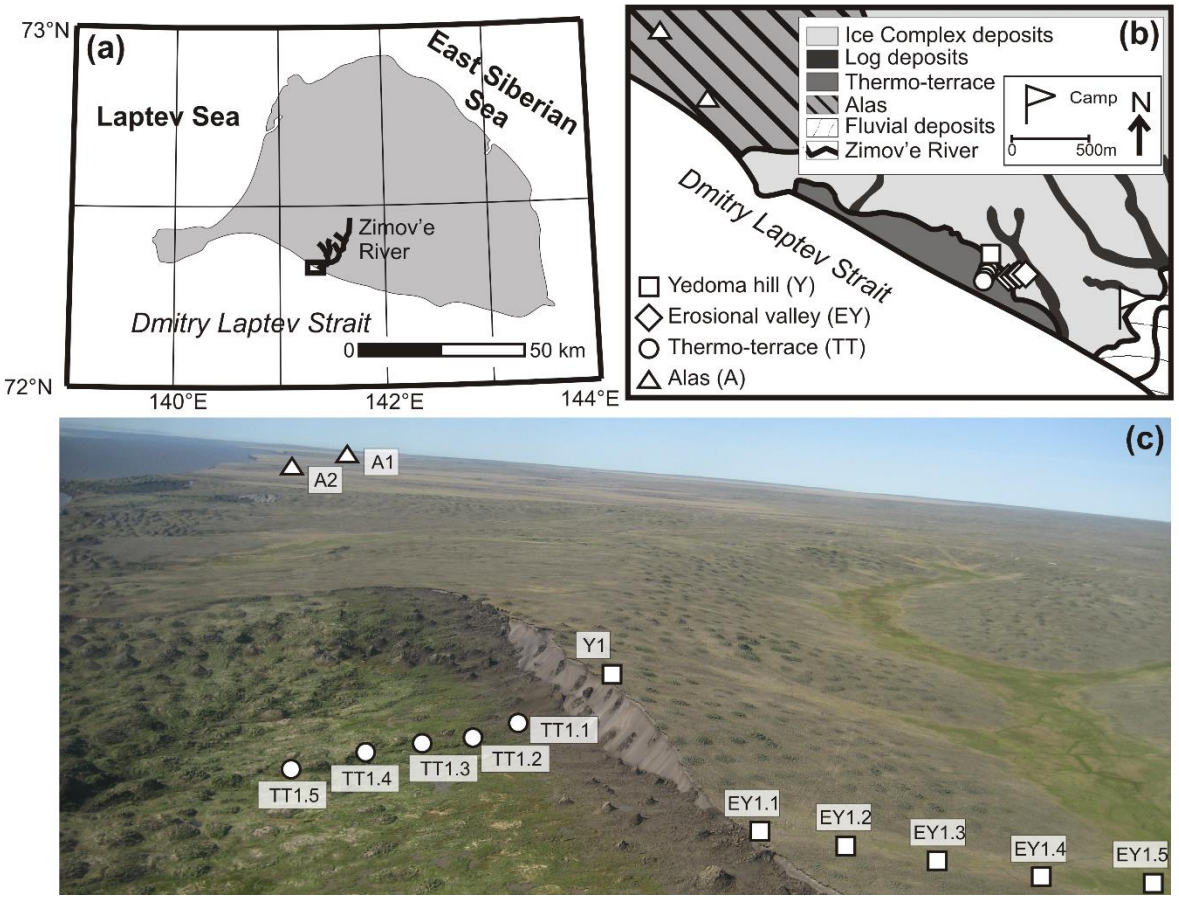

Figure 10: Overview map of the soil sampling locations on the southern coast of Bol'shoy Lyakhovsky. The black box in panel (a) frames the study area, while the enlarged view in panel (b) shows the different investigated landscape units (modified after Meyer *et al.*, 2000). The aerial photo (c, G. Schwamborn, AWI Potsdam) shows the locations of the soil profiles of the Yedoma (Y) IC, thermo-erosional valley (EY), thermo-terrace (TT), and the alas (A).

4.2 Coring and outcrop sampling

4.2.1 Muostakh Island

On the NE shore of Muostakh Island, the sedimentary sequence between 4.4–19.5 m above sea level (asl) was sampled in three sub-profiles (Meyer *et al.*, 2015b). Detailed stratigraphic and sedimentological studies will be published elsewhere (Meyer *et al.*, in prep). Briefly, two erosional plains separate three different units, evident by sharply intersected ice-wedges at ~17 m asl and a gravel layer at 9.5 m asl (Figure 11). The lowermost section between 4.4–9.5 m asl consists of sandy silts with ^{14}C ages >41 ka BP (MIS3, Kargin). The middle section between 9.5–17.5 m asl consists of coarser grained material with ^{14}C ages between 13–20 ka BP (MIS2, Sartan). The uppermost sections >17.5 m asl consists of silty material with many peaty patches and organic inclusions with ^{14}C ages of <13.7 ka BP (LGT-MIS1, Holocene, including the late glacial-early Holocene transition).

4.2.2 Buor Khaya Peninsula

A 18.9 m long core (BK8) was drilled on the Buor Khaya Peninsula in April 2012 (Grigoriev *et al.*, 2013). The drilling site (71°25.21’ N, 132°6.66’ E) was located approximately 100 m from the cliff edge on top of Yedoma ice complex hill (Figure 6). Core recovery was 100% and started at the ground surface at 34.2 m asl down to 15.3 m asl. Frozen core sections were packed in plastic bags and transported in a frozen state until further processing. Detailed field descriptions (Grigoriev *et al.*, 2013) and sedimentological, cryolithological, geochemical, and geochronological data (Schirrmeister *et al.*, 2017) have been published previously for the BK8 site. Briefly, the BK8 core consists of silty fine-grained sand with many plant remains and horizontal cryostructures (Schirrmeister *et al.*, 2017). An ice-wedge, which consisted of clear ice with entrapped gas bubbles, dissected the core between 3.2–8.5 m below surface (bs) or 31.0–25.7 m above sea level (asl). Between 8.5–10.1 m bs (25.7–24.1 m asl), diagonal cryostructures and upturned ice bands characterized the contact zone between the ice-wedge and sediment. Electrical conductivity in pore-space solution in the lowermost part of the core between 16.4–18.9 m bs (17.8–15.3 m asl) was with 7 000–14 000 µS cm^{-1} one to two order of magnitude higher than in the other sediment sections (100–1 000 µS cm^{-1}) and the ice-wedge (<100 µS cm^{-1}, Schirrmeister *et al.*, 2017).

Based on radiocarbon and IRSL ages (Schirrmeister *et al.*, 2017), the core was subdivided into three sections. The uppermost sample (0–0.5 m bs, 34.2–33.7 m asl) represents the active layer. Sediments above the ice-wedge between 0.5–3.2 m bs (33.7–31.0 m asl) yielded ages of 11.4–10.1 ka BP and represent the late glacial-early Holocene transition (LGT-MIS1). Sediments below the ice-wedge between 8.5–18.9 m bs (25.7–15.3 m asl) yielded ^{14}C and IRSL ages between 54.1–30.1 ka BP and thus represent the MIS3 (Kargin).

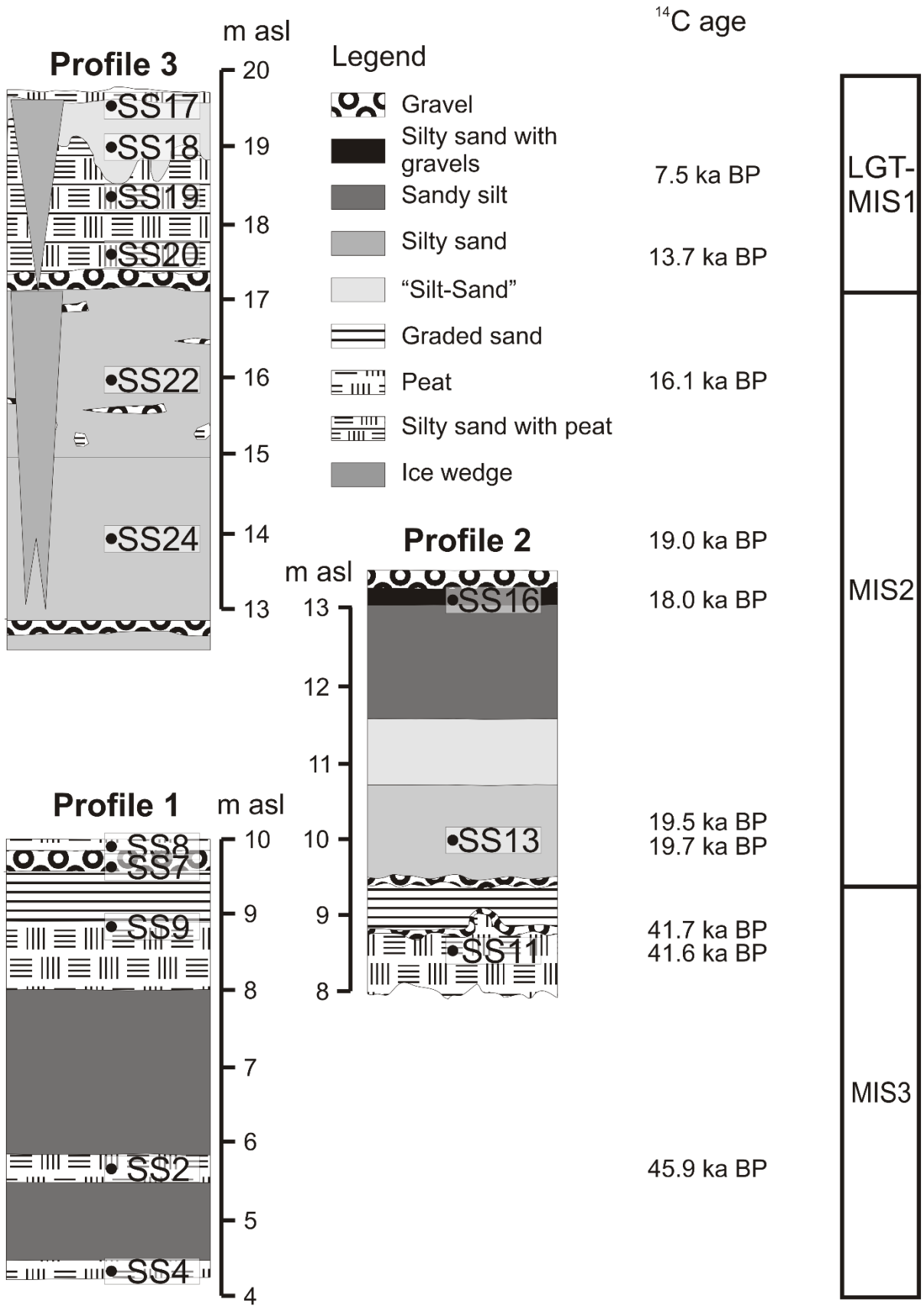

Figure 11: Stratigraphic scheme of the three sampled profiles on Muostakh Island (modified after C. Manthey, in Opel, 2015) with ages according to Meyer *et al.* (in prep) and subsample positions (compare with Table 11).

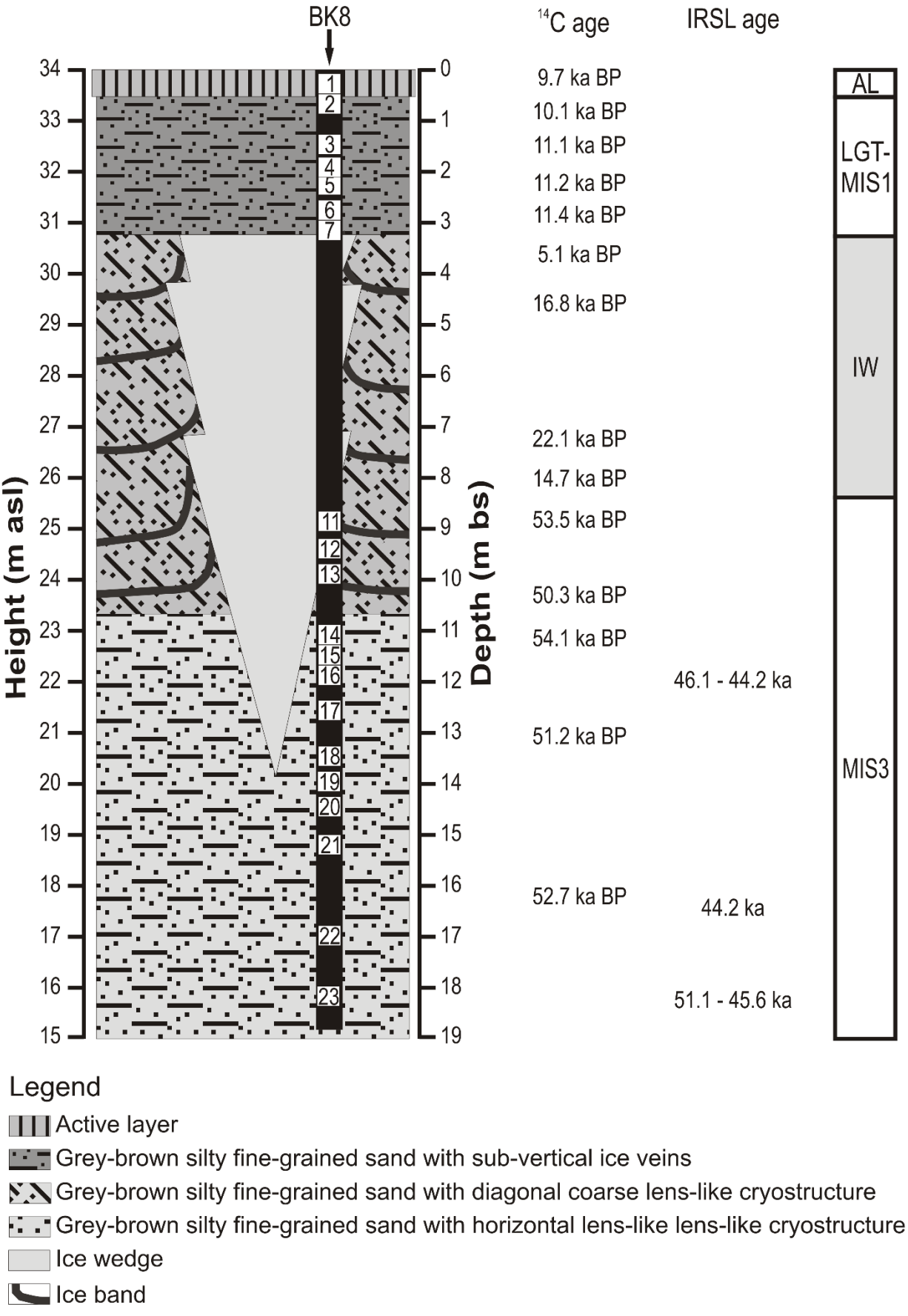

Figure 12: Stratigraphic scheme of the BK8 core with sediment (black) and ice-wedge (IW, grey) ages (modified after Schirrmeister *et al.*, 2017), chronostratigraphy, and subsample positions (compare with Table 12).

4.2.3 Bol'shoy Lyakhovsky

The permafrost deposits of Bol'shoy Lyakhovsky provide an important paleo-environmental archive of permafrost aggradation and degradation over at least two glacial-interglacial cycles. The sedimentary characteristics, pollen assemblages, and stable isotopes have been studied in detail previously and provide the basis for environmental interpretations for this work (compare with section 2.3). In 2014, the entire sedimentary record was sampled with four cores and five coastal permafrost outcrops (Figure 13). The permafrost cores were drilled in April 2014 with a mobile Russian drill rig (KMB3-15M) using a rotary mechanism in dry holes (Schwamborn & Wetterich, 2015) while the entire ground was frozen. The uppermost part (0–0.5 m bs) of each of the four cores represents the active layer. The outcrops were sampled in August 2014. The unfrozen material on the surface and the first few cm of frozen material were removed prior to sampling, to ensure that only permafrost material was sampled.

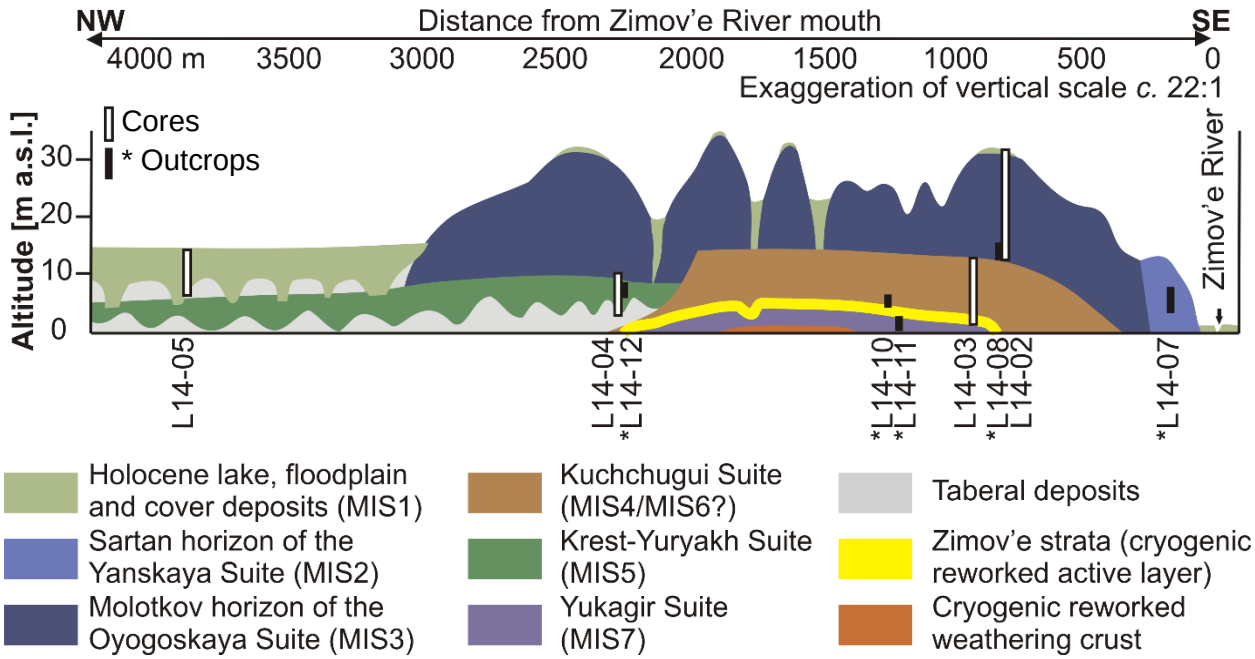

Figure 13: Stratigraphic scheme of the coastal sections west of the Zimov'e River mouth on the southern coast of Bol'shoy Lyakhovsky (modified after Andreev *et al.*, 2004 and updated according to Wetterich *et al.*, 2014 and references therein) with coring and outcrop sampling locations (compare with Table 13, Table 14).

The L14-05 core was drilled in an alas ~4 km west of the Zimov'e River mouth, which formed during the early Holocene. Drilling started at 11.4 m asl down to 3.6 m asl. Based on previous studies of coastal permafrost outcrops (Andreev *et al.*, 2004, 2009; Wetterich *et al.*, 2009) and sedimentary characteristics, the 7.9 m long recovered core was divided into two sections. The upper section between 0.5–5.5 m (10.9–5.9 m asl) represent the thermokarst deposits of MIS1 origin. They accumulated on top of the MIS3 Yedoma IC, which is captured in the lower part of L14-05 (5.5–7.9 m bs, 5.9–3.6 m asl). Five subsamples were taken from this core.

The L14-02 core was drilled on top of the Yedoma hill at 32.3 m asl. The first 0.5–10.9 m bs (31.8–21.4 m asl) consisted of ice-rich silt with many organic remains and peaty inclusions, which were correlated to the Molotkov horizon of the MIS3 interstadial (Wetterich *et al.*, 2014). An ice-wedge was encountered below 10.9 m bs (21.4 m asl). The ice-wedge continued down to at least 20.2 m bs (12 m asl), where drilling stopped. For this work, five subsamples were taken from the upper core section, but none from the ice-wedge.

The drill site of the L14-03 core was on the thermo-terrace from 17 m asl to 1.5 m asl and ended above the gravel of the Zimov'e strata. Core recovery was 15.5 m. The upper 0–4.9 m (17–12.1 m asl) consisted of ice-rich silt and the lower section between 4.9–15.5 m bs (12.1–1.5 m asl) is characterized by sandy deposits with many organic remains between 4.9–6.9 m bs (12.1–8.6 m asl), and only scattered organic remains between 6.9–15.5 m bs (8.6–1.5 m asl). These deposits have been correlated to the Kuchchugui Suite. Due to the lack of reliable ages, the stratigraphic position of the Kuchchugui Suite is still debated. Low pollen concentrations (Andreev *et al.*, 2004) and ice-wedge stable isotopes (Meyer *et al.*, 2002a) suggest very cold conditions. Since the Kuchchugui Suite is in places overlain by Eemian lacustrine thermokarst lake sediments (Unit II in Andreev *et al.*, 2004, Unit I in Opel *et al.*, 2017), it has been proposed that the Kuchchugui represents an extremely cold late Saalian stadial (MIS7/MIS6). In other places, the Kuchchugui overlies Eemian and underlies Yedoma IC deposits (Unit IV in Andreev *et al.*, 2004). It was therefore inferred, that the Kuchchugui represents an early Weichselian stadial (Zyryan, MIS4). In this work, it is assumed, that the Kuchchugui on Bol'shoy Lyakhovsky is of MIS4 origin, which is in agreement with the latest publication on this sample material (Stapel *et al.*, 2017). Six subsamples were taken from L14-03.

The drill site of core L14-04 was ~2.5 km west of the Zimov'e River mouth. Drilling started 12.0 m asl and continued down to 3.9 m asl. Core recovery was 8.1 m. The core was subdivided into two parts. The upper 0.5–5 m (11.5–7 m asl) consisted of ice-rich silty material, similar to Early Weichselian MIS4 floodplain deposits (Unit IV in Andreev *et al.*, 2004), while the lower section between 5–8.1 m bs (7–3.9 m asl) consisted of ice-poor laminated silt and fine sand, consistent with the lacustrine MIS5 deposits of the Krest Yuryakh Suite. For this work, five subsamples were taken from L14-04 (Table 13).

The five additionally sampled outcrops partly overlap with the cores, but also extent the record to MIS2 deposits of the Sartan horizon and deposits from the MIS7 Saalian glacial, which were not included in the core record. Briefly, profile *L14-07 corresponds to the Sartan horizon (MIS2) and consisted of brownish ice-rich, silty material with many fossil grass roots. Profile *L14-08 corresponds to the Molotkov horizon (MIS3), and consisted of light brown-greyish silt and fine sand with fine grass roots clustered in several areas and single dark-brown organic patches. Profile *L14-10 corresponds to the Kuchchugui Suite. The layered brown-yellowish silt and fine sand likely represent MIS4 floodplain deposits. Profile *L14-12 corresponds to the Krest Yuryakh

Suite. One sample from this profile (*BK5) was taken from the slightly layered silty sands with clustered black spots of organic material. A second sample (*BK6) was taken from the uppermost section, where many pockets of peaty material are intercalated into the mineral matrix. Profile *L14-11 corresponds to the Yukagir IC (MIS7) and consists of greenish-grey ice-rich fine-grained material (*BK7) overlain by 1 m thick peaty deposits (*BK4).

4.3 Laboratory work

4.3.1 Soil and sediment analysis

Soil water contents were calculated as the weight difference between wet and oven dried (105 °C, >24 h) samples. pH values were measured in a suspension of 5 g thawed soil in 12.5 ml distilled water (Hamburg: CG820, Schott AG, Mainz, Germany; Samoylov pH/Ion 340i, Wissenschaftlich-Technische Werkstätten (WTW) GmbH, Weilheim, Germany). For soil chemical analyses, bulk soil samples were dried at 70 °C for 24-48 h and milled. Total C and nitrogen (N) contents were measured with an element analyzer (VarioMAX cube, Elementar Analysensysteme GmbH, Hanau, Germany), while SOC contents were measured with a liquiTOC II coupled to a solids module (Elementar Analysensysteme GmbH, Hanau, Germany). The $\delta^{13}C$ values of SOC ($\delta^{13}C_{org}$) were measured with an isotope-ratio mass spectrometer (Delta V, Thermo Scientific, Dreieich, Germany) coupled to an elemental analyzer (Flash 2000, Thermo Scientific, Dreieich, Germany) after samples were treated with phosphoric acid to release inorganic C.

4.3.2 Incubation

Samples were prepared in three to five replicates. Frozen samples were slowly thawed from -18 °C to 4 °C over 48–60 h in a refrigerator. Samples for anaerobic incubations were prepared in a N_2 atmosphere in a glove box. All samples were homogenized and large roots were removed. Approximately 10–50 g thawed soil or sediment was weighed into 120 ml or 250 ml glass bottles. All bottles were sealed with butyl rubber stoppers to prevent gas exchange with the ambient air and to keep water content constant. 10–30 ml of N_2-flushed, CO_2-free distilled water was added to anaerobic samples to saturate them and displace any residual O_2 in the pore space. The headspace of anaerobic samples was exchanged with N_2. The headspace of aerobic samples was exchanged with synthetic air (20% O_2, 80% N_2).

The concentrations of CO_2 and CH_4 inside the headspace of each bottle were measured repeatedly via gas chromatography (7890A and 6890N, Agilent Technologies, Santa Clara, CA, USA). The gas chromatograph was equipped with a nickel catalyst to reduce CO_2 to CH_4 and a flame ionizing detector (FID). Gases were separated on a PorapakQ column with helium as carrier gas. If the concentration of CO_2 in the headspace of aerobic incubations approached 3%, the headspace was again exchanged with synthetic or ambient air, respectively. Gas concentrations were generally measured once to trice a week during the first three months of incubations.

Measuring intervals then gradually decreased once every 2–4 weeks for the next 3–6 months and finally to once every 3–6 months after the first incubation year.

The amount of gas inside each bottle was calculated from the gas concentration, headspace volume, incubation temperature, and pressure inside the bottle using the ideal gas law. The amount of dissolved gas was calculated from the gas concentration in the headspace, pressure inside the bottle, water content, and gas solubility in water. Solubility for CO_2 and CH_4 was calculated after Carroll *et al.* (1991) and Yamamoto *et al.* (1976), respectively. To account for the dissociation of carbonic acid in water, the amounts of dissolved C species were calculated using dissociation constants from Millero *et al.* (2007). Gas production rates were calculated by a linear fit of produced gas and incubation time using four to five consecutive measurements.

4.3.3 Environmental drivers of soil organic matter decomposition

Soil samples from Samoylov and Kurungnakh were used to investigate the influence of different environmental parameters (O_2 availability, freeze-thaw cycle, temperature, and substrate availability) on SOM decomposition in different soil layers (Table 9, Table 8). Due to the limited amount of soil collected, not all the experiments could be performed on each sample. Samoylov samples from Polygons 1 and 2 were used for aerobic and anaerobic incubations, as well as a freeze-thaw experiment. Temperature sensitivity and priming experiments were carried out with samples from Samoylov Polygon 3 as well as samples from Kurungnakh (Table 9, Table 8).

To examine the long-term production potentials in different soil layers under aerobic and anaerobic conditions, samples from Samoylov (Polygons 1 and 2) were aerobically and anaerobically incubated at a constant temperature of 4 °C for up to 1059 days. To account for the 34-times higher warming potential of CH_4 compared to CO_2 on a 100-year timescale (Myhre *et al.*, 2013), a relative climate forcing (RCF) factor was calculated as

$$RCF = \frac{Aerobic\ CO_2}{Anaerobic\ CO_2 + 34 \times Anaerobic\ CH_4} \quad (1)$$

The RCF was calculated based on the mean aerobic and anaerobic production per gram soil for each of the nine depth increments for Polygons 1 and 2. A RCF>1 suggest that the net warming effect on climate from aerobic decomposition processes is greater than from anaerobic decomposition, while a RCF<1 suggests the opposite.

To examine the effect of freezing and thawing on SOM decomposability, one surface active layer, one bottom active layer, and one permafrost from Polygon 1 (aerobic) and Polygon 2 (anaerobic) from Samoylov were used (Table 9). Samples were prepared in six replicates and incubated for 30 days at 4 °C. After 30 days, all aerobic and anaerobic samples were flushed with synthetic air or N_2, respectively. Three replicates of each sample were incubated for another 30 days at 4 °C. The other three replicates were refrozen inside the incubation bottle to -18 °C. After seven days at this temperature, samples were re-thawed and incubated at 4 °C for another 30

days. During the 7-day re-freezing period, gas concentrations in the headspace of refrozen bottles remained constant. Thus, both treatments were incubated for a total of 60 days at 4 °C, with a break of seven days at -18 °C for the freeze-thaw treatment. The relative freeze-thaw effect (FT%) was calculated as

$$FT\% = \frac{(FTc - c)}{c} \times 100\% \quad (2)$$

where FTc and c are the amounts of C decomposed to either CO_2 or CH_4 in freeze-thaw and control samples, respectively.

The temperature sensitivity of SOM decomposition was examined using samples from Samoylov (Polygon 3) and Kurungnakh (Böhme, 2015). Samples were aerobically incubated for 150–185 days (Kurungnakh) to 429 days (Samoylov) at 1 °C, 4 °C, or 8 °C. To assess the temperature response and to calculate Q_{10} values, the equal-C method was applied. Unlike the traditional approach to Q_{10} values, where decomposition rates at different temperatures over a fixed incubation period are compared (equal-time), this approach compares the time needed to decompose the same amount of SOC, thereby excluding temperature-induced differences in the depletion of the labile and stable SOC pools (Rey & Jarvis, 2006; Conant *et al.*, 2008). The temperature response of SOM decomposition was determined by fitting the data to an Arrhenius type equation

$$\ln(t) = m \times T^{-1} + b \quad (3)$$

where t is the incubation day when a certain amount of the initial SOC was decomposed in each sample, T^{-1} is the inverse incubation temperature, and m and b are the slope and intercept of the linear regression line, respectively. Q_{10} values were then calculated as

$$Q_{10} = \frac{t_0}{t_{10}} \quad (4)$$

where t_0 and t_{10} are derived from Equation 3 and represent the theoretical incubation days needed to decompose a certain amount of the initial SOC at 0 °C and at 10 °C, respectively. The temporal evolution of the temperature sensitivity was assessed by calculating Q_{10} values with increasing amounts of SOM decomposition from 0.1–5.5% of the initial SOC.

To examine the influence of labile OM availability on SOM decomposition samples from Samoylov (Polygon 3) and Kurungnakh were amended with ^{13}C-labelled OM from leaves of *Carex aquatilis*, which is the dominant vascular plant species in wet polygon centers at the study site. The plants were grown under a ^{13}C-CO_2 enriched atmosphere on Samoylov and the leaves harvested after about three weeks. The $\delta^{13}C$ value of the labelled *Carex* leaves ($\delta^{13}C_{Carex}$) was 744‰ relative to the Vienna Pee Dee Belemnite (VPDB) standard. Samples were individually amended with the *Carex* material at a rate of 1.3% of the initial SOC, and aerobically incubated at 1 °C, 4 °C, or 8 °C for 150 days. The concentration of CO_2 was measured every week. The

isotopic signature of the produced CO_2 in amended samples was also measured weekly by isotope-ratio mass spectroscopy (Finnigan Delta Plus, Thermo Scientific, Dreieich, Germany) coupled to a gas chromatograph (6890, Agilent Technologies, Santa Clara, CA, USA). To differentiate between SOM-derived and *Carex*-derived CO_2, a mixing model was used

$$f_{SOM} = \frac{\delta^{13}C_{CO_2} - \delta^{13}C_{Carex}}{\delta^{13}C_{org} - \delta^{13}C_{Carex}} \quad (5)$$

and

$$f_{Carex} = 1 - f_{SOM} \quad (6)$$

where f_{SOM} and f_{Carex} are the fractions of SOM- and *Carex*-derived CO_2, $\delta^{13}C_{Carex}$ and $\delta^{13}C_{org}$ are $\delta^{13}C$ values of the added *Carex* material and of SOC, and $\delta^{13}C_{CO_2}$ are the measured isotopic signatures of CO_2 inside each bottle. The same samples were also incubated for the temperature sensitivity experiment without *Carex* addition and thus served as a control group for quantifying the priming effect. In control samples, all CO_2 is SOM-derived. The relative priming effect (PE%) was then calculated as

$$PE\% = \frac{aSOM\ CO_2 - cSOM\ CO_2}{cSOM\ CO_2} \times 100\% \quad (7)$$

where $aSOM\ CO_2$ and $cSOM\ CO_2$ are the amounts of SOM-derived CO_2 in amended and control samples, respectively.

4.3.4 Climatic controls on soil organic matter decomposability

To examine the influence of climatic and environmental conditions during OM deposition on SOM characteristics and future GHG production potentials, age-diverse sediments from Muostakh Island (MUO12, Table 11), the Buor Khaya Peninsula (BK8, Table 12), and Bol'shoy Lyakhovsky (L14,Table 13,Table 14) were used. Based on ages and stratigraphical correlation, the sediments were pooled into six age periods; (1) the recent active layer, (2) the late glacial-early Holocene transition (LGT-MIS1), (3) the late Weichselian stadial (Sartan, MIS2), the middle Weichselian interstadial (Kargin, MIS3), (4) the early Weichselian stadial (Zyryan, MIS4), (5) the Eemian interglacial (Kazantsevo, MIS5), and (6) the Saalian glacial (Taz, MIS7). Only MIS1 and MIS3 deposits are preserved at all three study sites. MIS2 deposits were only available from Muostakh Island and Bol'shoy Lyakhovsky, and MIS5 and MIS7 deposits were only available from Bol'shoy Lyakhovsky.

All samples were aerobically and anaerobically incubated in generally three replicates at a constant temperature of 4 °C. The lengths of the incubation period varied between 134 days for samples from Muostakh Island and outcrop samples from Bol'shoy Lyakhovsky, 444 days for cores from Bol'shoy Lyakhovsky, and 903 days for samples from the Buor Khaya Peninsula.

4.4 Statistics

Prior to statistical testing, data were log transformed to meet the assumption of normally distributed data (Shapiro-Wilk test) with homogeneity (Levene's test). One-way analysis of variance (ANOVA) followed by Tukey's honest significant difference test were used to analyze the effect of soil depth, incubation temperature, and age on SOM decomposition. Two-sided t-test was used to test for the effect of freezing and thawing as well as substrate addition on SOM decomposition. Propagation of error theory was used to estimate uncertainties for freeze-thaw effects, Q_{10} values, and priming effects. Pearson's correlation was used to characterize the relationship between soil and sediment characteristics and SOM decomposition. All statistical analyses were performed using MATLAB® (MATLAB and Statistics Toolbox Release 2014b, The MathWorks Inc., Natick, MA, USA).

5 Results

5.1 Soils of Bol'shoy Lyakhovsky

Soils of the different landscape units on the southern coast of Bol'shoy Lyakhovsky were sampled (Figure 10). Five characteristic soil profiles are described in more detail below.

The first soil on the Yedoma hill (Profile Y1, Table 3) was classified as *Turbic Cryosol (Humic, Gleyic)*. The **Ah** horizon (0–5 cm bs) was clearly separated from the underlying horizons by its dark color (Munsell 10YR1/2) and high accumulation of OM. Below the **Ah** horizon, the soil was cryoturbated and exhibited gleyic properties. Mottling started to dominate the layers below 35 cm.

A transect of five soil pits was dug across the thermo-terrace. The five soil profiles (Profiles TT1.1–TT1.5) varied only slightly with regard to thaw depth (45–60 cm, August 2014), %SOC, (~2.5 wt% in topsoil, ~1.9 wt% in subsoil), C/N (10.0–11.6), and pH (5.7–6.9) and all exhibited signs of cryoturbation and gleyic properties (Profile TT1.2, Table 4). They were all classified as *Turbic Cryosol (Humic, Gleyic)*.

A second transect of five soil pits was dug from the edge of the IC wall along a thermo-erosional valley. The first four soil profiles (Profiles EY1.1–EY1.4) were similar to the soils of the thermo-terrace with strong signs of cryoturbation and clear indications of reductimorphic properties. They were classified as *Turbic Cryosol (Humic, Gleyic)*. The last sampling point (Profile EY1.5, Table 5), however, was located in the main erosional valley, which drains the Yedoma hill. The water-saturated conditions favored the formation of an **H** horizon above the bluish-grey mineral horizon. This soil was classified as *Rheic Fibric Cryic Histosol (Calcic)*.

The alas was sampled at two contrasting locations. The first location (Profile A1, Table 6) was in the center of a high-centered polygon. The thaw depth was only 13 cm (11 August 2014) but the organic **O** horizon was clearly separated from the cryoturbated soil layers below. However, since the **O** horizon was only 3 cm thick, this soil was also classified as *Turbic Cryosol (Humic, Gleyic)*. The second Alas location (Profile A2, Table 7) was located in a water-saturated low-centered polygon. The 15 cm thick **H** horizon consisted of moderately decomposed moss and was underlain by an organic rich (7.7 wt% SOC) mineral layer. This soil was classified as *Rheic Fibric Cryic Histosol*.

Table 3: Soil profile Y1 with selected soil properties (depth in cm below surafce (bs), soil organic carbon (SOC) content in weight percent (wt%), carbon to nitrogen ratios (C/N), isotopic signature of SOC ($\delta^{13}C_{org}$) in per mil relative to the Vienna Pee Dee Belemnite standard (‰VPDB) and pH) and classification according to international (IUSS Working Group WRB, 2014) and Russian soil classification systems (Gerasimova, 2001). The enlarged view framed by the red box shows organic matter that was reworked into lower horizons through cryoturbation.

Horizon	Depth cm bs	SOC wt%	C/N	$\delta^{13}C_{org}$ ‰VPDB	pH	Munsell color
Ah	0–5	3.7	10.5	-27.5	6.9	10YR1/2
ABg@	5–50	2.6	9.4	-27.7	7.1	7.5YR4/3
Bg@	50–55	1.3	9.0	-28.2	7.7	2.5Y6/2 and 7.5YR4/6
Bf	>55	-	-	-	-	-

Turbic Cryosol (Humic, Gleyic)

CR-tu-hu--gl

Russian classification: Raw-humus gleyic Cryozem

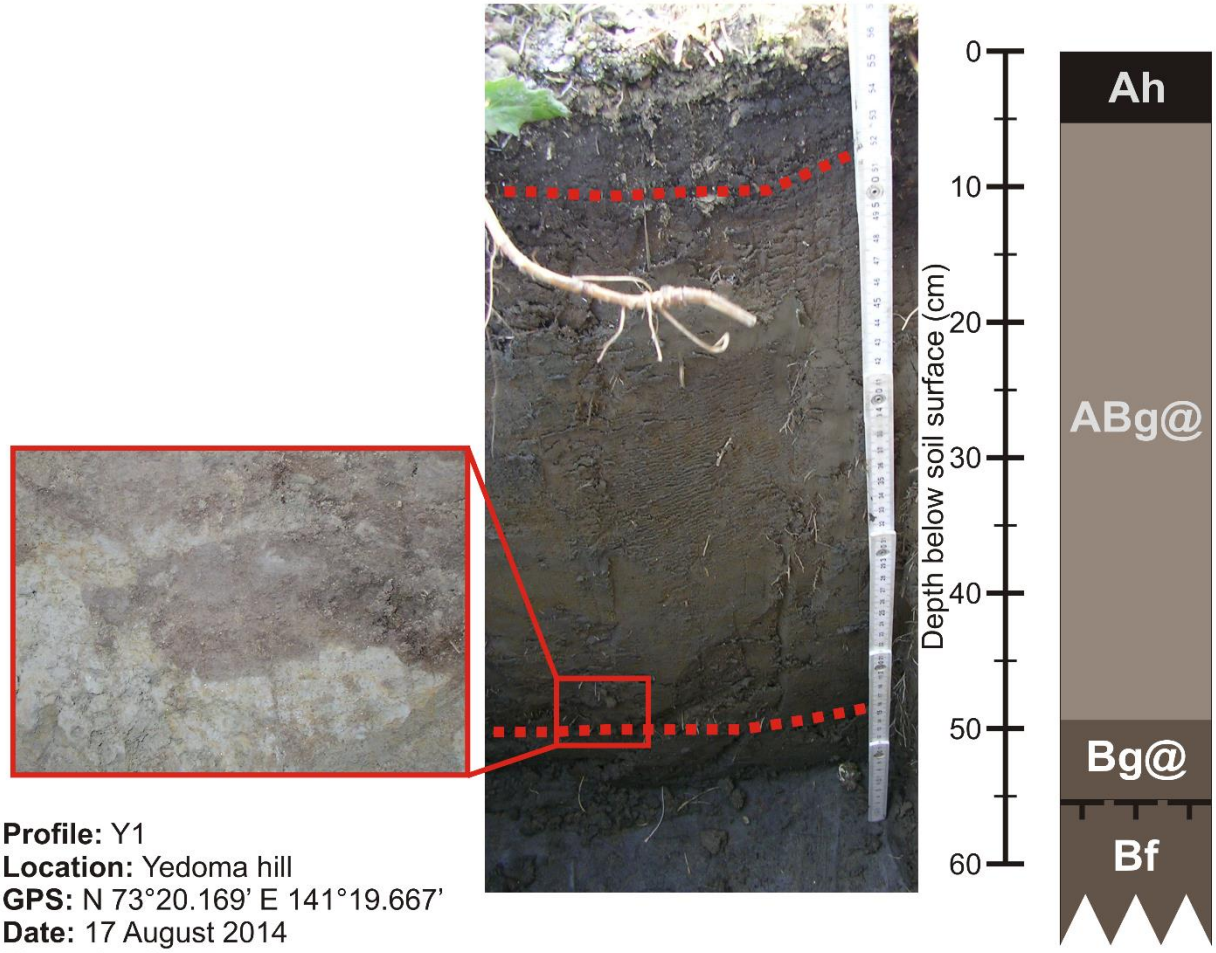

Profile: Y1
Location: Yedoma hill
GPS: N 73°20.169' E 141°19.667'
Date: 17 August 2014
Thaw depth: 55 cm
Description:
A cryoturbated soil with a thin topsoil layer enriched in organic matter (Ah) overlying mineral subsoil with distinct mottling. The transitional horizon (AB) is marked by brownish color with greyish mottles, gleyic (g) properties, and strong signs of cryoturbation (@). The lower B horizon is marked by greyish color with distinct brownish-orange mottles and gleyic properties. Below 55 cm, the soil was frozen (f).

Table 4: Soil profile TT1.2 with selected soil properties (depth in cm below surafce (bs), soil organic carbon (SOC) content in weight percent (wt%), carbon to nitrogen ratios (C/N), isotopic signature of SOC ($\delta^{13}C_{org}$) in per mil relative to the Vienna Pee Dee Belemnite standard (‰VPDB) and pH) and classification according to international (IUSS Working Group WRB, 2014) and Russian soil classification systems (Gerasimova, 2001). The enlarged section in the red box shows cryoturbated organic matter (encircled by dotted line) and mottling along roots (encircled by solid line).

Horizon	Depth cm bs	SOC wt%	C/N	$\delta^{13}C_{org}$ ‰VPDB	pH	Munsell color
Ah	0–20	2.5	10.2	-26.5	5.6	7.5YR4/3
Bg@1	20–42	1.6	11.4	-26.2	5.7	2.5Y6/2 and 7.5YR4/6
Bg@2	42–50	1.5	11.5	-26.8	5.9	2.5Y6/2 and 7.5YR4/6
Bf	>50	-	-	-	-	-

Turbic Cryosol (Humic, Gleyic)

CR-tu-hu--gl

Russian classification: Typic Cryozem

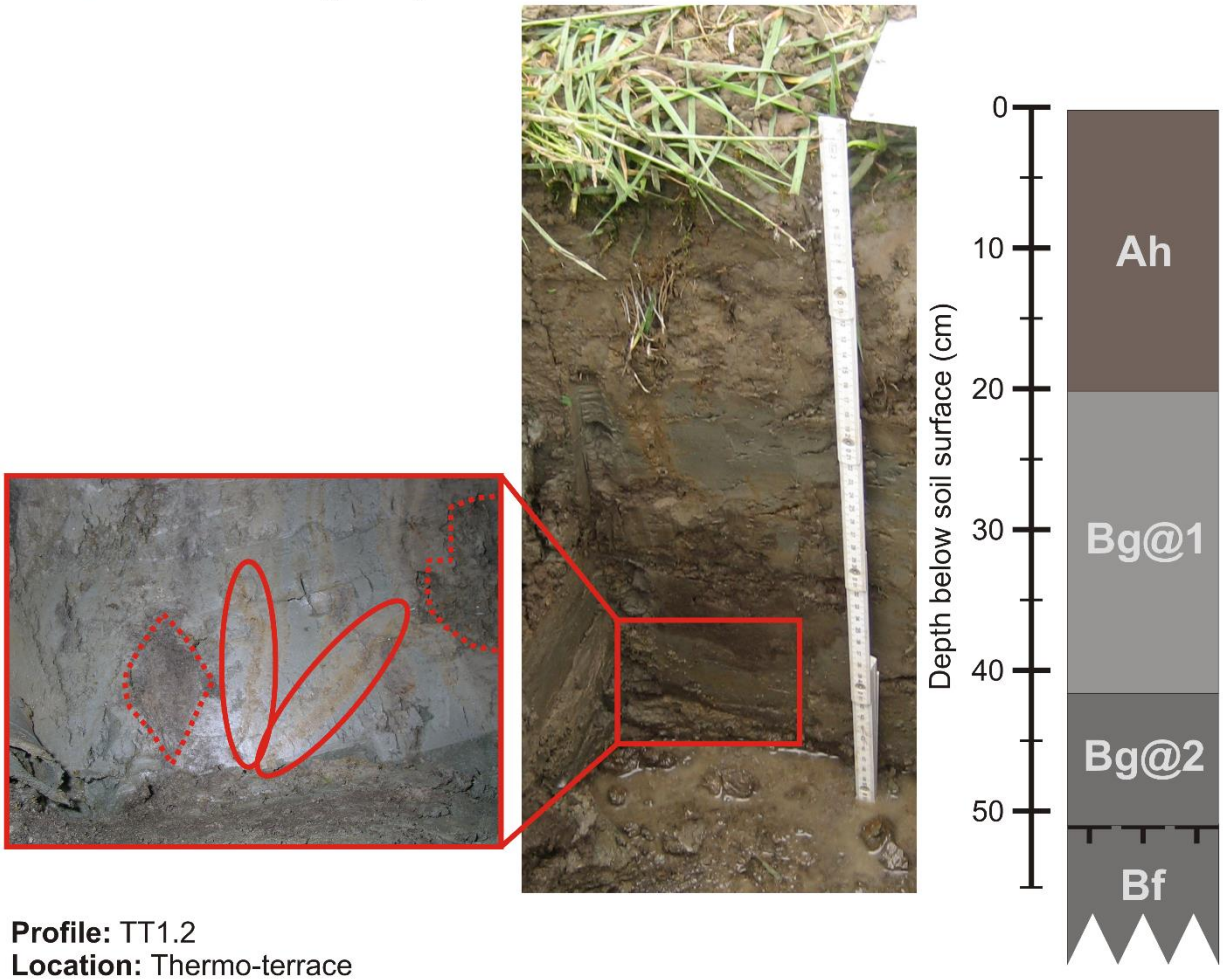

Profile: TT1.2
Location: Thermo-terrace
GPS: N 73°20.147' E 141°19.651'
Date: 02 August 2014
Thaw depth: 50 cm
Description:
The brownish Ah horizon is underlain by a cryoturbated (@) B horizon with strong reductimorphic and gleyic (g) properties. Oxidative properties, here evident as orange mottles, mainly occur along roots. Below 50 cm, the soil was frozen (f).

Table 5: Soil profile EY1.5 with selected soil properties (depth in cm below surafce (bs), soil organic carbon (SOC) content in weight percent (wt%), carbon to nitrogen ratios (C/N), isotopic signature of SOC ($\delta^{13}C_{org}$) in per mil relative to the Vienna Pee Dee Belemnite standard (‰VPDB) and pH) and classification according to international (IUSS Working Group WRB, 2014) and Russian soil classification systems (Gerasimova, 2001).

Horizon	Depth cm bs	SOC wt%	C/N	$\delta^{13}C_{org}$ ‰VPDB	pH	Munsell color
Hi	0–6	21.1	16.3	-27.1	5.3	5YR3/4
He	6–18	18.2	14.5	-31.3	5.6	10YR4/3
Bkr	18–33	2.2	6.9	-28.3	8.1	Gley 2 5/10B
Bf	>33	-	-	-	-	-

Rheic Fibric Cryic Histosol (Calcic)

Hi-cy.fi.rh-cc

Russian classification: Soddy light-humus soil

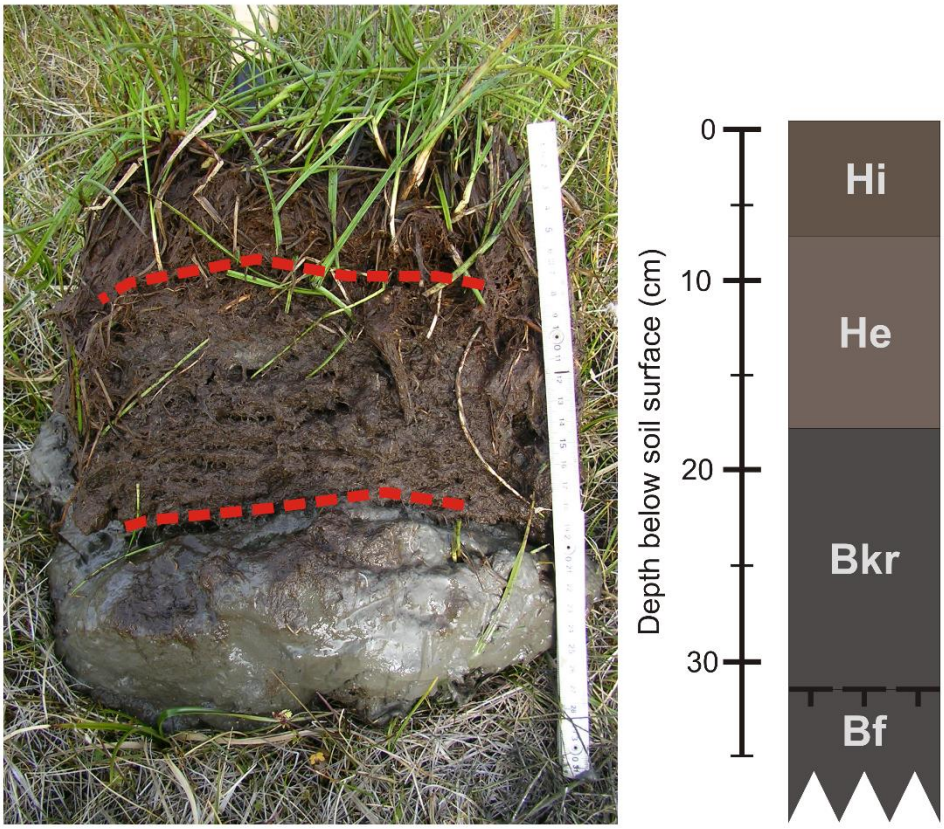

Profile: EY1.5
Location: Erosional valley
GPS: N 73°20.165' E 141°19.959'
Date: 03 August 2014
Thaw depth: 31 cm
Water table: 2 cm below soil surface
Description:
An organic-rich water-saturated soil with a thick organic horizon consisting of slightly (Hi) to moderately (He) decomposed organic material overlying mineral material, enriched in carbonates (Bkr). Below 33 cm, the soil was frozen (f).

Table 6: Soil profile A1 with selected soil properties (depth in cm below surafce (bs), soil organic carbon (SOC) content in weight percent (wt%), carbon to nitrogen ratios (C/N), isotopic signature of SOC ($\delta^{13}C_{org}$) in per mil relative to the Vienna Pee Dee Belemnite standard (‰VPDB) and pH) and classification according to international (IUSS Working Group WRB, 2014) and Russian soil classification systems (Gerasimova, 2001).

Horizon	Depth cm bs	SOC wt%	C/N	$\delta^{13}C_{org}$ ‰VPDB	pH	Munsell color
Oe	0–3	14.6	16.4	-29.5	5.1	-
Ah@	3–8	9.6	14.3	-27.4	5.5	7.5YR2.5/3
Bg@	9–13	2.2	10.7	-29.2	6.5	10YR3/2
Bf	>13	-	-	-	-	-

Turbic Cryosol (Humic, Gleyic)

CR-tu-hu--gl

Russian classification: Gleyic Cryozem

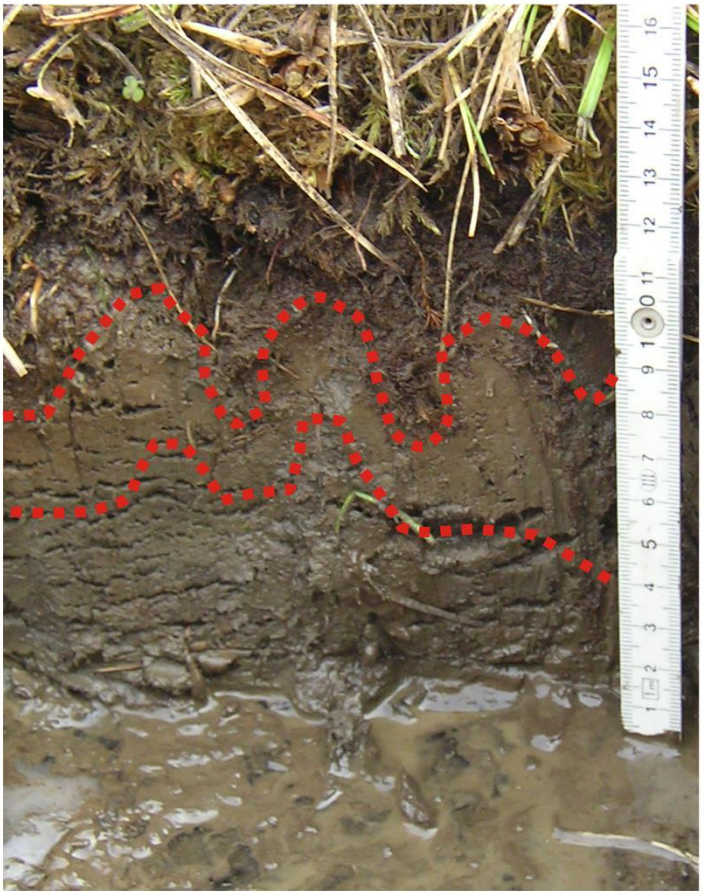

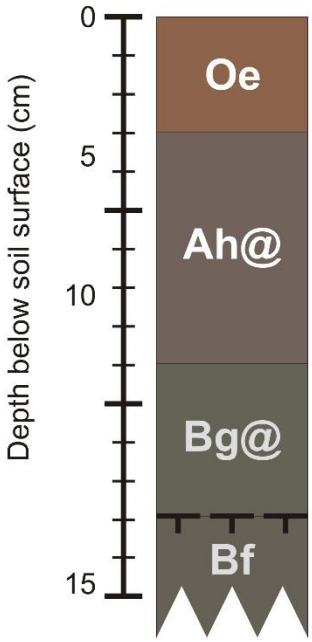

Profile: A1
Location: Alas (high-centered polygon)
GPS: N 73°21.513' E 141°14.806'
Date: 11 August 2014
Thaw depth: 13 cm
Description:
A cryoturbated permafrost-affected soil with a thin organic horizon with moderately decomposed organic material (Oe) overlying two croyturbated (@) mineral horizons with an accumulation of organic matter in the top layer (Ah) and gleyic properties below (Bg). Below 13 cm, the soil was frozen (f).

Table 7: Soil profile A2 with selected soil properties (depth in cm below surafce (bs), soil organic carbon (SOC) content in weight percent (wt%), carbon to nitrogen ratios (C/N), isotopic signature of SOC ($\delta^{13}C_{org}$) in per mil relative to the Vienna Pee Dee Belemnite standard (‰VPDB) and pH) and classification according to international (IUSS Working Group WRB, 2014) and Russian soil classification systems (Gerasimova, 2001).

Horizon	Depth cm bs	SOC wt%	C/N	$\delta^{13}C_{org}$ ‰VPDB	pH	Munsell color
Hi	0–15	37.0	16.7	-29.3	5.1	10YR4/3
Ahr	15–31	7.7	15.3	-25.7	5.7	10YR3/2
Bf	>31	-	-	-	-	-

Rheic Fibric Cryic Histosol

HS-cy.fi.rh

Russian classification: Raw-humus Gleyzem

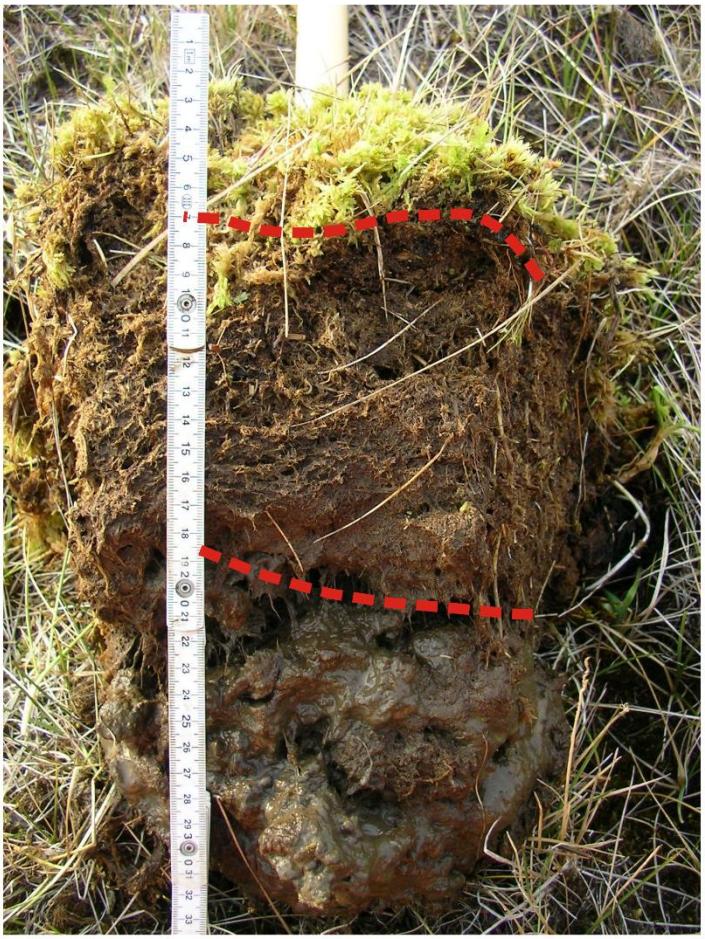

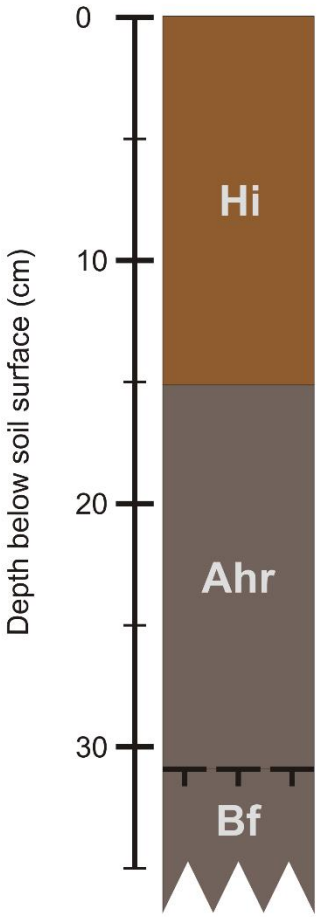

Profile: A2
Location: Alas (low-centered polygon)
GPS: N 73°20.865' E 141°15.525'
Date: 11 August 2014
Thaw depth: 31 cm
Water table: 3 cm below soil surface
Description:
A organic-rich water-saturated soil with a thick organic horizon consisting moderately decomposed moos (Hi) overlying mineral horizons with high amounts of organic matter and reducing conditions (Ahr). Below 31 cm, the soil was frozen (f).

5.2 Near-surface processes

5.2.1 Soil characteristics

Frozen soil cores from Samoylov and Kurungnakh in the Lena River Delta were divided into four soil layers: (1) the surface active layer (0–11 cm) including relatively undecomposed plant material, (2) the bottom active layer (11–41 cm), both thawing every year, (3) the transition zone (41–60 cm), which only thaws in some years, and (4) permafrost (>60 cm), presumably not thawed for several decades to centuries. Cores were further subdivided into depth increments of approximately 10 cm, resulting in a total of nine subsamples per core: one from the surface active layer, three from the bottom active layer, two from the transition zone, and three from the permafrost. However, not all subsamples were used for further analysis. All investigated soil layers are mineral soils and were classified (IUSS Working Group WRB, 2014) as *Reductaquic Cryosol (Hyperhumic)*, with intermediate to high SOC contents (4.1–18.7 wt%, Table 8, Table 9), a wide range in C/N ratios (21–40), and strongly acidic to neutral pH values (5.4–6.7). $\delta^{13}C_{org}$ ranged between -28.7‰VPDB and -25.3‰VPDB. Generally, SOC contents were highest in the surface layers and decreased with depth, while $\delta^{13}C_{org}$ values were lowest in the surface layers and highest in the deeper layers.

Table 8: Soil characteristics and treatments for Kurungnakh samples with depth in cm below surface (bs), soil organic carbon (SOC) content in weight percent (wt%), carbon to nitrogen ratios (C/N), isotopic signature of SOC ($\delta^{13}C_{org}$) in per mil relative to the Vienna Pee Dee Belemnite standard (‰VPDB) and pH.

Layer	Depth			Treatment[a)]	SOC	C/N	$\delta^{13}C_{oc}$	pH
	upper	lower	mean					
	cm bs				wt%		‰VPDB	
Active layer	20	30	25	Ae, T, Pr	8.3	14.3	-28.4	5.28
Permafrost	80	90	85	Ae, T, Pr	4.7	16.5	-24.3	6.28

a) Ae=aerobic, FT=freeze-thaw, T=temperature, Pr=priming

Table 9: Soil characteristics and treatments for Samoylov samples with depth in cm below surface (bs), soil organic carbon (SOC) content in weight percent (wt%), carbon to nitrogen ratios (C/N), isotopic signature of SOC ($\delta^{13}C_{org}$) in per mil relative to the Vienna Pee Dee Belemnite standard (‰VPDB) and pH

Layer	Depth			Treatment[a)]	SOC	C/N	$\delta^{13}C_{org}$	pH
	upper	lower	mean					
	cm bs				wt%		‰VPDB	
Polygon 1, 72° 22.5' N, 126° 29.3' E								
Surface active layer	0	11	5.5	Ae, An, FT	14.6	27.5	-28.7	5.63
Bottom active layer	11	22	16.5	Ae, An	10.0	36.4	-27.9	5.91
Bottom active layer	22	32	27.0	Ae, An, FT	4.1	25.0	-27.5	6.40
Bottom active layer	32	42	37.0	Ae, An	8.1	29.3	-26.3	6.66
Transition zone	42	51	46.5	Ae, An	5.9	27.4	-26.4	6.44
Transition zone	51	59	55.0	Ae, An	6.7	31.9	-26.3	6.31
Permafrost	59	67	63.0	Ae, An	6.5	30.7	-26.9	6.13
Permafrost	67	74	70.5	Ae, An	7.3	29.0	-26.0	6.15
Permafrost	74	82	78.0	Ae, An, FT	10.1	29.0	-26.5	6.21
Polygon 2, 72° 22.3' N, 126° 29.9' E								
Surface active layer	0	11	5.5	Ae, An, FT	13.7	31.5	-28.1	6.28
Bottom active layer	11	22	16.5	Ae, An	9.9	29.6	-27.3	5.36
Bottom active layer	22	32	27.0	Ae, An, FT	8.7	28.6	-27.4	5.50
Bottom active layer	32	42	37.0	Ae, An	10.6	28.2	-26.4	5.69
Transition zone	42	51	46.5	Ae, An	17.7	32.7	-25.3	5.64
Transition zone	51	61	56.0	Ae, An	10.7	31.4	-26.0	5.62
Permafrost	61	68	64.5	Ae, An	5.5	23.4	-26.6	5.61
Permafrost	68	77	72.5	Ae, An	13.7	31.8	-26.5	5.41
Permafrost	77	86	81.5	Ae, An, FT	8.4	20.5	-26.1	5.37
Polygon 3, 72° 22.5' N, 126° 29.4' E								
Surface active layer	0	10	5.0	Ae, T, Pr	11.0	40.3	-27.4	6.02
Bottom active layer	20	30	15.0	Ae, T, Pr	5.2	23.6	-25.4	6.53
Permafrost	70	80	75.0	Ae, T, Pr	11.5	21.3	-26.3	6.45

a) Ae=aerobic, An=anaerobic, FT=freeze-thaw, T=temperature, Pr=priming

5.2.2 Aerobic and anaerobic decomposition processes

For the two investigated soils from Samoylov (Polygons 1 and 2), the highest production per gram soil (g^{-1}) was observed in the surface active layer, where between 9.5–10.5 mg CO_2-C g^{-1} were aerobically produced (Figure 14). This was significantly more (ANOVA, p<0.001) than in deeper layers. Total aerobic C production in the bottom active layer, transition zone, and permafrost ranged between 0.7–2.5 mg CO_2-C g^{-1}, but did not differ significantly between the layers (ANOVA, p>0.05). Anaerobically, 22–50% less SOM was decomposed to CO_2 and CH_4 than under aerobic conditions, but the depth pattern was similar under both aerobic and anaerobic conditions. In the surface active layer, 3.2–4.6 mg CO_2-C g^{-1} and 3.2–4.5 mg CH_4-C g^{-1} were anaerobically produced, which was also significantly more (ANOVA, p<0.001) than in deeper layers. Total anaerobic C production in the bottom active layer, transition zone, and permafrost ranged between 0.3–1.4 mg CO_2-C g^{-1} and 0.1–1.2 mg CH_4-C g^{-1}. The total amount of C produced after

1059 incubation days at 4 °C was positively correlated with %SOC and %N and negatively correlated with $\delta^{13}C_{org}$ (Table 10). Aerobic CO_2 production also correlated with C/N.

To highlight qualitative differences in the SOM available for microbial decomposition, C production was normalized to %SOC (g^{-1} SOC). Aerobically, 23–47% more SOM was decomposed than anaerobically. The highest decomposability was again observed in the surface active layer, where after 1059 days 65.1–77.0 mg CO_2-C g^{-1} SOC were produced aerobically and 23.5–31.6 mg CO_2-C g^{-1} SOC and 23.8–31.2 mg CH_4-C g^{-1} SOC were produced anaerobically (Figure 15). The decomposability of the bottom active layer, transition zone, and permafrost did not differ significantly (ANOVA, p>0.05) under both aerobic and anaerobic conditions. In the deeper soil layers, 11.3–25.0 mg CO_2-C g^{-1} SOC were aerobically produced and 2.5–13.5 mg CO_2-C g^{-1} SOC and 1.6–12.3 mg CH_4-C g^{-1} SOC were produced anaerobically.

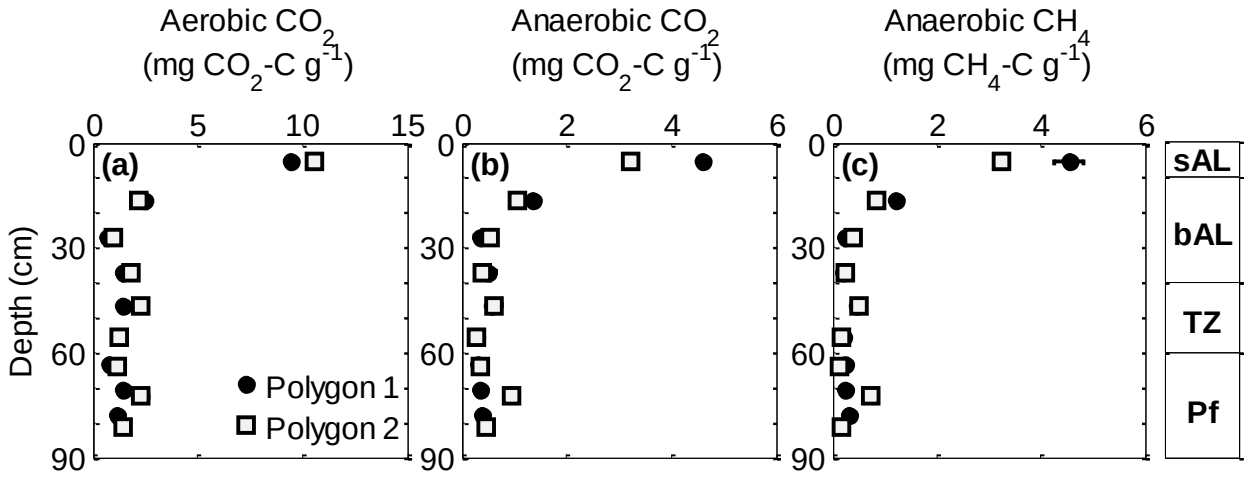

Figure 14: Samoylov: Depth profiles of total CO_2 and CH_4 production per gram dry soil (g^{-1}) after 1059 incubation days at 4 °C under aerobic (a) and anaerobic (b, c) conditions in the surface active layer (sAL), bottom active layer (bAL), transition zone (TZ), and permafrost (Pf) of Polygons 1 and 2. Data are mean values (n = 3) and error bars represent one standard deviation. Note the different scale in panel (a).

Table 10: Samoylov: Correlation matrix for total C production in Polygon 1 and 2 (log transformed) after 1059 incubation days at 4 °C for the two investigated polygons from Samoylov.

		%SOC	%N	C/N	$\delta^{13}C_{org}$	pH
log(aerobic CO_2-C g^{-1})	*r*	0.68	0.66	0.33	0.49	0.09
	p	0.000	0.000	0.021	0.000	0.535
log(anaerobic CO_2-C g^{-1})	*r*	0.60	0.61	0.18	0.77	0.22
	p	0.000	0.000	0.277	0.000	0.185
log(anaerobic CH_4-C g^{-1})	*r*	0.61	0.57	0.30	0.77	0.20
	p	0.000	0.000	0.063	0.000	0.218

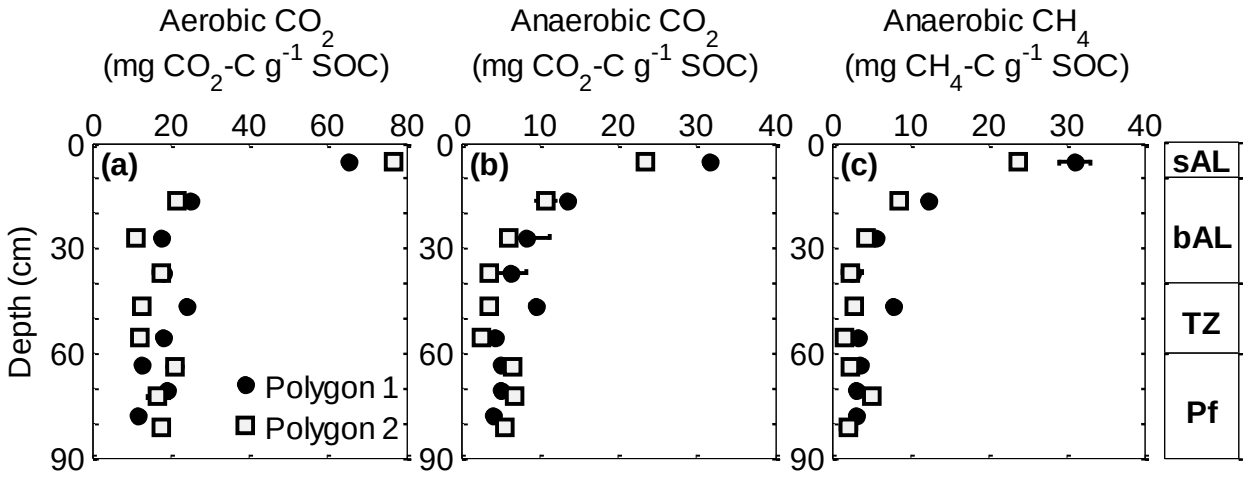

Figure 15: Samoylov: Depth profiles of total CO_2 and CH_4 production per gram soil organic carbon (g^{-1} SOC) after 1059 incubation days at 4 °C under aerobic (a) and anaerobic (b, c) conditions in the surface active layer (sAL), bottom active layer (bAL), transition zone (TZ), and permafrost (Pf) of Polygons 1 and 2. Data are mean values (*n* = 3) and error bars represent one standard deviation. Note the different scale in panel (a).

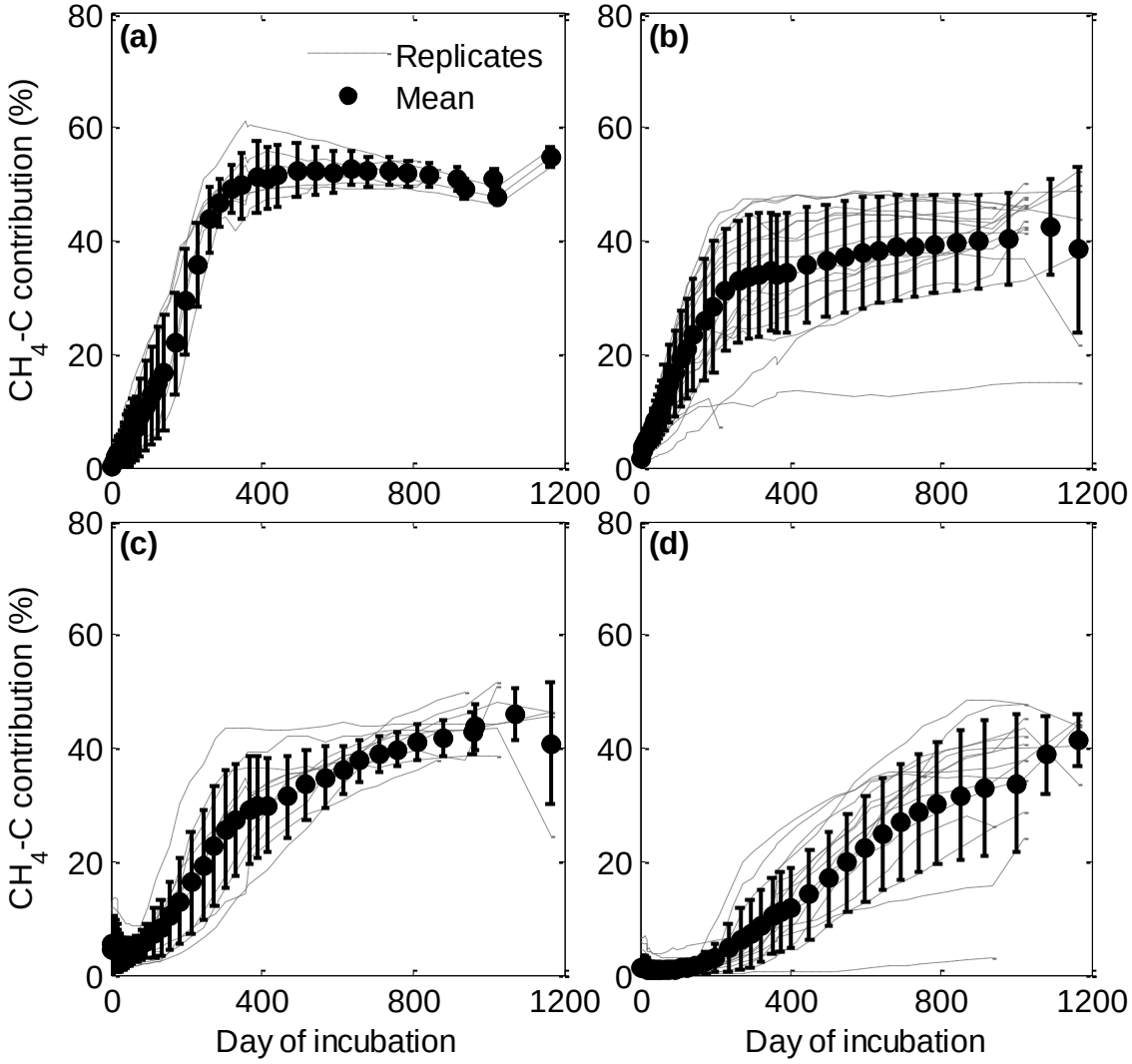

Figure 16: Samoylov: Contribution of CH_4-C to total anaerobic C release over 1059 incubation days at 4 °C for the surface (a) and bottom active layer (b), transition zone (c), and permafrost (d) in Polygons 1 and 2. Data are mean values (surface active layer *n* = 6; bottom active layer *n* = 24; transition zone *n* = 12; permafrost *n* = 18) and error bars represent one standard deviation.

After 1059 incubation days, the amount of anaerobically produced CO_2 and CH_4 did not differ significantly (t-test, $p>0.05$) from each other, except in permafrost, where significantly more (t-test, $p<0.001$) CO_2 than CH_4 was produced. Overall, CH_4 contributed 41 ± 13% to the total anaerobic C production (Figure 16). However, while CO_2 production rates were highest during the initial incubation (0–30 incubation days) and decreased sharply afterwards, methanogenesis was initiated after a lag phase of several days (active layer) to months (permafrost). CH_4 production rates were generally lowest in the beginning of the incubation and increased with incubation time (Figure 17). Maximum CH_4 production rates where reached after 568 ± 332 days. The lag phase was generally shorter in the surface active layer (308 ± 37 days) than in permafrost (803 ± 193 days). In contrast, maximum aerobic and anaerobic CO_2 production rates were reached after 12 ± 4 days and 14 ± 9 days, respectively.

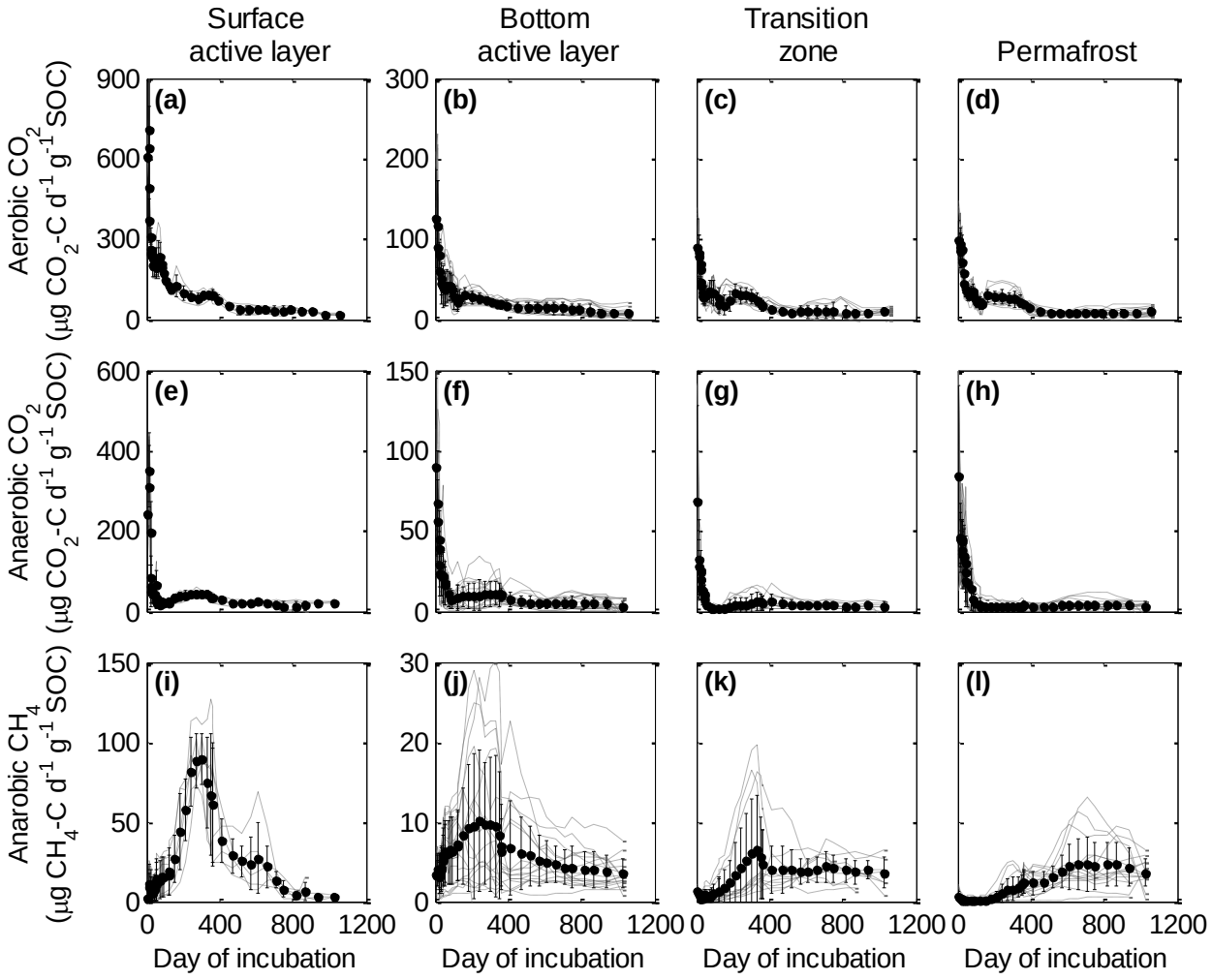

Figure 17: Samoylov: Cumulative aerobic CO_2 (a–d), anaerobic CO_2 (e–h), and anaerobic CH_4 (i–l) production rates per day (d^{-1}) and gram soil organic carbon (g^{-1} SOC) over 1059 incubation days at 4 °C for the surface (a, e, i) and bottom active layer (b, f, j), transition zone (c, g, k), and permafrost (d, h, l) of Polygons 1 and 2. Error bars represent one standard deviation from the mean (surface active layer *n* = 6; bottom active layer *n* = 24; transition zone *n* = 12; permafrost *n* = 18). Note the different scales for aerobic and anaerobic production rates and for the surface active layer.

At the beginning of the incubation, anaerobic CO_2 production rates exceeded CH_4 production rates by a factor of >1000 (Figure 18). Over the course of the 1059-day incubation period, the production ratio approached 1:1. The increasing contribution of CH_4 with time combined with the higher warming potential of CH_4 resulted in a shift of a greater net warming effect of aerobic C production (RCF>1) at the beginning of the incubation to a greater net warming effect of anaerobic C production (RCF<1). In the active layer, anaerobic decomposition processes dominated the relative climate forcing after about 120 incubation days, while in permafrost anaerobic decomposition processes dominated only after 550 incubation days (Figure 19).

Because no significant differences in the SOM decomposability was observed between the bottom active layer, transition zone, and permafrost, the following experiments only concentrated on the different response of the seasonally thawed active layer and perennially frozen permafrost. The subdivision of the surface and bottom active layer, however, was kept, because decomposition in the surface layer was 2–4 times higher than in deeper soil layers and thus represents the main GHG production zone in permafrost-affected soils.

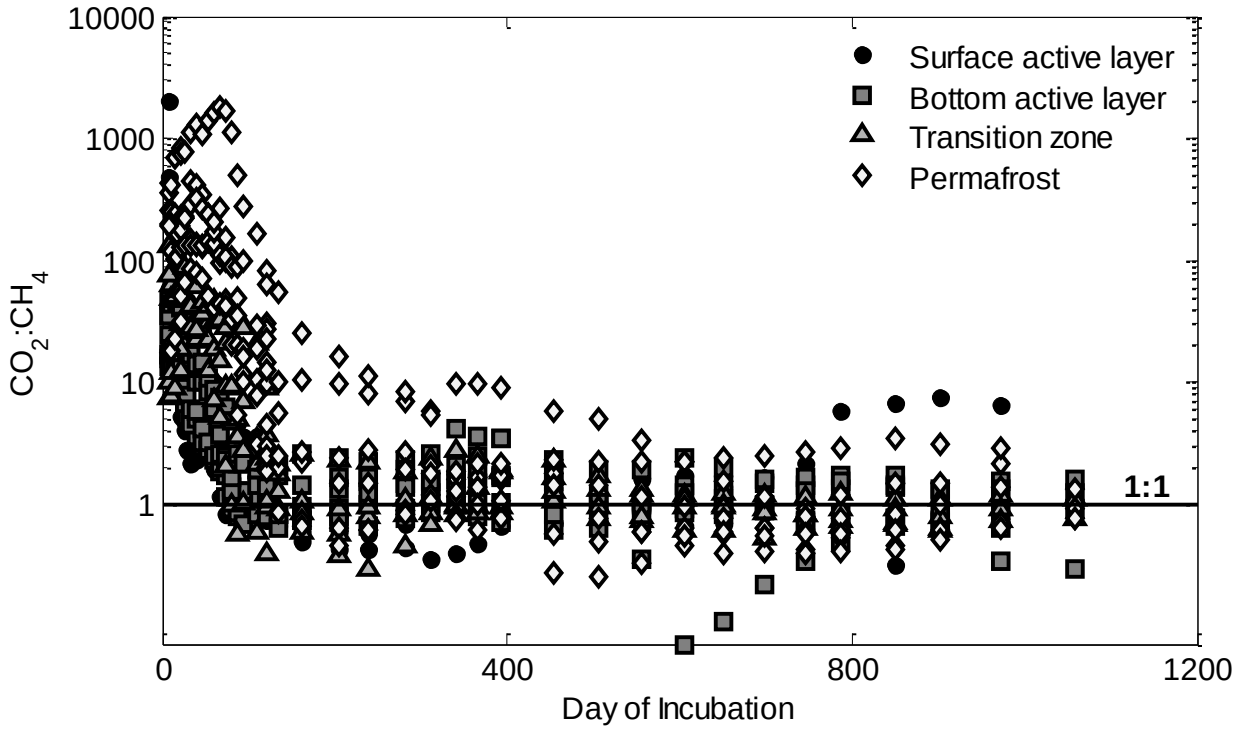

Figure 18: Samoylov: Anaerobic CO_2:CH_4 production rate ratio over 1059 incubation days at 4 °C for the surface and bottom active layer, transition zone, and permafrost of Polygons 1 and 2. Data are measurements in each anaerobic replicate (surface active layer *n* = 6; bottom active layer *n* = 24; transition zone *n* = 12; permafrost *n* = 18). Note the logarithmic y-axis.

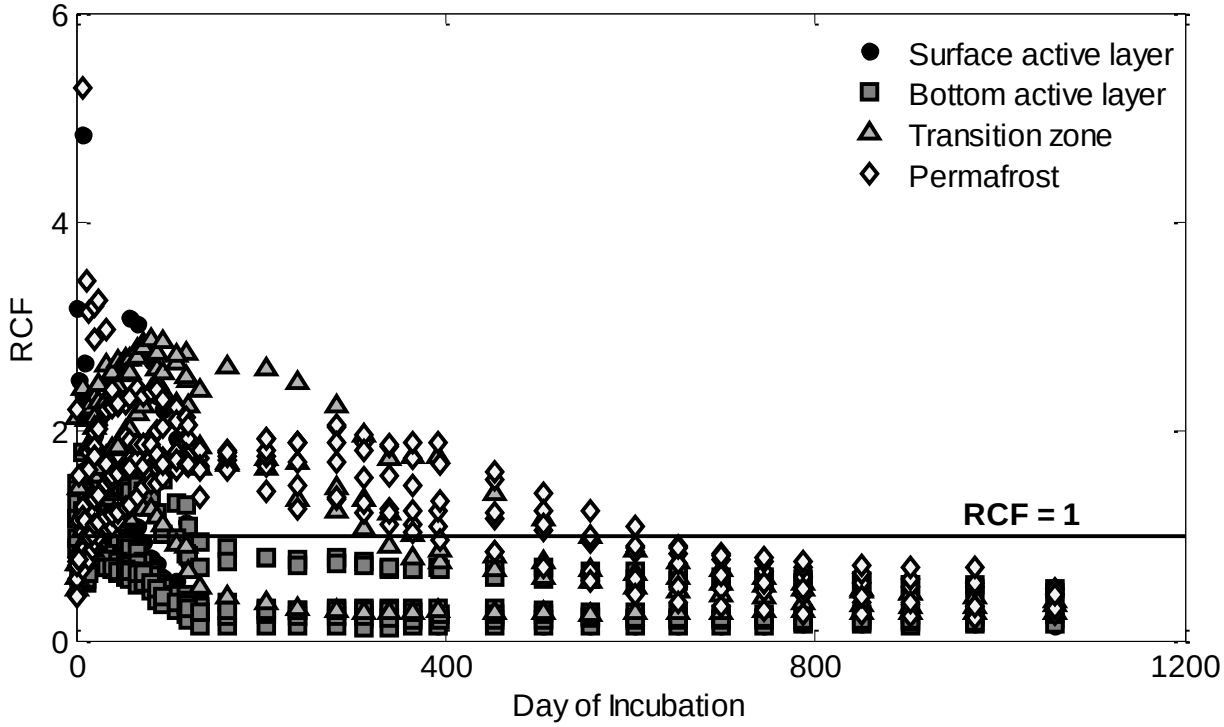

Figure 19: Samoylov: Relative climate forcing (RCF) over 1059 incubation days at 4 °C for the surface and bottom active layer, transition zone, and permafrost of Polygons 1 and 2. Data are mean (*n* = 3) of C production in aerobic and anaerobic incubations for each of the nine respective depth increments for the two investigated polygons.

5.2.3 Freeze-thaw effects

Both aerobic and anaerobic CO_2 production rates in the surface active layer, the bottom active layer, and the permafrost were highest at the beginning of the incubations and declined sharply within the first 7–10 days (Figure 20). Production rates in the control and the freeze-thaw replicates did not differ significantly at the end of the first 30-day period. During the 7-day freezing period at -18 °C the concentration of CO_2 and CH_4 inside the headspace of freeze-thaw samples did not increase. Aerobic and anaerobic CO_2 production rates in the control samples remained constant between 30–60 incubation days, but CO_2 production rates in the freeze-thaw samples of the surface and bottom active layer increased after re-thawing and remained significantly higher (t-test, $p<0.05$) for up to 14 days after re-thawing. By the end of the 60-day incubation period at 4 °C, rates between freeze-thaw and the control group were again not significantly different. After 60 days at 4 °C, freeze-thaw samples from the surface active layer had produced 23.3 ± 6.7% more CO_2 aerobically (t-test, $p<0.01$) and 28.0 ± 10% more CO_2 anaerobically (t-test, $p<0.001$) than control incubations. The bottom active layer produced 24.7 ± 5.5% more CO_2 aerobically and 20.4 ± 4.5% more CO_2 anaerobically (t-test, $p<0.01$) (Figure 21). Within the permafrost, CO_2 production rates only increased in anaerobic samples for about three days after re-thawing (Figure 20f) but the cumulative amount of aerobically as well as anaerobically produced CO_2 after 60 days did not differ significantly (t-test, $p>0.05$) between the two treatments (Figure 21b). Methanogenesis only occurred in surface and bottom active layer samples and rates increased with time (Figure 21g, h). Neither the CH_4 production rates nor the amount of CH_4 produced after

60 days differed significantly (t-test, p>0.05) between control and freeze-thaw treatments (Figure 21c). No CH_4 was produced in any permafrost samples with the 60-day incubation period.

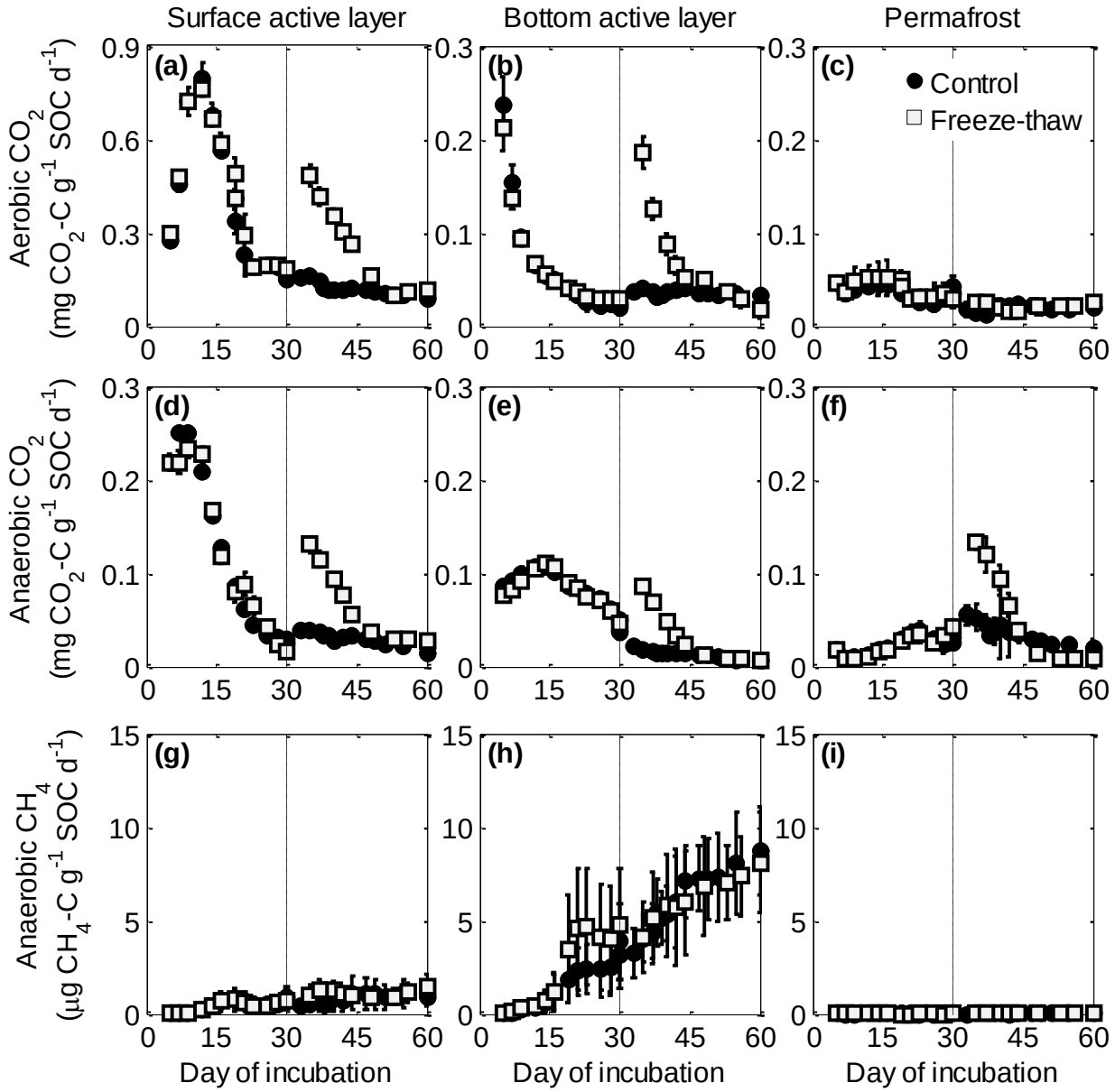

Figure 20: Samoylov: Cumulative CO_2 and CH_4 production rates in control and freeze-thaw incubations under aerobic (a–c) and anaerobic (d–i) conditions for the surface active layer (a, d, g), bottom active layer (b, e, h), and permafrost (c, f, i) of Polygons 1 and 2. Data are mean values (n = 3) and error bars represent one standard deviation. The vertical line separates the two 30-day incubation periods at 4 °C pre- and post-refreezing for the freeze-thaw treatment. Note the different scales and units for CO_2 and CH_4. Note the different scales for CO_2 and CH_4 production rates and for the surface active layer.

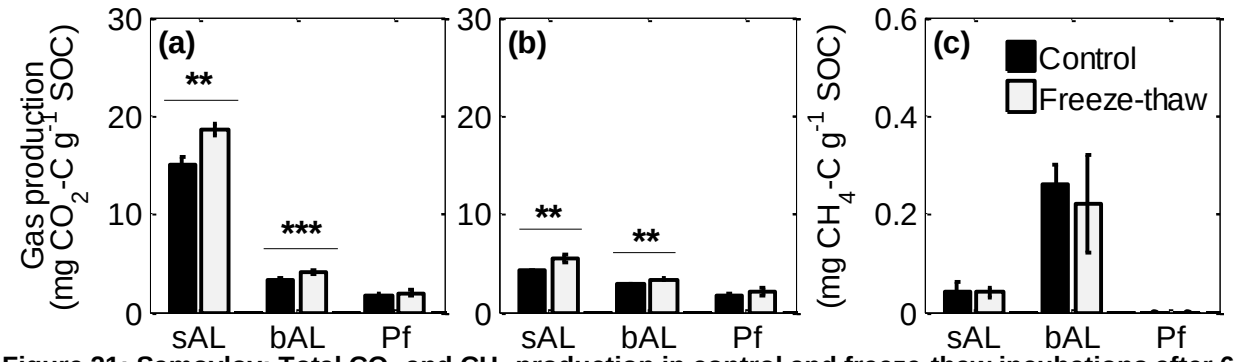

Figure 21: Samoylov: Total CO_2 and CH_4 production in control and freeze-thaw incubations after 60 incubation days at 4 °C under aerobic (a) and anaerobic (b, c) conditions in the surface active layer (sAL), bottom active layer (bAL), permafrost (Pf) of Polygons 1 and 2. Data are mean values (*n* = 3) and error bars represent one standard deviation. Significant differences (t-test) in the total production are indicated by the vertical line and asterisks (*p*<0.01, *** *p*<0.001). Note the different scale in panel (c).**

5.2.4 Temperature sensitivity

Higher temperatures significantly (ANOVA, $p<0.001$) increased CO_2 production in all soil layers from Polygon 3 on Samoylov (Figure 22). After 426 incubation days, aerobic CO_2 production in the surface active layer was 65.9 ± 6.2 mg CO_2-C g^{-1} SOC at an incubation temperature of 1 °C, 106.9 ± 8.3 mg CO_2-C g^{-1} SOC at a temperature of 4 °C, and 143.9 ± 11.1 mg CO_2-C g^{-1} SOC at 8 °C. In the bottom active layer and permafrost, CO_2 production was significantly lower (ANOVA, $p<0.001$) than in the surface active layer. At 1 °C, CO_2 production after 426 incubation days was 14.7 ± 1.3 mg CO_2-C g^{-1} SOC in the bottom active layer and 10.8 ± 0.6 mg CO_2-C g^{-1} SOC in permafrost. At 4 °C production was 19.7 ± 0.8 mg CO_2-C g^{-1} SOC and 15.2 ± 0.8 mg CO_2-C g^{-1} SOC in the bottom active layer and in permafrost, respectively. At 8 °C, production was 28.6 ± 3.6 mg CO_2-C g^{-1} SOC (bottom active layer) and 24.3 ± 1.4 mg CO_2-C g^{-1} SOC (permafrost), respectively.

The temperature sensitivity of SOM decomposition differed between soil layers, especially between seasonally and perennially frozen soil layers (Figure 23). To account for differential depletion of SOC pools at different temperatures, Q_{10} values were calculated via the equal-C method. Q_{10} values were calculated in steps of 0.1% until 1% of the initial SOC was decomposed. This represents the maximum amount that was decomposed in the bottom active layer and permafrost at 1 °C (Figure 22b, c). For the surface active layer, Q_{10} were further calculated in steps of 0.5% until 5.5% of the initial SOC was decomposed, which was the maximum amount decomposed in the surface active layer at 1 °C (Figure 22a).

In all three investigated soil layers, Q_{10} values were lowest for the decomposition of the first 0.1% of SOC. As expected, decomposition was most rapid in the surface active layer, where it took 1.5 ± 0.1 days at 1 °C, 1.2 ± 0.2 days at 4 °C, and 0.9 ± 0.1 days at 8 °C to decompose 0.1% of the initial SOC. In the bottom active layer, it took 5.5 ± 0.4 days (1 °C), 3.7 ± 0.2 days (4 °C), and 2.7 ± 0.3 days (8 °C). In permafrost, it took 11.6 ± 0.3 days (1 °C), 7.8 ± 0.2 days (4 °C), and

2.7 ± 0.3 days (8 °C). Fitting these data to Equation 3 and Equation 4 gave respective Q_{10} values of 2.1 ± 0.8 (surface active layer), 2.8 ± 0.9 (bottom active layer), and 4.2 ± 1.0 (permafrost). Q_{10} values increased with increasing amounts of SOC decomposition, especially in permafrost. To decompose 0.5% of the initial permafrost SOC, it took 126.2 ± 6.3 days (1 °C), 85.4 ± 12.1 days (4 °C), and 36.3 ± 4.8 days (8 °C) and to decompose 1% of the initial permafrost SOC it took 372.2 ± 30.2 days (1 °C), 229.1 ± 19.8 (4 °C), and 89.2 ± 8.1 (8 °C). Permafrost Q_{10} values therefore increased from 6.1 ± 2.8 (0.5%) to 7.8 ± 3.0 (1%).

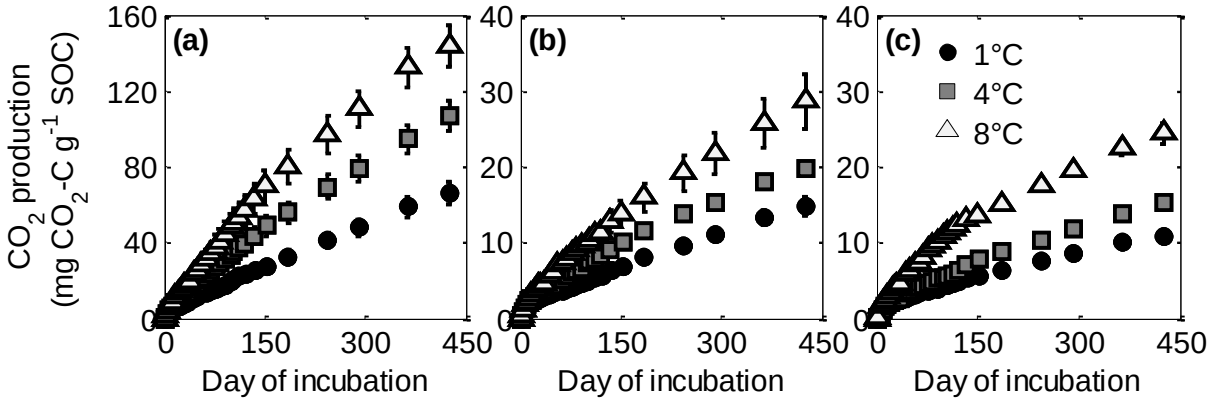

Figure 22: Samoylov: Cumulative aerobic CO_2 production over 426 incubation days at different temperatures in the surface active layer (a), bottom active layer (b), and permafrost (c) of Polygon 3. Data are mean values (*n* = 4) and error bars represent one standard deviation. Note the different scale in (a).

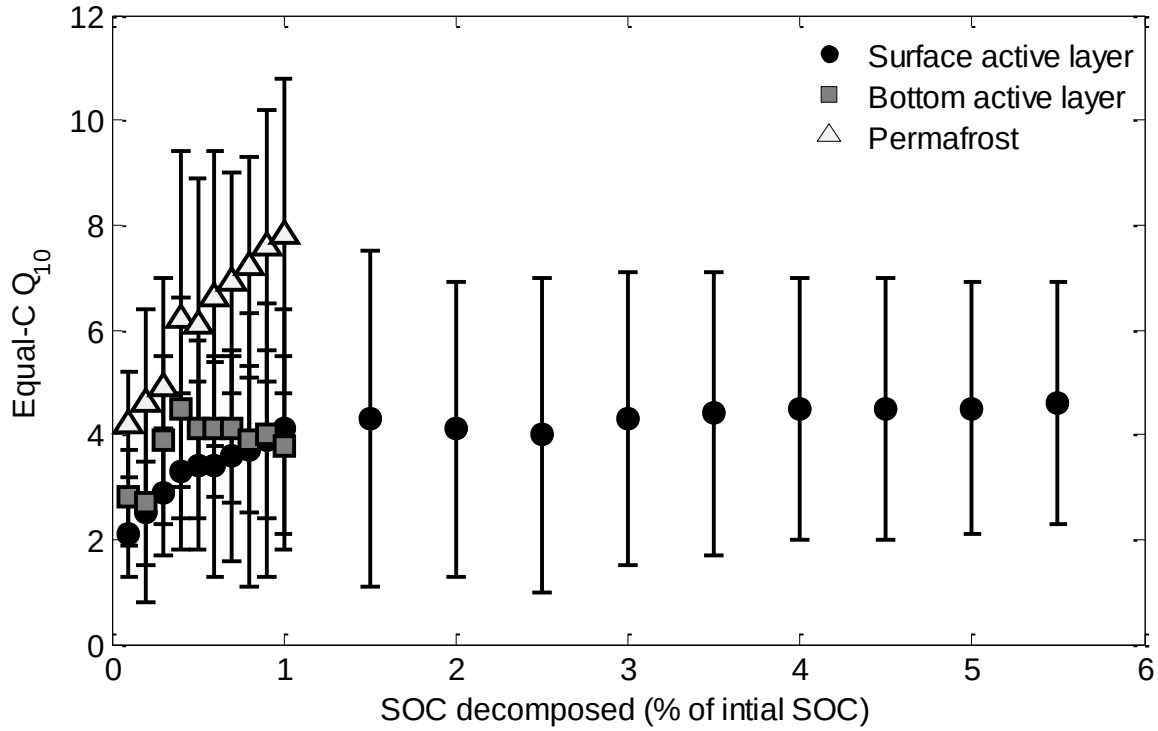

Figure 23: Samoylov: Equal-C Q_{10} values for different soil layers of Polygon 3. Uncertainties for calculated Q_{10} values were obtained by error propagation.

In Kurungnakh samples, higher temperatures also significantly increased aerobic CO_2 production in both the (bottom) active layer and permafrost (Figure 24). After 150 incubation days, CO_2 production in the active layer was 5.1 ± 0.1 mg CO_2-C g^{-1} SOC (1 °C), 6.9 ± 0.3 mg CO_2-C g^{-1} SOC (4 °C), and 10.3 ± 0.4 mg CO_2-C g^{-1} SOC (8 °C). In permafrost, production after 150 incubation days was 9.7 ± 0.3 mg CO_2-C g^{-1} SOC (1 °C), 12.9 ± 0.5 mg CO_2-C g^{-1} SOC (4 °C), and 15.9 ± 0.9 mg CO_2-C g^{-1} SOC (8 °C).

Q_{10} values were calculated in steps of 0.1% until 0.5% of the initial SOC was decomposed, which required an additional measurement at 185 incubation days for active layer samples incubated at 1 °C. For permafrost, Q_{10} values were calculated in steps of 0.1% until 0.9% of the initial permafrost SOC was decomposed. Kurungnakh Q_{10} (Figure 25) were less variable than Samoylov Q_{10}. To decompose 0.1% of the initial active layer SOC at different temperatures, it took 36.2 ± 1.1 mg CO_2-C g^{-1} SOC (1 °C), 19.6 ± 1.8 mg CO_2-C g^{-1} SOC (4 °C), and 12.3 ± 0.5 mg CO_2-C g^{-1} SOC (8 °C). This resulted in a Q_{10} of 4.6 ± 1.5 for the active layer. The Q_{10} value for the first 0.1% of permafrost SOC was 2.2 ± 0.5. Permafrost-Q_{10} values slightly increased with the amount of initial SOC decomposed to 3.3 ± 1.2 (0.9%).

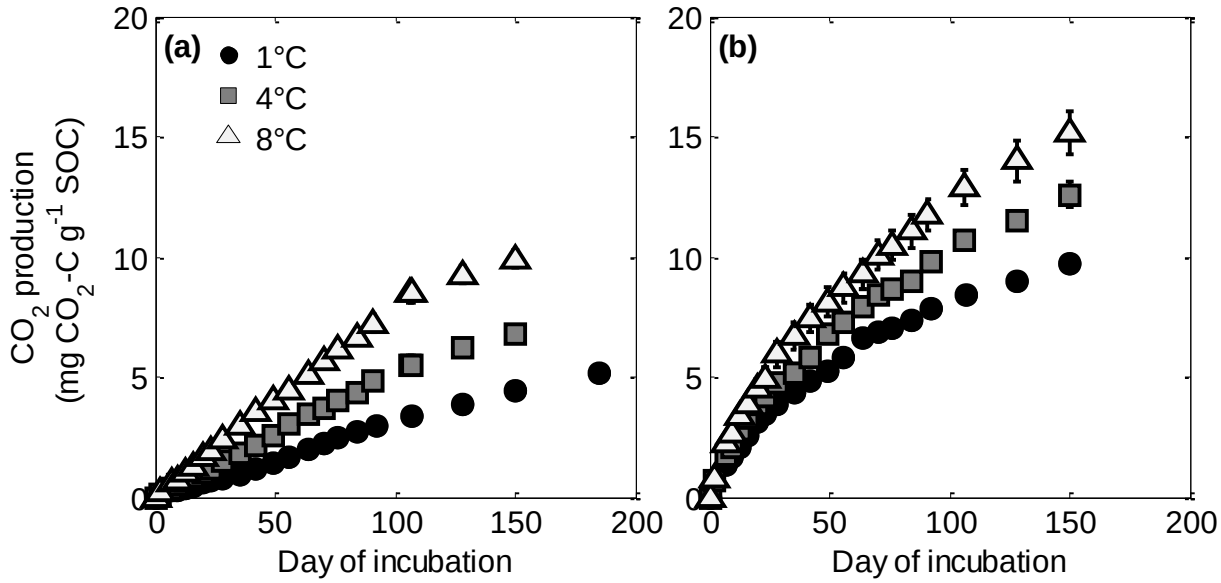

Figure 24: Kurungnakh: Cumulative aerobic CO_2 production over 150–185 incubation days at different temperatures in the active layer and permafrost (b). Data are mean values (*n* = 5) and error bars represent one standard deviation.

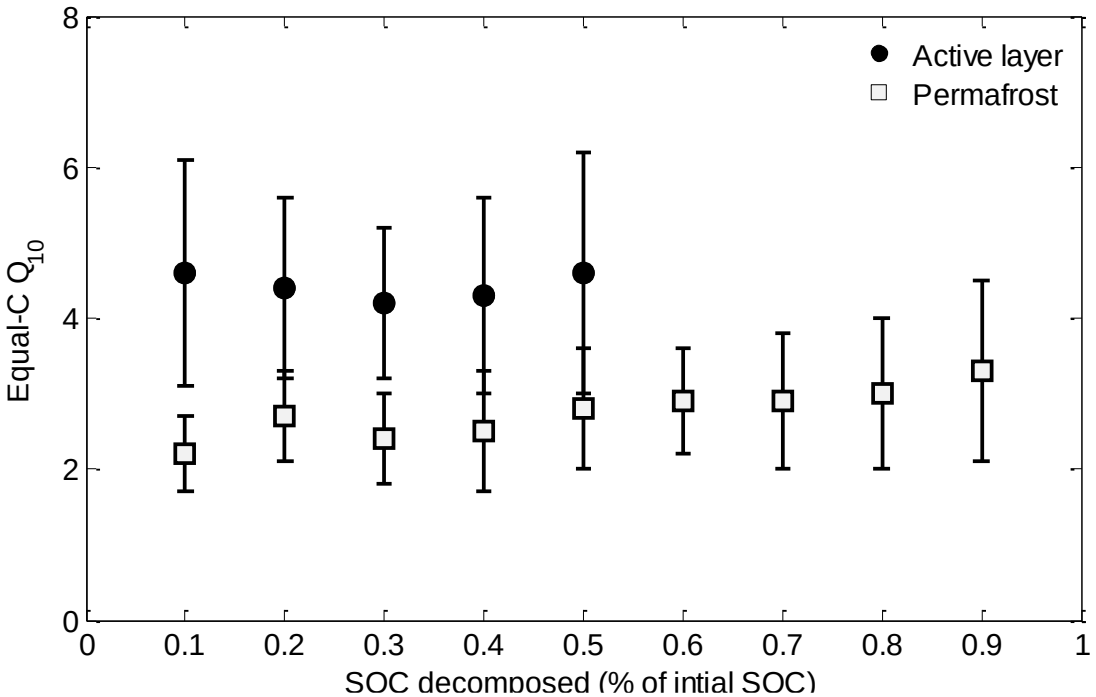

Figure 25: Kurungnakh: Equal-C Q_{10} values for different soil layers. Uncertainties for calculated Q_{10} values were obtained by error propagation.

5.2.5 Labile organic matter availability

In Samoylov samples from Polygon 3, the addition of *Carex* significantly (t-test, p<0.01) increased total CO_2 production in all soil layers at all temperatures, except in surface active layer soils incubated at 1 °C and 4 °C (Figure 26). The amount of additional CO_2 varied with depth and temperature. Total CO_2 production after 150 incubation days in the surface active layer increased by 13–18% compared to the control incubations. In deeper soil layers the increase in CO_2 production ranged between 28–39% in the bottom active layer and 46–71% in the permafrost. However, partitioning the amount of CO_2 in *Carex*-amended samples into SOM- and *Carex*-derived CO_2 revealed that most of the additional CO_2 came from the amendment. The *Carex*–derived fraction (f_{Carex}, Equation 6) of total CO_2 (Figure 27) showed considerable differences between soil layers but varied only slightly with temperatures, while the percentage of the added *Carex* that was decomposed (Figure 28) varied less with temperature and more with depth. Generally, the f_{Carex} was highest in permafrost and lowest in the surface active layer, while the amount of decomposed *Carex* was higher at high incubation temperatures. In the surface active layer, f_{Carex} at 1 °C, 4 °C, and 8 °C ranged between 0.06 at the beginning of the incubation and 0.13 after 150 incubation days (mean 0.08 ± 0.01). In the bottom active layer and permafrost, the f_{Carex} ranged between 0.04–0.27 (mean 0.18 ± 0.04) and 0.16–0.33 (mean 0.23 ± 0.05), respectively. The amount of the added *Carex* that was decomposed after 150 incubation days in the surface active layer, bottom active layer, and permafrost was 18.3 ± 5.3% at 1 °C, 30.6 ± 3.8% at 4 °C, and 39.4 ± 7.6% at 8 °C. A significant (t-test, p<0.01) increase in SOM-derived CO_2 (positive priming) was only evident in permafrost samples. Compared to control incubations, SOM-derived CO_2 at 1 °C and 4 °C increased by 15.6 ± 7.2% and 14.6 ± 7.8%, respectively.

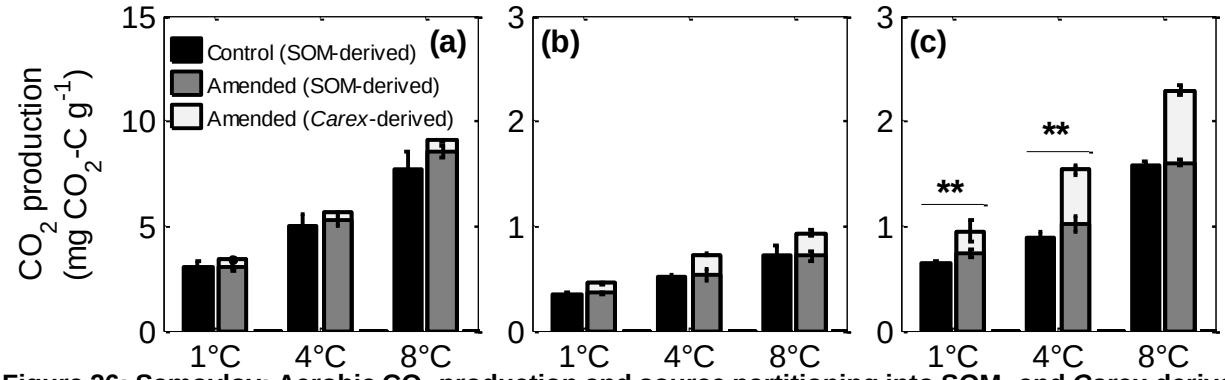

Figure 26: Samoylov: Aerobic CO_2 production and source partitioning into SOM- and *Carex*-derived CO_2 in control and amended incubations after 150 incubation days at different temperatures in the surface active layer (a), bottom active layer (b), and permafrost (c) of Polygon 3. Data are mean values (*n* = 4) and error bars represent one standard deviation. Significant differences (t-test) between SOM-derived CO_2 in control and amended samples (priming effect) are indicated by the vertical lines and asterisks (*p*<0.01). Note the different scale in panel (a).**

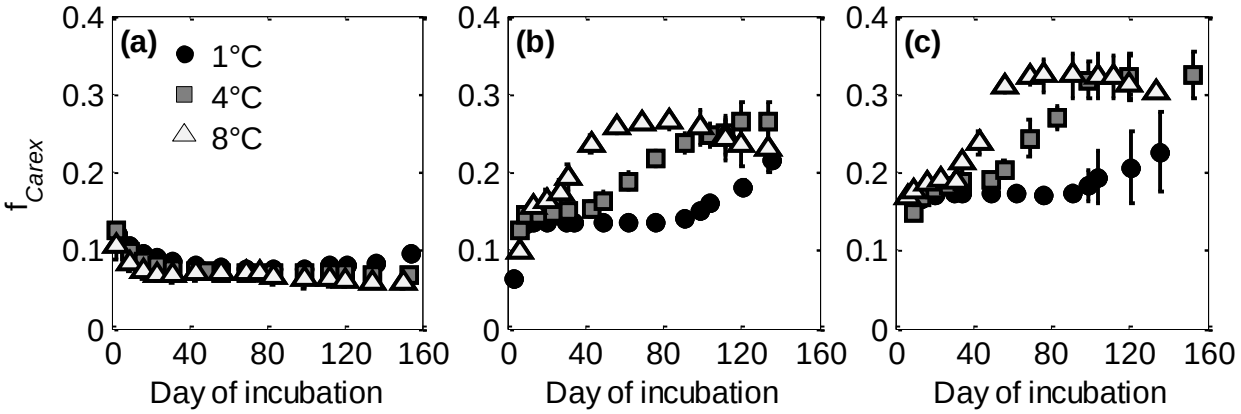

Figure 27: Samoylov: Fraction of *Carex*-derived CO_2 in amended incubations over 150 incubation days at different temperatures for the surface active layer (a), bottom active layer (b), and permafrost (c) of Polygon 3. Data are mean values (*n* = 4) and error bars represent one standard deviation.

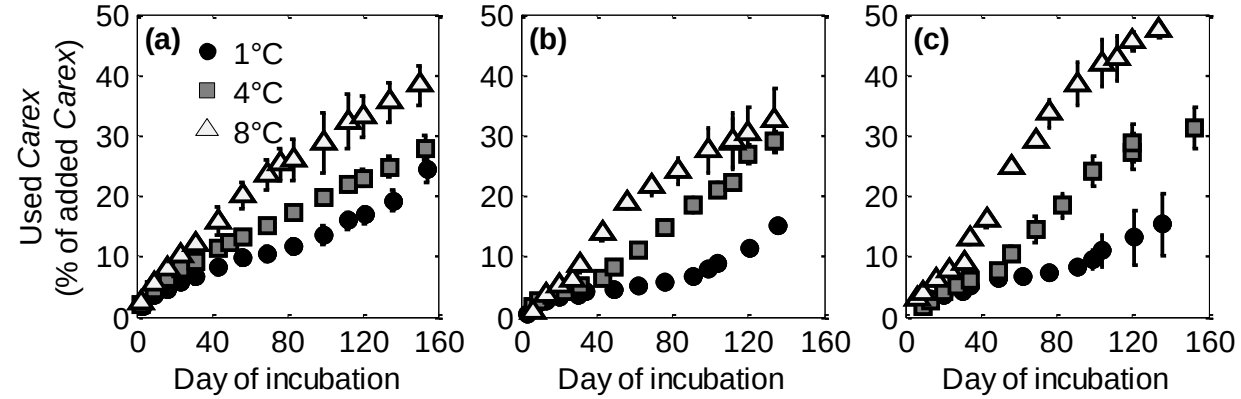

Figure 28: Percentage of added *Carex* material that was decomposed over 150 incubation days at different temperatures in the surface active layer (a), bottom active layer (b), and permafrost (c) of Polygon 3. Data are mean values (*n* = 4) and error bars represent one standard deviation.

In Kurungnakh samples, the addition of *Carex* also significantly increased (t-test, $p<0.01$) total CO_2 production after 150 incubation days in all soil layers and at all temperatures (Figure 29). In the active layer, total CO_2 production increased by 11–24% compared to control incubations. In permafrost, CO_2 production increased by 26–29%. f_{Carex} in the active layer varied little with temperature, but decreased from 0.36 at the beginning of the incubation to 0.13 after 150 incubation days (mean 0.22 ± 0.06, Figure 30). The mean f_{Carex} in permafrost was similar (0.20 ± 0.08), but much more variable with incubation time, especially at 4 °C and 8 °C, when f_{Carex} increased sharply between 28–76 incubation days. The amount of the added *Carex* that was decomposed during the incubation also varied considerably between the active layer and permafrost (Figure 31). At 1 °C, 4 °C, and 8 °C, only 9.6 ± 3.1% of the added *Carex* was decomposed in active layer samples. In permafrost, 16.9 ± 2.9% were decomposed at 1 °C, but 49.6 ± 5.3% and 48.5 ± 3.9% at 4 °C and 8 °C (mean 38.3 ± 18.6%). Partitioning the amount of CO_2 in *Carex*-amended samples into SOM- and *Carex*-derived CO_2 (Figure 29) revealed that most of the additional CO_2 came from the amendment. The amount of SOM-derived CO_2 in permafrost samples incubated at 4 °C and 8 °C significantly decreased (t-test, $p<0.05$) by 21.5 ± 4.2% and 8.7 ± 3.8% compared to control incubations (negative priming).

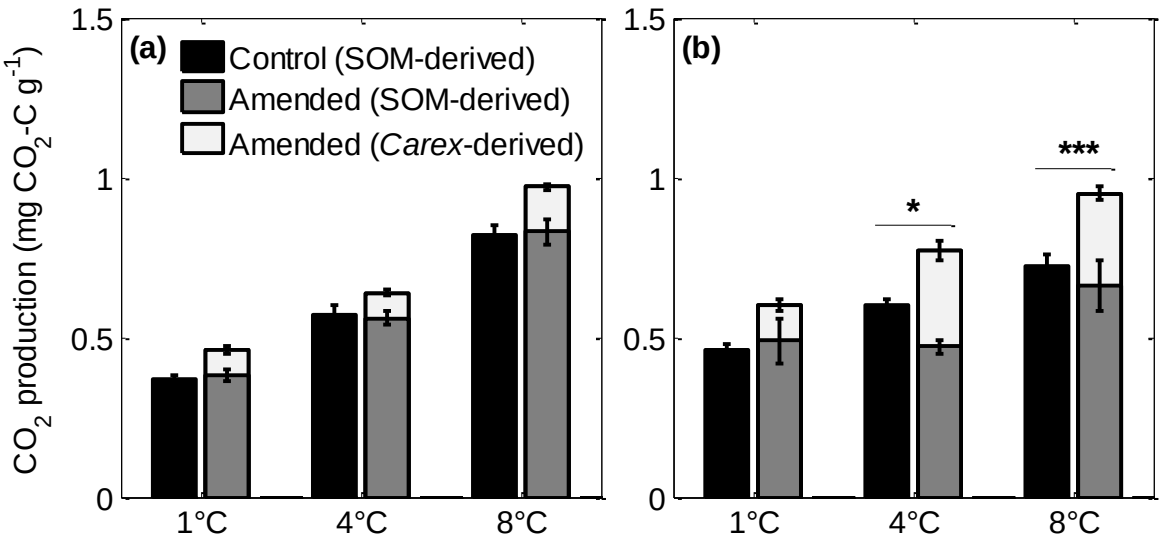

Figure 29: Kurungnakh: Aerobic CO_2 production and source partitioning into SOM- and *Carex*-derived CO_2 in control and amended incubations after 150 days of incubation at different temperatures in the active layer (a) and permafrost (b). Data are mean values (n = 5) and error bars represent one standard deviation. Significant differences (t-test) between SOM-derived CO_2 in control and amended samples (priming effect) are indicated by the vertical lines and asterisks (* $p<0.05$, *** $p<0.001$).

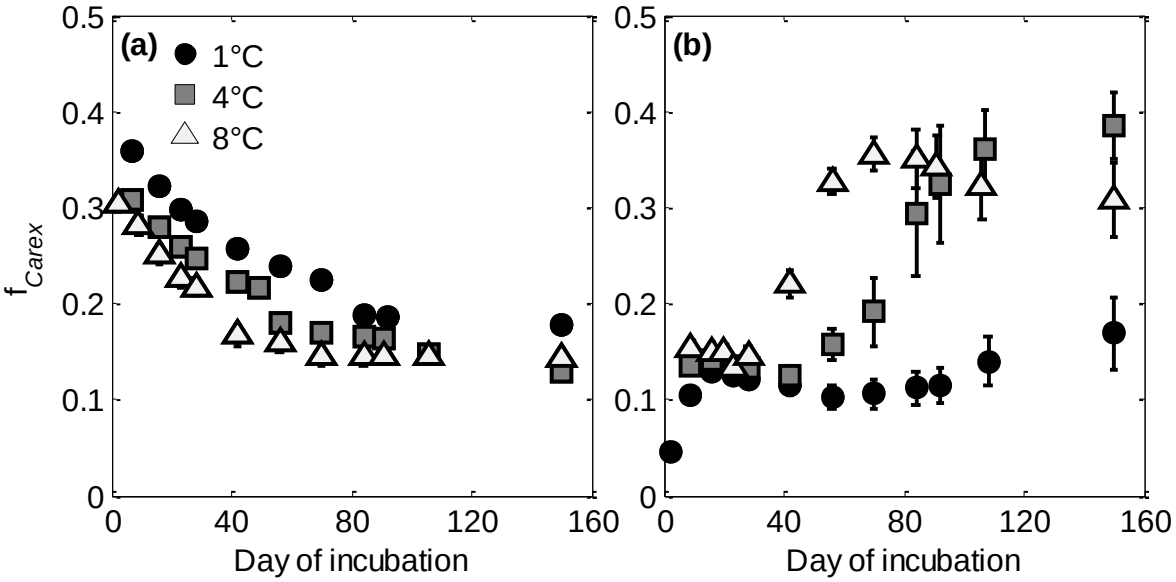

Figure 30: Kurungnakh: Fraction of *Carex*-derived CO_2 in amended incubations over 150 incubation days at different temperatures for the active layer (a) and permafrost (b). Data are mean values (*n* = 4) and error bars represent one standard deviation.

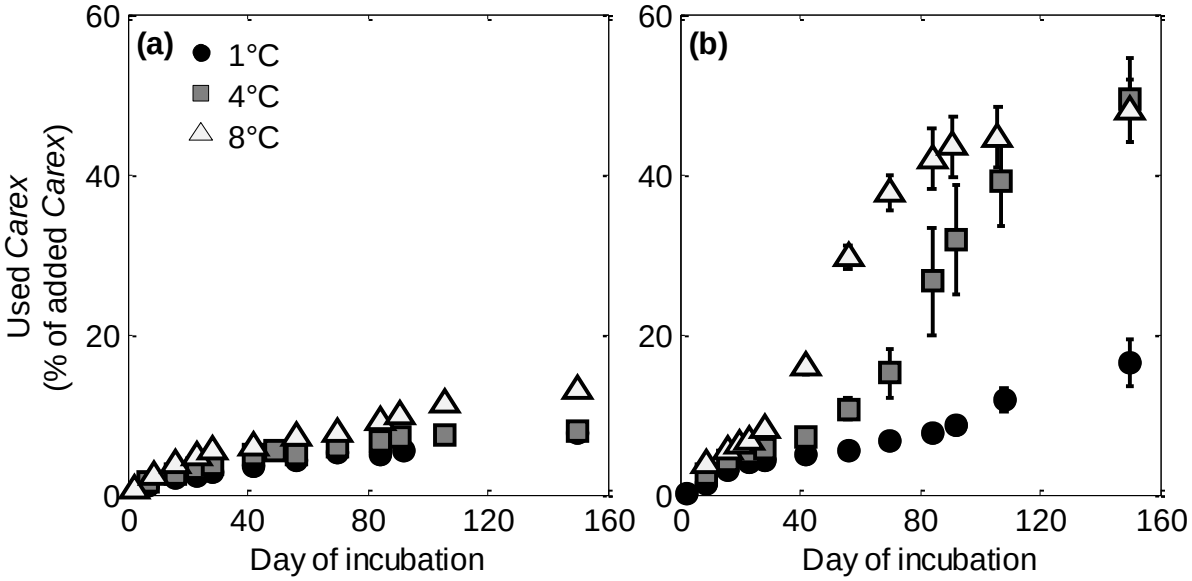

Figure 31: Kurungnakh: Percentage of added *Carex* material that was decomposed over 150 incubation days at different temperatures the active layer (a) and permafrost (b). Data are mean values (*n* = 5) and error bars represent one standard deviation.

5.3 Deep carbon

The decomposability of deep SOC of age-diverse permafrost deposits (MIS1-MIS7) from three different study sites was investigated. The preservation of different stratigraphic units, however, varied between the sites. Also, the lengths of the incubation period varied from 134 incubation days for outcrop samples from Muostakh Island (MUO12) and Bol'shoy Lyakhovsky (L14 outcrops) to 444 days for core sampled from Bol'shoy Lyakhovsky (L14 cores) and 903 days for core samples from the Buor Khaya Peninsula (BK8). For better comparability between the sites, cumulative SOM decomposition is first presented based on 134 incubation days, which reflects about one thaw period, and then for the whole incubation period.

5.3.1 Muostakh Island

For this work, 14 subsamples from the three sampled profiles on Muostakh Island were investigated with variable %SOC, C/N, $\delta^{13}C_{org}$, and pH (Tigges, 2014, Table 11). Overall, higher %SOC were observed in MIS1 and MIS3 deposits (1.9–6.3 wt%) than in MIS2 deposits (0.8–3.2 wt%). MIS2 deposits also showed higher $\delta^{13}C_{org}$ and pH values.

Table 11: Sediment characteristics and chronostratigraphy for Muostakh Island samples with height in m above sea level (asl), soil organic carbon (SOC) content in weight percent (wt%), carbon to nitrogen ratios (C/N), isotopic signature of SOC ($\delta^{13}C_{org}$) in per mil relative to the Vienna Pee Dee Belemnite standard (‰VPDB) and pH.

Sample	Height	Chrono-stratigraphy	SOC	C/N	$\delta^{13}C_{org}$	pH
	m asl		wt%		‰VPDB	
MUO12-SS17	19.5	MIS1	5.5	23.4	-27.5	5.0
MUO12-SS18	19.0	MIS1	5.8	16.2	-27.8	5.0
MUO12-SS19	18.4	MIS1	3.1	10.8	-27.1	5.5
MUO12-SS20	17.6	LGT-MIS1	1.9	7.6	-26.5	7.2
MUO12-SS22	16.0	MIS2	1.8	6.2	-24.3	7.2
MUO12-SS24	14.0	MIS2	1.0	4.6	-23.9	7.4
MUO12-SS16	13.2	MIS2	1.1	7.8	-23.4	8.2
MUO12-SS13	10.0	MIS2	0.8	6.9	-22.8	7.2
MUO12-SS8	10.0	MIS2	3.2	11.1	-25.0	7.7
MUO12-SS7	9.5	MIS2	1. 0	6.5	-22.9	7.3
MUO12-SS9	8.7	MIS3	5.1	12.6	-26.5	6.0
MUO12-SS11	8.7	MIS3	6.3	15.8	-26.5	6.4
MUO12-SS2	5.7	MIS3	2.1	9.6	-25.8	7.9
MUO12-SS4	4.4	MIS3	1.7	8.6	-25.5	6.7

On a gram sediment basis, aerobic and anaerobic CO_2 production ranged between 0.05–1.4 mg CO_2-C g^{-1} and 0.03–0.4 mg CO_2-C g^{-1}, respectively (Figure 32). Generally, 4–14 times more CO_2 was produced aerobically than anaerobically, except in MIS2 deposits between 10.0–17.6 m asl. In these cases, the ratio of aerobic to anaerobic CO_2 was 2.0 ± 1.3. Based on %SOC, CO_2 production ranged between 4.7–60.7 mg CO_2-C g^{-1} SOC under aerobic conditions and 0.5–20.9 mg CO_2-C g^{-1} SOC under anaerobic conditions (Figure 33). Higher aerobic CO_2 production was generally observed in the lowermost MIS3 deposits between 4.4–8.7 m asl but elevated CO_2 production levels were also observed at 10 m asl, 14 m asl, and 18.4 m asl. Under anaerobic conditions, the highest production was observed at 14 m asl (19.3 ± 1.4 mg CO_2-C g^{-1} SOC), which was nearly twice as much as in most other samples. No methanogenesis was observed in any Muostakh Island samples over the 134-day incubation period.

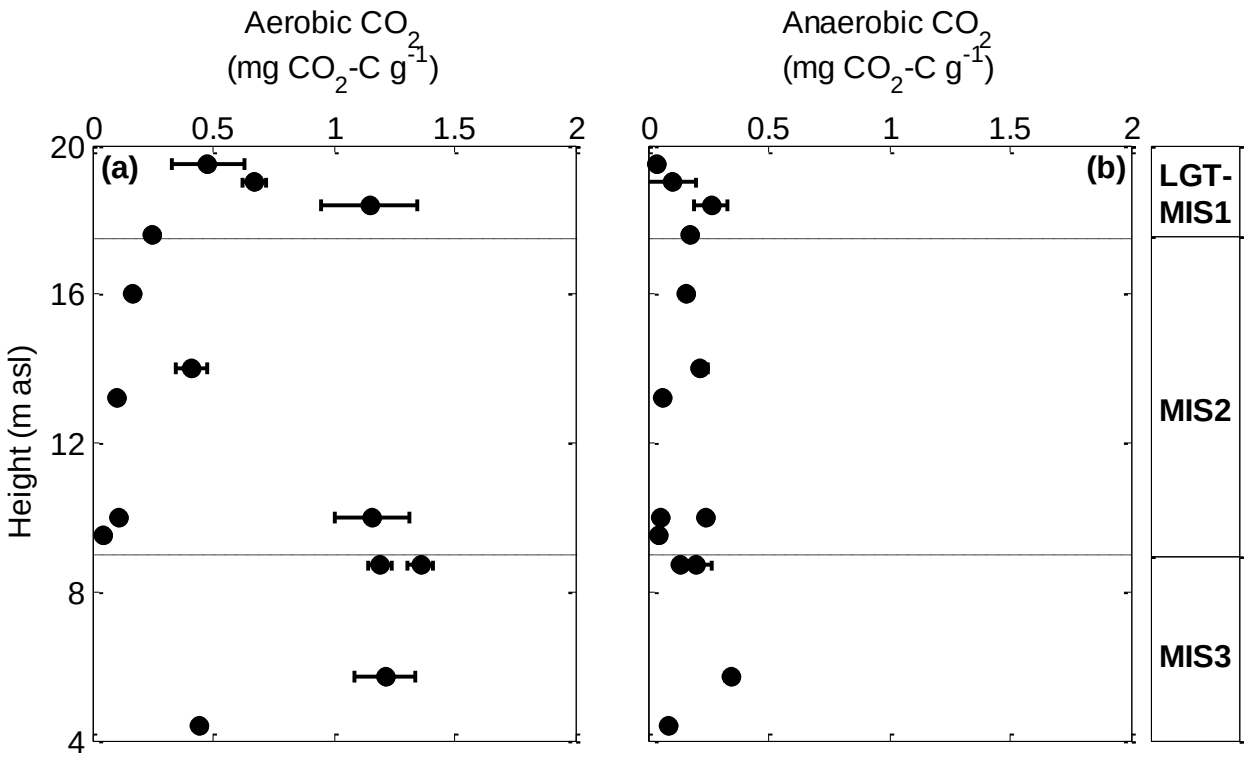

Figure 32: MUO12: Depth profiles of total CO_2 production per gram dry soil (g^{-1}) after 134 incubation days at 4 °C under aerobic (a) and anaerobic (b) conditions. Data are mean values (generally *n* = 3) and error bars represent one standard deviation.

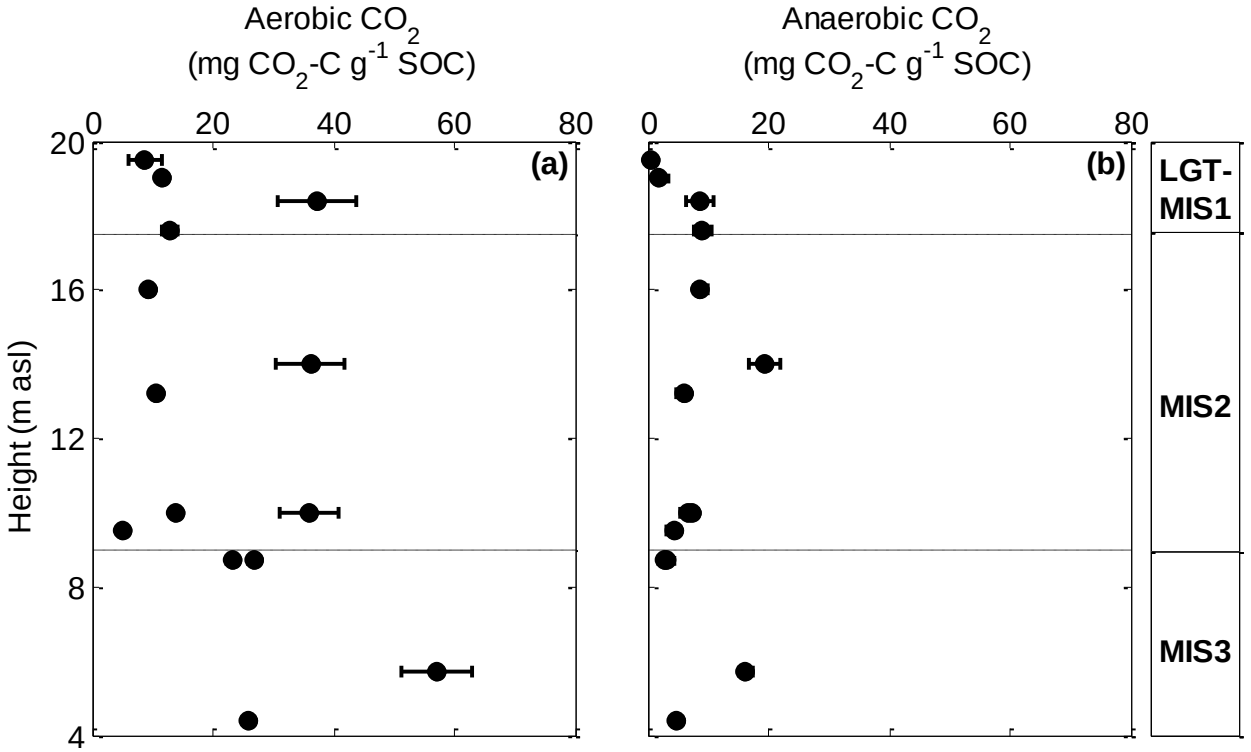

Figure 33: MUO12: Depth profiles of total CO_2 production per gram soil organic carbon (g^{-1} SOC) after 134 incubation days at 4 °C under aerobic (a) and anaerobic (b) conditions. Data are mean values (generally *n* = 3) and error bars represent one standard deviation.

To test for qualitative differences in the SOM deposited under different climatic conditions, the amounts SOC decomposed after 134 incubation days at 4 °C under aerobic and anaerobic conditions were pooled for samples from the MIS1, MIS2, and MIS3. Under aerobic conditions, that highest amount of SOC was decomposed in MIS3 deposits (3.2 ± 1.6% of initial SOC), which was significantly more (ANOVA, $p<0.05$) than in MIS1 (1.7 ± 1.1% of initial SOC) and MIS2 deposits (1.7 ± 1.3% of initial SOC, Figure 34). Under anaerobic conditions, the highest amount was decomposed in MIS2 deposits (0.9 ± 0.5% of initial SOC), which was significantly more (ANOVA, $p<0.05$) than in MIS1 deposits (0.5 ± 0.4%). Anaerobic decomposition in MIS3 deposits (0.7 ± 0.6%) ranged between MIS1 and MIS2.

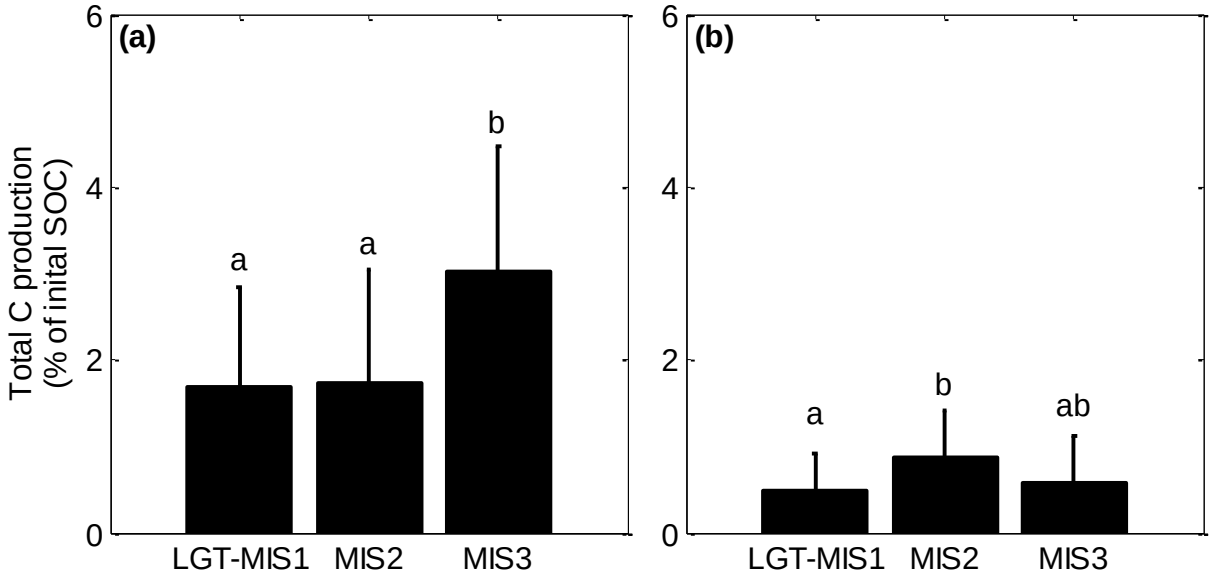

Figure 34: MUO12: Total C production in different age groups after 134 incubation days at 4 °C under aerobic (a) and anaerobic (b) conditions. Data are mean values (LGT-MIS1 *n* = 12; MIS2 *n* = 17, MIS3 *n* = 15) and error bars represent one standard deviation. Different letters indicate significant differences between the age groups (ANOVA, *p*<0.05).

5.3.2 Buor Khaya Peninsula

In this work, 20 sediment subsamples spread evenly over the entire core were analyzed (Figure 12, Table 12). The ice-wedge was not sampled. The highest %SOC (4.1 wt% was observed in the active layer, but also below ranged %SOC between 1.4–3.9. $\delta^{13}C_{org}$ and pH values increased slightly with depth.

Table 12: Sediment characteristics and chronostratigraphy for BK8 core samples with height in m above sea level (asl), depth in m below surface (bs), soil organic carbon (SOC) content in weight percent (wt%), carbon to nitrogen ratios (C/N), isotopic signature of SOC ($\delta^{13}C_{org}$) in per mil relative to the Vienna Pee Dee Belemnite standard (‰VPDB) and pH.

Sample	Height	Depth	Chrono-stratigraphy	SOC	C/N	$\delta^{13}C_{org}$	pH
	m asl	m bs		wt%		‰VPDB	
BK8-1	33.9	0.3	AL	4.1	11.4	-28.5	6.09
BK8-2	33.5	0.7	LGT-MIS1	3.9	12.0	-27.6	6.66
BK8-3	32.7	1.5	LGT-MIS1	2.8	11.7	-26.8	6.58
BK8-4	32.2	2.0	LGT-MIS1	3.5	10.6	-27.1	6.47
BK8-5	31.9	2.3	LGT-MIS1	3.6	11.0	-27.5	6.50
BK8-6	31.4	2.8	LGT-MIS1	4.0	11.9	-27.3	6.58
BK8-7	31.0	3.2	LGT-MIS1	3.4	12.1	-27.4	6.34
BK8-11	25.5	8.7	MIS3	2.7	8.2	-26.6	6.45
BK8-12	24.7	9.5	MIS3	2.0	10.2	-28.4	6.71
BK8-13	24.2	10.0	MIS3	1.8	9.2	-28.6	7.37
BK8-14	23.0	11.2	MIS3	1.4	8.7	-26.3	7.16
BK8-15	22.6	11.6	MIS3	2.0	9.3	-27.1	7.06
BK8-16	22.2	12.0	MIS3	3.1	10.1	-27.3	6.80
BK8-17	21.5	12.7	MIS3	3.3	11.6	-26.8	6.83
BK8-18	20.6	13.6	MIS3	3.1	12.0	-27.3	6.21
BK8-19	20.1	14.1	MIS3	3.2	11.6	-26.9	6.84
BK8-20	19.6	14.6	MIS3	3.7	12.0	-26.4	7.48
BK8-21	19.1	15.1	MIS3	3.6	12.2	-25.8	6.80
BK8-22	17.4	16.9	MIS3	2.9	9.7	-26.0	7.62
BK8-23	16.1	18.1	MIS3	1.6	8.6	-25.8	7.52

After 134 incubation days, between 0.08–2.6 mg CO_2-C g^{-1} were aerobically, and 0.08–0.7 mg CO_2-C g^{-1} were anaerobically produced (Figure 35), which is within the same range as production in samples from Muostakh Island. The highest decomposition was observed in the active layer and decreased sharply between 0.7–3.2 m bs (33.3–30.8 m asl). Both aerobic and anaerobic CO_2 production then increased again in deposits below the ice-wedge. Methanogenesis was only observed in one of the three replicates in the active layer, but in much smaller quantity than CO_2 (0.02 mg CH_4-C g^{-1} compared to 0.55 mg CO_2-C g^{-1} in the same replicate after 134 incubation days). After 903 incubation days, aerobic CO_2 production ranged between 0.2–5.3 mg CO_2-C g^{-1}. On average, more than 50% (55 ± 13%) of the aerobically produced CO_2 after 903 days was already produced within the first 134 incubation days. After 903 incubation days under anaerobic conditions, CO_2 production ranged between 0.07–1.5 mg CO_2-C g^{-1}. On average, 84 ± 13% of the CO_2 after 903 days was produced within the first 134 days. Methanogenesis was now observed in all of the three replicates from the active layer, where 0.5 ± 0.2 mg CH_4-C g^{-1} were produced. Additionally, CH_4 production was also observed in two subsamples from below the ice-wedge at 10 m bs (24 m asl). In these two samples, CH_4 production (0.11 mg CH_4-C g^{-1} and 0.41 mg CH_4-C g^{-1}) was equal to or higher than anaerobic CO_2 production in the same replicates (0.13 mg CO_2-C g^{-1} and 0.14 mg CO_2-C g^{-1}, respectively).

Based on %SOC, the depth pattern of high production in the active layer as well as in deposits from below the ice-wedge persisted (Figure 36). After 134 incubation days, 2.6–50.2 mg CO_2-C g^{-1} SOC were aerobically and 2.1–13.3 mg CO_2-C g^{-1} SOC were anaerobically produced. After 903 incubation days, production increased to 6.5–129.2 mg CO_2-C g^{-1} SOC aerobically and 2.2–36.2 mg CO_2-C g^{-1} SOC anaerobically. Methanogenesis in the active layer increased from just 0.4 ± 0.2 mg CH_4-C g^{-1} SOC after 134 incubation days to 13.3 ± 3.8 mg CH_4-C g^{-1} SOC after 903 days. In the two subsamples at 10 m bs, CH_4 production after 903 incubation days was 22.4 mg CH_4-C g^{-1} SOC and 6.1 mg CH_4-C g^{-1} SOC.

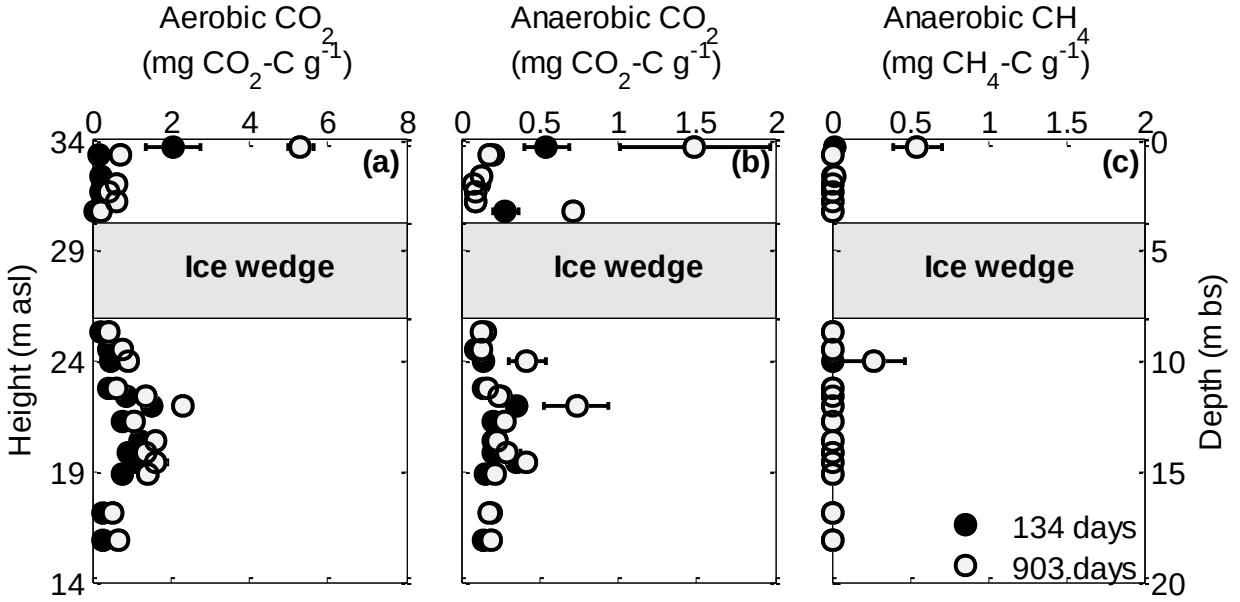

Figure 35: BK8: Depth profiles of total CO_2 and CH_4 production per gram dry soil (g-1) after 134 and 903 incubation days at 4 °C under aerobic (a) and anaerobic (b, c) conditions. Data are mean values (n = 3) and error bars represent one standard deviation. Note the different scale in panel (a).

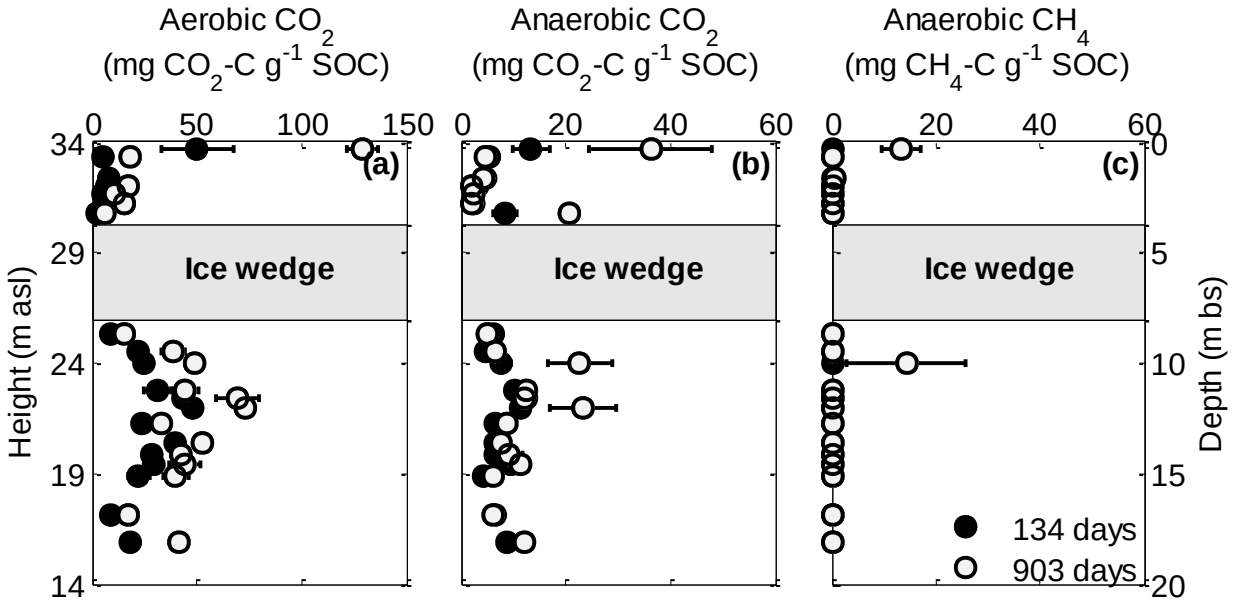

Figure 36: BK8: Depth profiles of total CO_2 and CH_4 production per gram soil organic carbon (g^{-1} SOC) after 134 and 903 incubation days at 4 °C under aerobic (a) and anaerobic (b, c) conditions. Data are mean values (*n* = 3) and error bars represent one standard deviation. Note the different scale in panel (a).

Similar to the data from Muostakh Island, BK8 data were pooled for samples from the active layer, late glacial-early Holocene transition, and MIS3. After 134 days 5.0 ± 1.7% of the initial SOC was aerobically and 1.3 ± 0.4% of the initial SOC was anaerobically decomposed to CO_2 in the active layer, which was in both cases significantly more than in the other two age groups (Figure 37). In MIS3 samples 2.7 ± 1.1% of the initial SOC were aerobically and 0.8 ± 0.3% of the initial SOC were anaerobically decomposed after 134 days, which was significantly more than in samples from the late glacial-early Holocene transition (0.6 ± 0.2% of initial SOC aerobically, and 0.4 ± 0.2% of the initial SOC anaerobically).

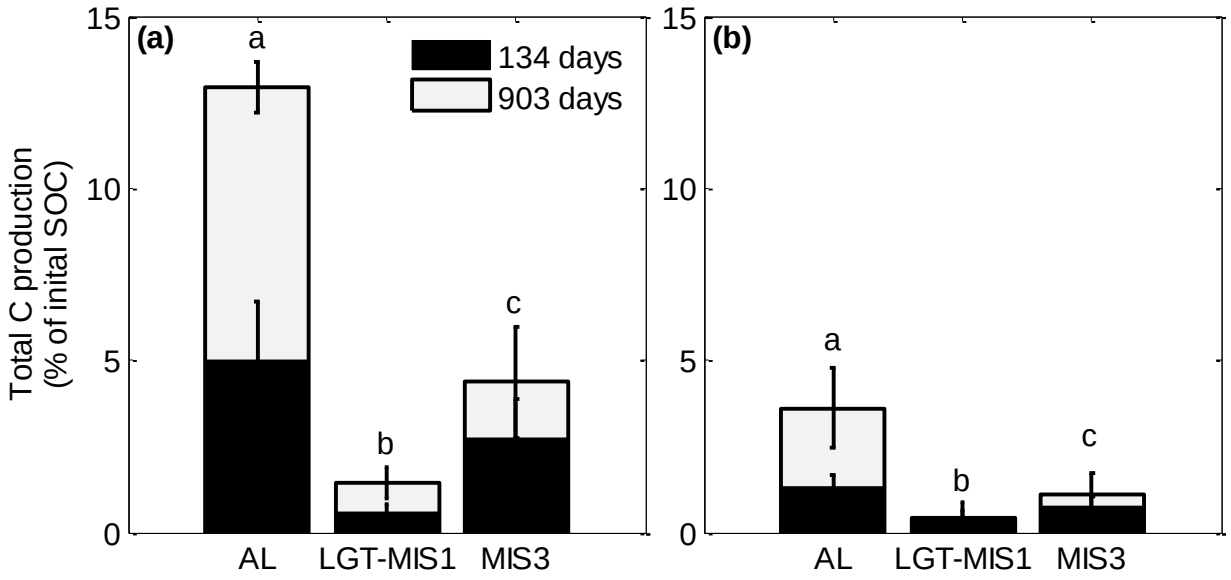

Figure 37: BK8: Total C production in different age groups after 134 and 903 incubation days at 4 °C under aerobic (a) and anaerobic (b) conditions. Data are mean values (AL *n* = 3; LGT-MIS1 *n* = 17, MIS3 *n* = 38) and error bars represent one standard deviation. Different letters indicate significant (ANOVA, *p*<0.05) differences between the age groups.

5.3.3 Bol'shoy Lyakhovsky

21 subsamples from four cores (Table 13) and eight samples from five different permafrost outcrops (Table 14) from Bol'shoy Lyakhovsky were investigated with a wide range in sediment characteristics (%SOC, C/N, $\delta^{13}C_{org}$, pH). Overall, %SOC in core samples ranged between 0.4–3.2 wt%. The highest %SOC were observed in a Saalian sample from the Yukagir Suite (*BK8, 14.6 wt%) and the peaty layer on top of the Krest-Yuryakh Suite (*BK6, 8.8 wt%). Lower %SOC and C/N values were generally observed in MIS4 and MIS5 deposits.

Table 13: Sediment characteristics and chronostratigraphy for Bol'shoy Lyakhovsky core samples with height in m above sea level (asl), depth in m below surface (bs), soil organic carbon (SOC) content in weight percent (wt%), carbon to nitrogen ratios (C/N), isotopic signature of SOC ($\delta^{13}C_{org}$) in per mil relative to the Vienna Pee Dee Belemnite standard (‰VPDB) and pH.

Sample	Height	Depth	Chrono-stratigraphy	SOC	C/N	$\delta^{13}C_{org}$	pH
	m asl	m bs		wt%		‰VPDB	
L14-05							
L14-05_01	11.3	0.2	AL	3.2	8.8	-28.7	5.3
L14-05_02	11.0	0.7	MIS1	1.4	4.0	-27.4	5.3
L14-05_05	8.2	3.3	MIS1	1.8	8.4	-27.6	6.2
L14-05_07	5.4	6.1	MIS3	1.5	7.6	-28.0	6.1
L14-05_08	4.5	7.0	MIS3	4.2	9.8	-29.0	5.9
L14-02							
L14-02_01	32.1	0.2	AL	3.4	8.3	-27.6	6.0
L14-02_02	31.4	0.9	MIS3	4.2	9.2	-28.0	6.1
L14-02_03	30.6	1.7	MIS3	4.4	11.0	-27.9	6.3
L14-02_06	27.0	5.4	MIS3	1.7	6.3	-26.5	7.1
L14-02_10	21.8	10.5	MIS3	1.5	5.8	-27.4	6.7
L14-03							
L14-03_01	16.7	0.3	AL	2.1	8.7	-28.1	6.3
L14-03_02	16.2	0.8	MIS4	1.9	9.4	-28.4	5.5
L14-03_06	13.8	3.2	MIS4	2.0	10.5	-27.5	7.2
L14-03_11	8.1	8.9	MIS4	0.6	4.2	-27.0	7.6
L14-03_14	4.5	12.5	MIS4	1.4	10.9	-29.0	7.4
L14-03_15	2.9	14.1	MIS4	1.0	9.4	-28.6	7.3
L14-04							
L14-04_01	11.7	0.3	AL	2.6	7.1	-28.1	6.5
L14-04_03	7.9	4.2	MIS4	0.5	4.9	-28.2	7.2
L14-04_04	7.0	5.0	MIS5	1.4	7.5	-28.0	7.2
L14-04_05	6.0	6.1	MIS5	0.4	4.0	-27.6	7.8
L14-04_07	4.3	7.7	MIS5	0.4	3.4	-27.1	7.4

Table 14: Sediment characteristics and chronostratigraphy for Bol'shoy Lyakhovsky outcrop samples (compare with Figure 13).

Outcrop	Sample	Height	Horizon/Suite	Chrono-stratigraphy	SOC	C/N	$\delta^{13}C_{org}$	pH
		m asl			wt%		‰VPDB	
L14-07	***BK1**	7.5	Sartan	MIS2	2.0	8.9	-25.6	7.59
	***BK2**	6.5	Sartan	MIS2	2.0	8.3	-27.1	7.54
L14-08	***BK8**	23	Molotkov	MIS3	1.4	8.4	-27.9	7.67
L14-10	***BK3**	2.5	Kuchchugui	MIS4[a]	0.6	7.5	-26.3	7.73
L14-12	***BK6**	7.5	Krest-Yuryakh	MIS5	8.8	13.2	-27.4	5.74
	***BK5**	4.5	Krest-Yuryakh	MIS5	0.5	7.0	-25.2	7.86
L14-11	***BK4**	3.5	Yukagir	MIS7	14.5	21.0	-26.2	5.73
	***BK7**	2.0	Yukagir	MIS7	2.4	11.1	-23.8	6.85

a) The stratigraphic position of the Kuchchugui Suite is still debated due to the lack of reliable ages. In this work, it is assumed that the sampled Kuchchugui Suite is of MIS4 origin, which is consistent with the latest publication on similar sample material (Stapel *et al.*, 2017).

CO_2 production in the four cores from Bol'shoy Lyakhovsky was highly variable between different cores, as well as within individual cores. Based on gram sediment, CO_2 production ranged between 0.004–0.5 mg CO_2-C g^{-1} under aerobic conditions and 0.004–0.3 mg CO_2-C g^{-1} under anaerobic conditions (Figure 38). Based on %SOC (Figure 39), the range was similarly high, with aerobic and anaerobic production ranging between 0.1–18.8 mg CO_2-C g^{-1} SOC and 0.1–11.7 mg CO_2-C g^{-1} SOC, respectively. Generally higher production was observed in the active layer samples (0–0.5 m bs for each of the cores), but some MIS3 deposits showed production levels similar or even higher than the active layer. Lower production was generally observed in MIS4 and MIS5 deposits. Extending the incubation period from 134 days to 444 days showed that 50 ± 13% of the total aerobic CO_2 and 73 ± 17% of the total anaerobic CO_2 after 444 incubation days was already produced in the first 134 incubation days. Especially MIS4 and MIS5 deposits showed little to no additional CO_2 production after 134 incubation days. Methanogenesis was only observed in some active layer samples (5 out of 12 replicates) and all MIS5 samples, except in one out of nine replicates. In the five active layer samples, CH_4 production after 444 incubation days ranged between 6.4–166.9 µg CH_4-C g^{-1} (196.2–6 451.2 µg CH_4-C g^{-1} SOC). In the Eemian lacustrine MIS5 sediments, CH_4 production ranged between 0.4–9.3 µg CH_4-C g^{-1} (3.0–262.7 µg CH_4-C g^{-1} SOC).

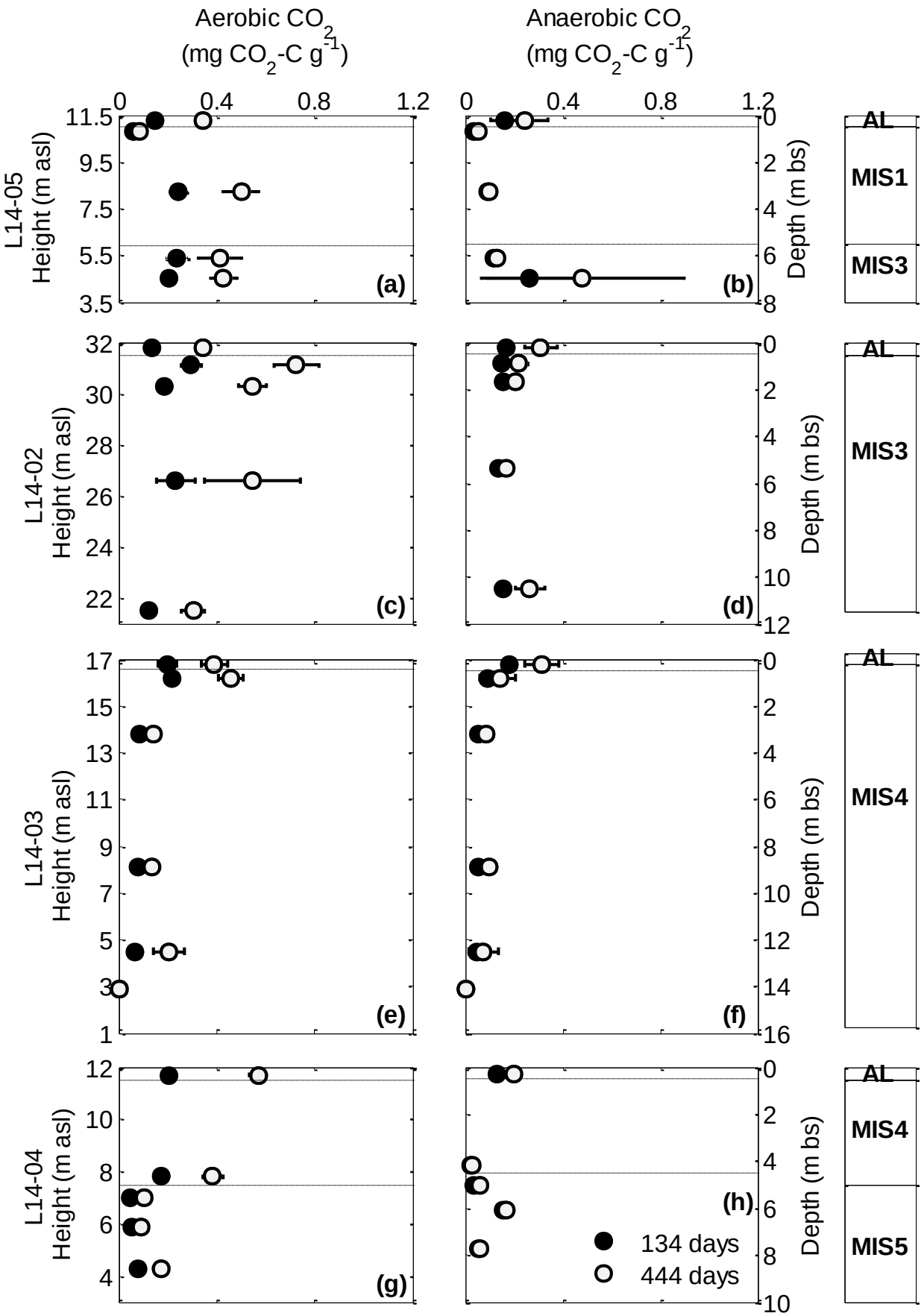

Figure 38: L14 cores: Depth profiles of total CO_2 production per gram dry soil (g^{-1}) after 134 and 903 incubation days at 4 °C under aerobic (a, c, e, g) and anaerobic (b, d, f, h) conditions. Data are mean values (generally *n* = 3) and error bars represent one standard deviation.

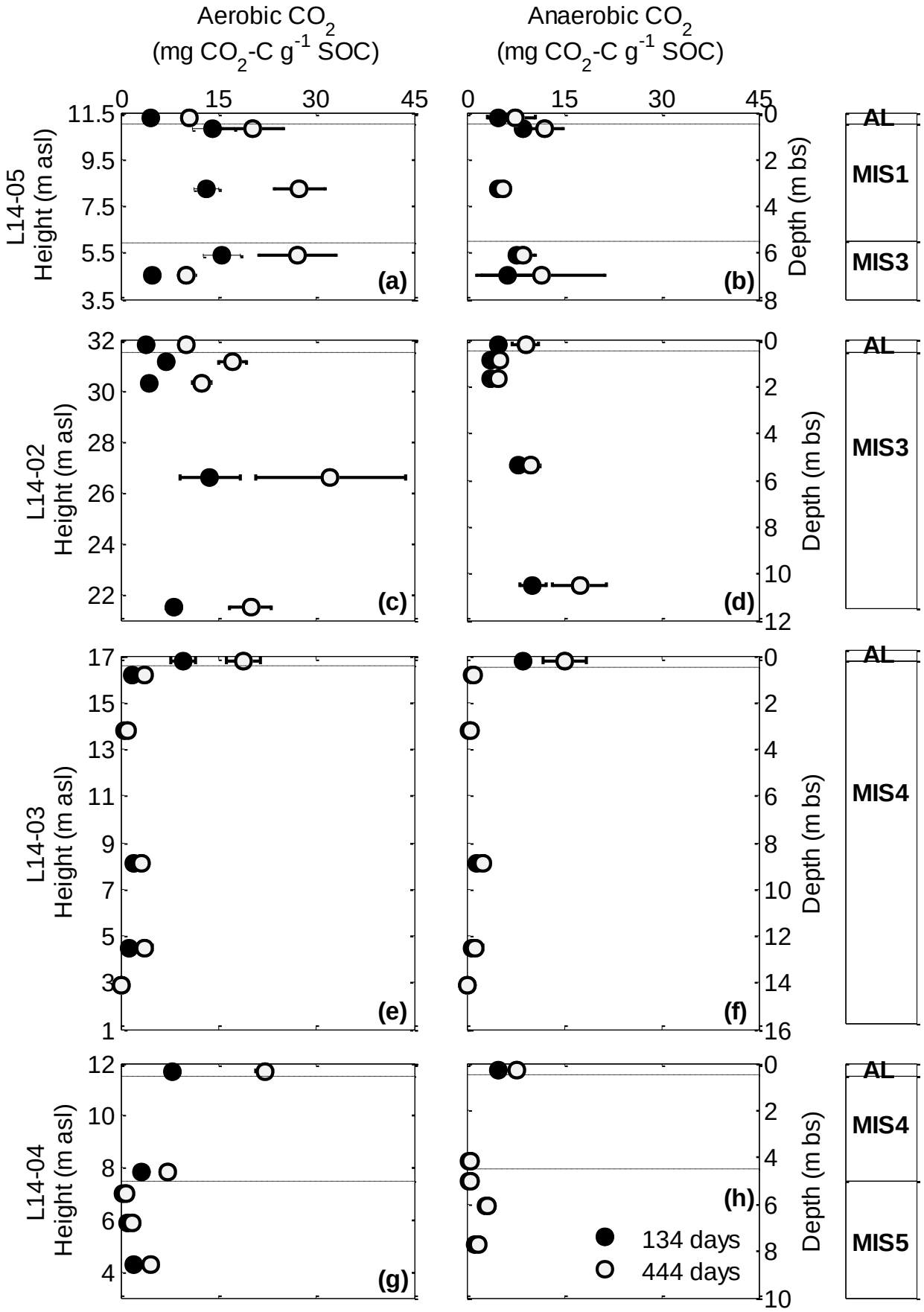

Figure 39: L14 cores: Depth profiles of total CO_2 production per gram soil organic carbon (g^{-1} SOC) after 134 and 903 incubation days at 4 °C under aerobic (a, c, e, g) and anaerobic (b, d, f, h) conditions. Data are mean values (generally *n* = 3) and error bars represent one standard deviation.

Pooling data from all cores for the active layer, MIS1, MIS3, MIS4, and MIS5 showed that the oldest deposits (MIS4 and MIS5) had only decomposed 0.1–0.2% of the initial SOC after 134 incubation days, which was significantly less than in younger deposits both under aerobic and anaerobic conditions (Figure 40). In MIS3 deposits, only 0.9 ± 0.5% of the initial SOC were aerobically decomposed after 134 days, which is ~3 times less than what was decomposed in MIS3 deposits from Muostakh Island (3.2 ± 1.6% of initial SOC, Figure 34a) and Buor Khaya Peninsula (2.7 ± 1.1% of the initial SOC, Figure 37a) over the same incubation period. Anaerobic CO_2 production was 0.7 ± 0.3% of the initial SOC, which was within the same range as for Muostakh Island and the Buor Khaya Peninsula.

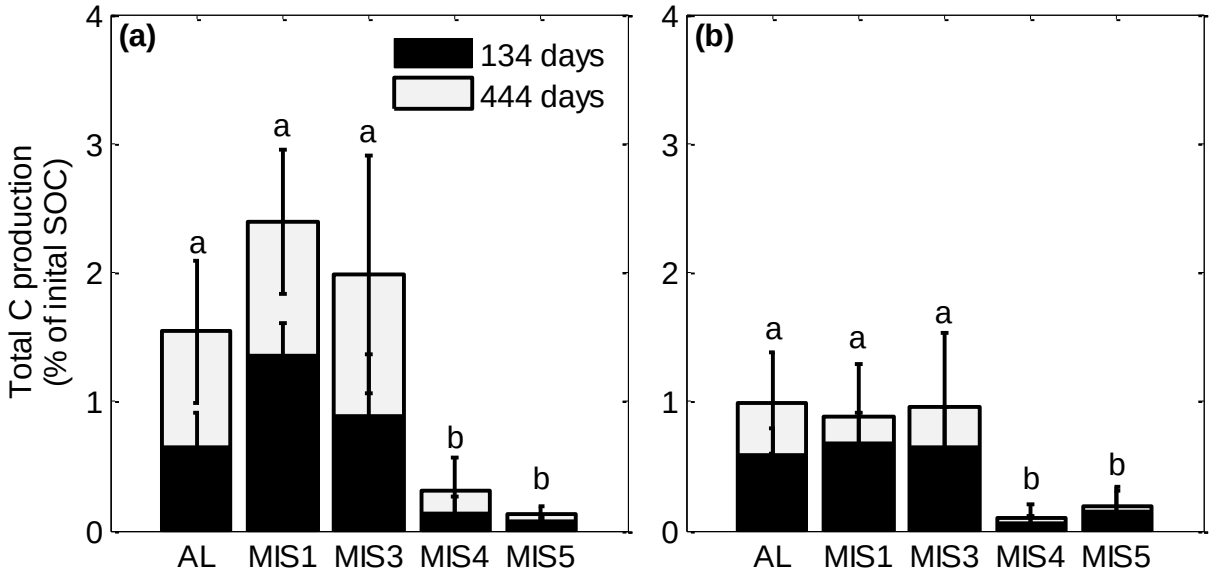

Figure 40: L14 cores: Total C production in different age groups after 134 and 444 incubation days at 4 °C under aerobic (a) and anaerobic (b) conditions. Data are mean values (AL *n* = 12; MIS1 *n* = 6; MIS3 *n* = 18; MIS4 *n* = 15; MIS5 *n* = 9) and error bars represent one standard deviation. Different letters indicate significant (ANOVA, *p*<0.05) differences between the age groups.

To extent the sedimentary record from Bol'shoy Lyakhovsky, eight additional samples from five permafrost outcrops were incubated at 4 °C for 134 days. Samples *BK8, *BK3, and *BK5 (
Table 14) were taken in close proximity to the core sites and can be correlated to the corresponding core depths in L14-02, L14-03, and L14-04 based on their relative height, but the production in these three samples was generally higher than in the corresponding core sections. The other samples extent the record to MIS2 (*BK1 and *BK2) and MIS7 (*BK6 and *BK7) deposits, which were not captured in the core record. Generally, about 2–7 times more SOM was decomposed under aerobic than anaerobic conditions, except in *BK3, where anaerobic production equaled aerobic production (Figure 41). The highest cumulative aerobic production per gram sediment was observed in the peat sample *BK4 from the Yugakir Suite (2.7 ± 0.3 mg CO_2-C g^{-1}) while the lowest production was observed in the Eemian lake sediments (*BK5, 0.1 ± 0.004 mg CO_2-C g^{-1}). *BK5 also produced the least amount of CO_2 under anaerobic

conditions (0.07 ± 0.002 mg CO_2-C g^{-1}). Otherwise, anaerobic CO_2 production was less variable between samples than aerobic production and ranged between 0.16 ± 0.02 mg CO_2-C g^{-1} (*BK8) and 0.39 ± 0.02 CO_2-C g^{-1}(*BK2). Based on gram SOC, the productions pattern between the different samples shifted. Now, the highest aerobic CO_2 production was observed in MIS2 deposits (*BK2, 37.4 ± 1.6 mg CO_2-C g^{-1} SOC) while the highest anaerobic production was observed in MIS4 deposits (*BK3, 35.7 ± 1.6 mg CO_2-C g^{-1} SOC). Methanogenesis only occurred in one sediment sample (*BK5) but was with just 0.040 ± 0.003 µg CH4-C g^{-1} (7.9 ± 0.5 µg CH4-C g^{-1} SOC) several orders of magnitude smaller.

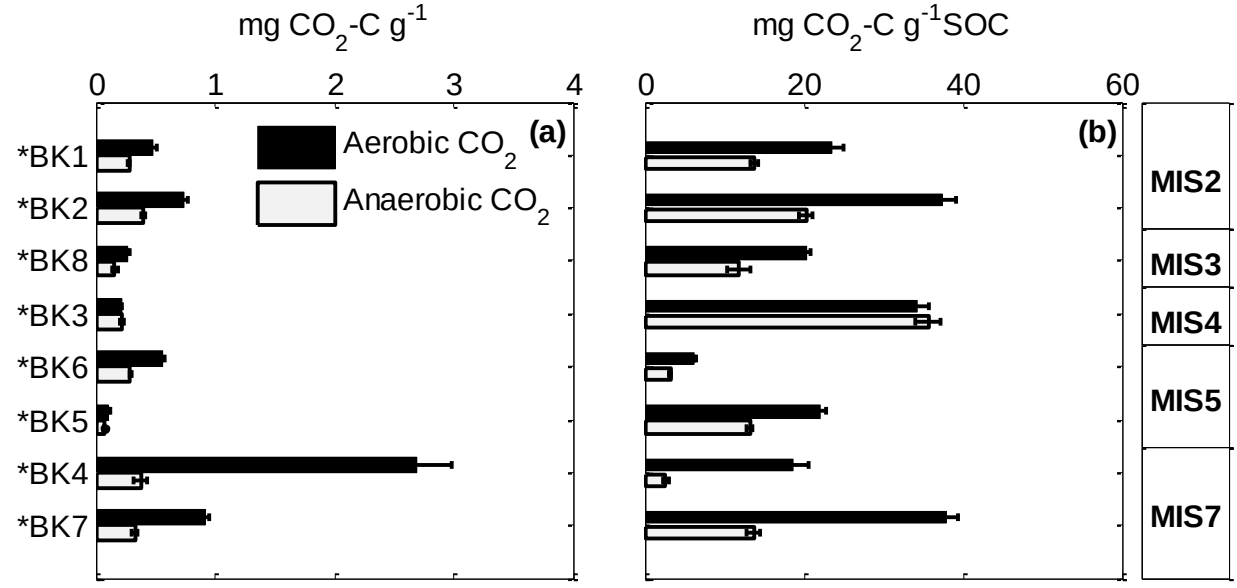

Figure 41: L14 outcrops: Total C production in different age groups after 134 incubation days at 4 °C under aerobic (a) and anaerobic (b) conditions. Data are mean values (*n* = 4) and error bars represent one standard deviation.

5.3.4 Relationship between sediment characteristics and decomposition

The sediment characteristics (%SOC, %N, C/N, $\delta^{13}C_{org}$), were variable both within the sedimentary records at one study site as well as between the study sites and followed neither a clear depth nor age trend. The highest %SOC (14.5 wt%) and %N (0.7 wt%) was measured in the Saalian peat sample (L14-11 *BK4). %SOC in the other investigated sediments ranged between 0.4–6.3 wt% (mean 2.4 ± 1.4, Figure 42), %N and C/N ranged between 0.08–0.5 wt% (0.2 ± 0.1) and 3–29 (9 ± 4), respectively, with lower values generally found in MIS5 deposits. $\delta^{13}C_{org}$ ranged between -29.0‰VPDB and -23.1‰VPDB (-26.8 ± 1.5).

The total aerobic and anaerobic CO_2 production after 134 incubation days also was highly variable between the different deposits (Figure 43) and significantly correlated with %SOC, %N, and C/N (Table 15). MIS3 deposits are preserved at all three study sites. However, aerobic CO_2 production in MIS3 deposits from Bol'shoy Lyakhovsky in the eastern Laptev Sea was nearly three times less (0.9 ± 0.5% of the initial SOC after 134 days) than what was observed for MUO12 (3.2 ± 1.6 of initial SOC) and BK8 (2.7 ± 1.1% of the initial SOC) in the central Laptev Sea.

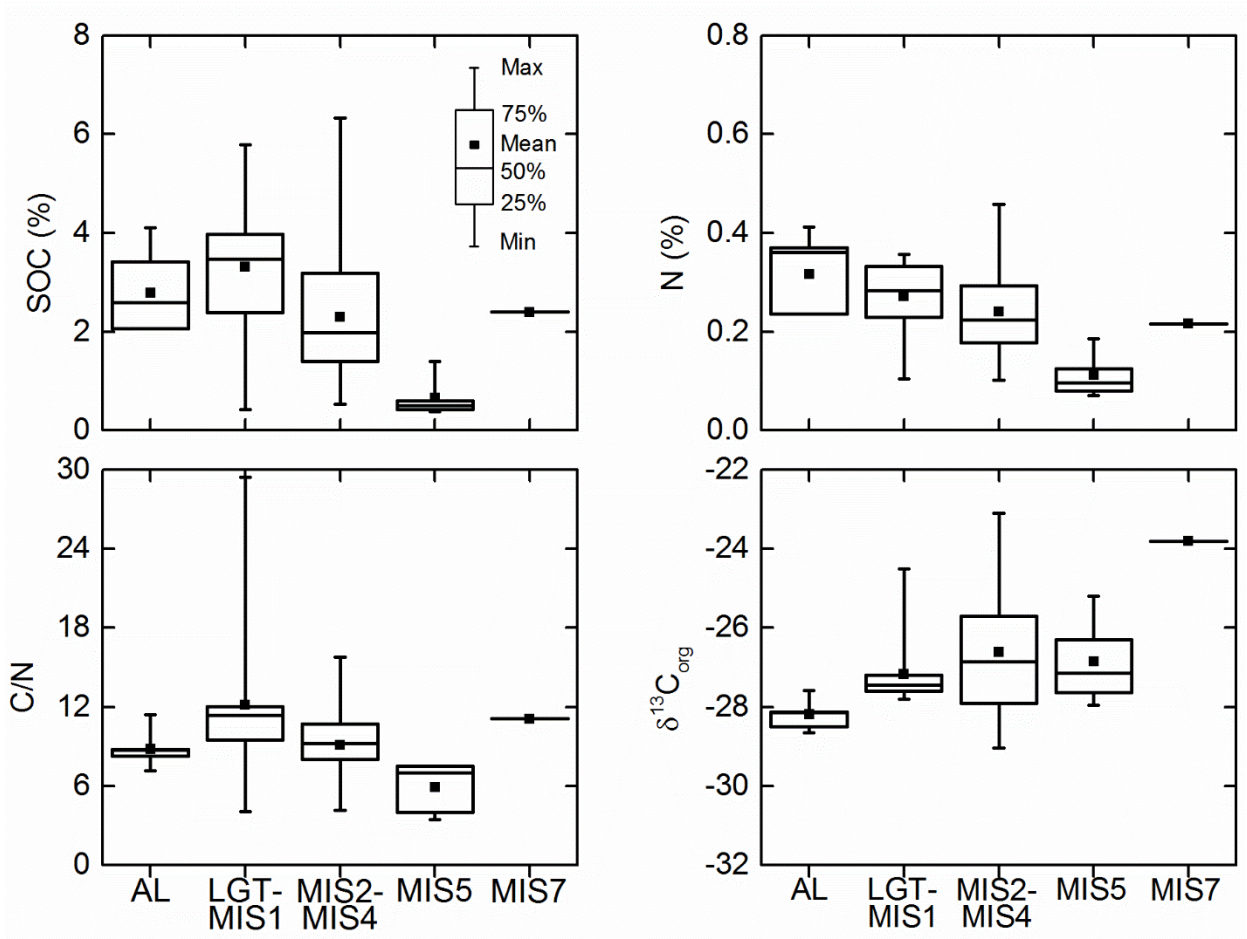

Figure 42: Boxplots of sediment characteristics for all three study sites. Samples were grouped into active layer (AL, *n* = 5), Holocene, including the late glacial transition (LGT-MIS1, *n* = 12), Yedoma IC (MIS2–MIS4, *n* = 40), Eemian lacustrine (MIS5, *n* = 6), and Saalian IC (MIS7, *n* = 1) deposits. The whiskers illustrate minimum and maximum values, while the box indicates the 25th and 75th percentiles. The vertical line inside each box is the median (50th percentile) and the square is the mean.

Table 15: Deep C: Correlation matrix for the total aerobic and anaerobic CO_2 production (log transformed) after 134 incubation days at 4 °C for all samples from Muostakh Island, the Buor Khaya Peninsula, and Bol'shoy Lyakhovsky (*n* = 197).

		%SOC	%N	C/N	$\delta^{13}C_{org}$	pH
log(aerobic CO_2-C g^{-1})	*r*	0.57	0.56	0.54	0.08	0.29
	p	0.000	0.000	0.000	0.286	0.000
log(anaerobic CO_2-C g^{-1})	*r*	0.36	0.48	0.19	0.10	0.09
	p	0.000	0.000	0.007	0.178	0.214

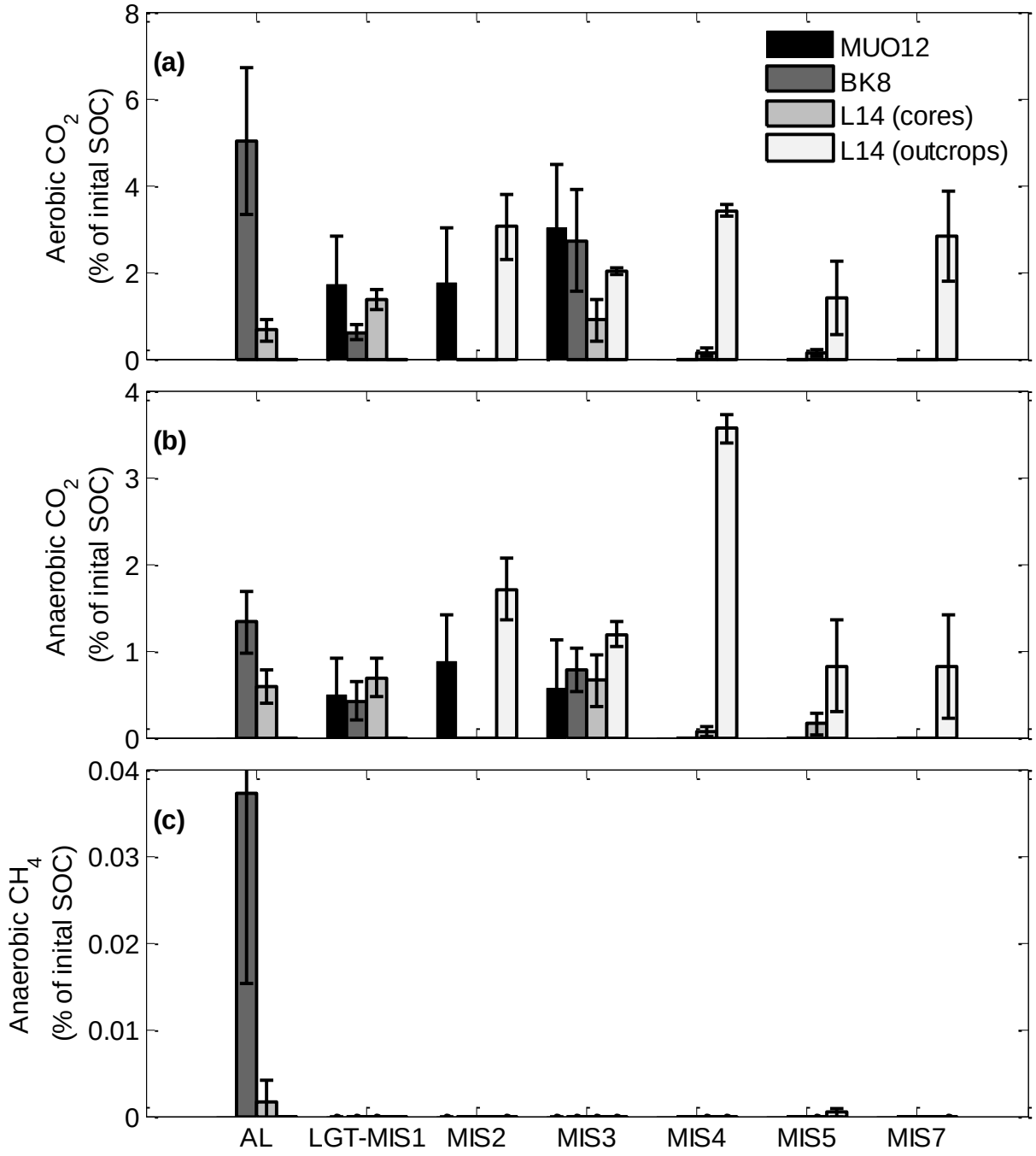

Figure 43: Deep C: Potential cumulative C release as aerobic CO_2 (a), anaerobic CO_2 (b) and anaerobic CH_4 (c) after 134 incubation days in percentage of initial soil organic carbon (SOC) content for different age groups for the three investigated study sites of Muostakh Island (MUO12), Buor Khaya Peninsula (BK8) and core and outcrop samples from Bol'shoy Lyakhovsky (L14). Data are mean values and errorbars are one standard deviation (variable *n* and replicates for different sites and periods, compare with Table 16). Note the different scales in the different panels.

Table 16: Deep C: Number of subsamples and replicates (in brackets) for sediments from marine isotope stage (MIS) MIS7–MIS1 and the active layer (AL) from Muostakh Island (MUO12), the Buor Khaya Peninsula (BK8), and core (L14 cores) and outcrop samples from Bol'shoy Lyakhovsky (l14 outcrops).

	AL	LGT-MIS1	MIS2	MIS3	MIS4	MIS5	MIS7
MUO12	-	4 (12)	6 (17)	4 (12)	-	-	-
BK8	1 (3)	6 (17)	-	13 (38)	-	-	-
L14 (cores)	4 (12)	2 (6)	-	6 (18)	6 (18)	3 (12)	-
L14 (outcrops)	-	-	2 (8)	1 (4)	1 (4)	2 (8)	2 (8)

6 Discussion

6.1 Regulation of soil organic matter decomposition in near-surface layers

The potential positive feedback between climate warming and GHG release from thawing permafrost is a topic of intensive scientific debate (Zimov *et al.*, 2006; Koven *et al.*, 2011; Schuur *et al.*, 2015). Environmental conditions in the seasonally thawed active layer and perennially frozen permafrost are substantially different and may therefore respond differently to warming-induced environmental changes (Gillespie *et al.*, 2014). It was hypothesized that older SOM currently stored in permafrost is less easily decomposable than SOM stored in the active layer. As SOM is incorporated into soils, easily decomposable OC compounds are decomposed and lost to the atmosphere. Consequently, fewer, but more stable C compounds, such as aromatic ring structures (von Lützow *et al.*, 2008), remain within soils. An increase in the stable SOM fraction within deeper permafrost soils in Siberia, Alaska, and Greenland has been shown in a study by Schädel *et al.* (2014). In the current work, significantly higher SOM decomposability was only observed in the surface active layer, while CO_2 production in soil layers below did not differ significantly from those in the permafrost. This suggests that labile C from root exudates and plant litter, which is incorporated at the soil surface where microbial abundance and diversity are also highest (Liebner *et al.*, 2008), dominates SOM turnover. Thus, most of the labile pool is decomposed in near-surface layers within one thaw period and less decomposable compounds from vascular plants and mosses are the source of deeper SOM.

Under anaerobic conditions, 2–6 times less CO_2 was produced than under aerobic conditions. Schädel *et al.* (2016) reported on average a 3.4 lower C release under anaerobic than aerobic conditions for different high-latitude ecosystems (tundra, boreal forests, and northern peatlands) and found this pattern to be independent of active layer or permafrost material as well as incubation temperature. CH_4 production in the current study was only observed after a lag phase of several days (surface active layer) to weeks (bottom active layer) to months (permafrost) and at a much lower rate than CO_2 production, most likely due to the overall low abundance of methanogenic microbes in permafrost (Waldrop *et al.*, 2010; Treat *et al.*, 2014). Initial CH_4 production in the surface active layer was high in Polygon 1, but low in Polygon 2, which can be explained by differences in the water table. While the entire active layer of Polygon 1 is water-saturated under *in situ* conditions, the water table depth in Polygon 2 is 9–12 cm bs (measured in August 2013). Under *in situ* conditions, soil microbial communities will develop depending on the environmental conditions, and increased CH_4 production under anaerobic conditions can be expected. By the end of the 1059-day incubation period, Polygon 1 and Polygon 2 had produced similar amounts of CH_4.

The late onset of CH_4 production has been observed in several anaerobic incubation studies (Waldrop *et al.*, 2010; Lee *et al.*, 2012; Lipson *et al.*, 2012; Knoblauch *et al.*, 2013; Treat *et al.*, 2014). The length of the lag time varies strongly between studies and has been discussed in detail

by Treat *et al.* (2015). For studies with incubation temperatures <10 °C, a mean lag time of 341 ± 65 days until maximum CH_4 production rates were reached has been reported (Treat *et al.*, 2015) and most studies suggest that CO_2 production dominates in permafrost-affected soils (Treat *et al.*, 2015; Schädel *et al.*, 2016). However, most of the anaerobic incubation studies are shorter than the lag time of methanogenesis and the importance of CH_4 production on time scales beyond several years remains unclear. In this work, all soil samples eventually produced CH_4. Maximum CH_4 production rates were reached after 333 ± 255 days in the active layer and 803 ± 193 days in permafrost. The increasing contribution of CH_4 with increasing incubation length shifted the relative climate forcing from being dominated by aerobic decomposition to anaerobic decomposition after ~120 days for the active layer and ~550 days in permafrost. Anaerobic decomposition processes may therefore play a more important role in some Arctic ecosystems in the long-term, than assumed previously.

Seasonal freezing and thawing characterizes the active layer. It was hypothesized that freeze-thaw cycles increase the microbial decomposition of SOM and result in short-lived bursts of GHG after thawing (Schimel & Clein, 1996; Herrmann & Witter, 2002). There are several explanations for the increase in CO_2 production after freeze-thaw cycles. In non-permafrost soils, the increase in decomposition has been related to the death of up to 50% of microorganisms and the release of easily decomposable OC compounds from lysis (Soulides & Allison, 1961). Herrmann and Witter (2002) estimated that about 65% of the CO_2-flush after a freeze-thaw cycle was due to microbial necromass. However, soil microorganisms in arctic soils are well adapted to low temperatures and prolonged freezing (Morozova & Wagner, 2007). Some studies have shown that moderate frost events (-5 °C) had no effect on microbial biomass in tundra soils (Lipson & Monson, 1998; Grogan *et al.*, 2004), while others reported a decrease in microbial biomass C after repeated moderate freeze-thaw cycles (Schimel & Clein, 1996; Larsen *et al.*, 2002). In the current study, a lower freezing temperature of -18 °C was applied, which is close to the average soil temperature during the coldest month (-24.4 °C at 20 cm depth in February) at the study site (Boike *et al.*, 2013). An increase in decomposition after one freeze-thaw cycle has only been observed in the active layer, while in the permafrost, the pronounced peaks in decomposition rates were absent after the initial thawing and only weak after one freeze-thaw cycle. The immediate start and continuous production of CO_2 after thawing, however, indicate that the microorganisms of the NE Siberian tundra survive the very low temperatures. Therefore, it seems unlikely that microbial necromass and lysis are solely responsible for the burst in GHG production after thawing. Permafrost was frozen for the longest time. If microbes would not survive the low temperatures, the large amounts of necromass should lead to a large peak in CO_2 production.

Another possible explanation for the increase in decomposition rates after thawing is the destruction of soil aggregates and exposure of previously physically protected labile substrate to microbial decomposition (van Bochove *et al.*, 2000). In experiments with repeated freeze-thaw

cycles, the size of the C-flush often decreased with each freezing event, which has been connected to the depletion of labile SOM, which is most susceptible to freeze-thaw cycles (Herrmann & Witter, 2002; Feng *et al.*, 2007). However, under *in situ* conditions, the additional input of fresh OM during each vegetation period would supply every year labile substrate to be physically broken down by frost action, resulting in a flush of CO_2 right at the beginning of each thaw period. Although the current data do not allow to identify the source of the CO_2 flush after thawing, they demonstrate the importance of freeze-thaw dynamics for SOM decomposition which should be considered for estimates of long-term GHG production in thawing permafrost-affected soils. However, an effect of freeze-thaw cycles on CH_4 production could not be shown. Rising CH_4 production rates during the incubations indicate that methanogenic communities were not substrate limited, which might explain why additional substrate availability through a freeze-thaw cycle did not increase CH_4 production.

Temperature is a main driver of microbial soil processes. It was hypothesized that less decomposable permafrost SOM is more sensitive to temperature than more decomposable active layer material. This is consistent with the third component of kinetic theory and has been shown across a range of ecosystems (Davidson & Janssens, 2006). In permafrost-affected soils, the slowly decomposing C pool has also been shown to have a higher temperature sensitivity (equal-C Q_{10} = 2.19) than the fast (1.16) decomposing C pool (Bracho *et al.*, 2016). In the current work, the lowest Q_{10} values were observed for the decomposition of small quantities of the initial SOC (<1%) and increased with increasing amounts of SOC decomposition. For different tundra ecosystems, a mean Q_{10} of 3.4 has been reported (Hamdi *et al.*, 2013). Q_{10} values in the current study ranged between 2.1–7.8, but a lower temperature range (1–8 °C) was used than most other studies from tundra soils (>10 °C). This lower temperature range might be one reason for the generally higher Q_{10} values in the current study. According to the second component of kinetic theory, temperature sensitivities exponentially increase with decreasing temperatures. SOC pools in colder regions therefore respond stronger to increasing temperatures than those in temperate environments (Kirschbaum, 1995; Hamdi *et al.*, 2013).

Estimations of temperature sensitivity are dependent on methods and assumptions (Liang *et al.*, 2015). Dutta *et al.* (2006) reported a range of equal-time Q_{10} values of 1.7–2.9 for different permafrost soils but found that rates between temperatures treatments (5–15 °C) did not differ after 200 incubation days, possibly due to the differential depletion of labile SOM at different temperatures. This suggests that SOM quality is more important than temperature and that SOM decomposition at temperatures close to freezing might not respond strongly to small temperature changes until more favorable conditions are established (Schädel *et al.*, 2014). A similar effect was observed for Samoylov samples in the current study, where decomposition of low quality permafrost SOM was similar at 1 °C and 4 °C but much higher at 8 °C (Figure 22c).

Taken together, the different responses of the active layer and shallow permafrost to warming-

induced environmental changes, suggest that thawing permafrost SOM can contribute substantially to future GHG production. Higher GHG production from these soils can be expected due to the combined effect of higher soil temperatures in the active layer and successive permafrost thaw. In the current study, aerobic CO_2 production in Samoylov polygon centers in different soil layers at different temperatures can be used for estimating the effect of thawing permafrost on total SOM decomposition under rising temperatures. The current mean active layer depth at the study site is ~50 cm (Boike *et al.*, 2013). Assuming a mean soil temperature of 4 °C for the surface active layer (0–10 cm) and 1 °C for the bottom active layer (10–50 cm), the surface active layer could potentially produce 4.5 g C kg^{-1} and the bottom active layer 0.5 g C kg^{-1} within one thaw period of 150 days. To get absolute production, potential production is multiplied with the dry bulk density (300 kg m^{-3} for the surface active layer and 500 kg m^{-3} for the bottom active layer, Zubrzycki *et al.*, 2013) and the respective layer thickness. This results in a contribution of 135 g C m^{-2} from the surface active layer and 100 g C m^{-2} from the bottom active layer and a total of 235 g C m^{-2}. No SOM decomposition is assumed in the currently frozen permafrost layer below 50 cm. In a future warmer Arctic, the active layer may deepen to 100 cm in NE Siberia until 2100 (Koven *et al.*, 2011). Assuming a future mean soil temperature of 8 °C in the surface active layer, 4 °C in the bottom active layer, and 1 °C in the newly thawed permafrost, potential production would increase to 6.5 g C kg^{-1}, 1.0 g C kg^{-1}, and 0.5 g C kg^{-1} in the respective soil layers. This would result in absolute productions of 195 g C m^{-2}, 200 g C m^{-2}, and 225 g C m^{-2} in these three soil layers (with a dry bulk density of 900 kg m^{-3} for newly thawed permafrost, Zubrzycki *et al.*, 2013) and a total of 620 g C m^{-2}. Hence, under this scenario, the newly thawed permafrost would account for 36% of total SOM decomposition.

Although laboratory results cannot be directly transferred to *in situ* conditions, they do highlight the importance of temperature effects on slow decomposing low quality C pools (Bracho *et al.*, 2016; Schädel *et al.*, 2016). In addition to SOM quality, temperature sensitivity has been shown to negatively correlate with SOC content (Balogh *et al.*, 2011). Especially in forest and grassland ecosystems, lower Q_{10} values have been observed in soils with high amounts of SOC (Hamdi *et al.*, 2013). Organic soils generally show higher greenhouse gas production than mineral soils (Schädel *et al.*, 2014), but GHG production in mineral soils, which are more wide spread in the permafrost region and contain together a larger fraction of the permafrost SOC stock (Hugelius *et al.*, 2014), may respond more strongly to warming. However, a recent study (Čapek *et al.*, 2015) reported that Q_{10} values of organic surface layers, cryoturbated, and non-cryoturbated mineral soils were not significantly different from each other.

The addition of labile plant-derived OM increased overall CO_2 production in all samples. It was hypothesized that the addition of *Carex* material would increase the decomposition of SOM in the whole soil profile. A significant change in SOM-derived CO_2 (priming effect), however, was only observed in permafrost samples. In Samoylov samples, SOM-derived CO_2 production increased

by ~15% (positive priming) compared to control incubations (Figure 26c). This suggests that soil microorganisms living in deeper soil layers with older, more degraded SOM as substrate were energy limited (Fontaine *et al.*, 2007) and that microbial activity can be stimulated by additional substrate and nutrients. In contrast, CO_2 production in amended permafrost samples from Kurungnakh decreased by 9–22% (negative priming) compared to control incubations (Figure 29b). Negative priming effects are seen as a switch in substrate utilization from less decomposable SOM to more easily decomposable substrate (Blagodatskaya & Kuzyakov, 2008). The size and direction of priming effects depend on the frequency of labile OM inputs (Fan *et al.*, 2013) as well as the amount (Blagodatskaya & Kuzyakov, 2008) and quality of the added material (Wang *et al.*, 2015a). Also, the nutrients already present in the soil can affect priming effects (Cheshire & Chapman, 1996). *In situ* nutrient availability in Arctic soils under future warming scenarios and additional inputs will therefore influence SOM turnover. Permafrost thaw can increase N availability (Natali *et al.*, 2012), which in turn has been shown to result in higher microbial activity and SOC losses in surface soils (Sistla *et al.*, 2012) as well as subsoils (Mack *et al.*, 2004). De Baets *et al.* (2016), however, observed positive priming effects in mineral and shallow permafrost soils after C additions, but simultaneous C and N additions diminished the effect. In contrast, Hartley *et al.* (2010) reported that SOM decomposition in organic surface soils did not respond to C additions, but increased by ~8% following simultaneous N and phosphor additions. In mineral soils, the increase was 57%. Similarly, a strong priming effect was observed for active layer soils as well as permafrost (Wild *et al.*, 2014, 2016) after the addition of amino acids and proteins, which increased SOM decomposition by 22–120%. Weak negative priming effects were only observed in some organic surface samples (Wild *et al.*, 2016).

Without further insight into the microbial community and growth strategies, it is difficult to deduce, why Samoylov and Kurungnakh permafrost responded differently to the addition of *Carex*. In general ecological theory, organisms pursue strategies that focus either on fast growth by utilizing easily accessible resources (*r*-strategy) or on slower growth but diversified resource use as well as the ability to utilize more complex substrate (K-strategy, Pianka, 1970). Adding labile substrate usually favors *r*-strategist, which can quickly utilize the easily decomposable substrate, but after these compounds are gone, K-strategists outcompete *r*-strategists, because they are able to also utilize more complex substrate (Fontaine *et al.*, 2003). If K-strategist then also preferentially utilize the added substrate instead to the SOM, a negative priming effect can be observed (Blagodatskaya *et al.*, 2007), especially in N-limited systems (Fontaine *et al.*, 2011; Chen *et al.*, 2014). In long-term fertilization experiments from Alaska, Campbell *et al.* (2010) showed, that the microbial community structure and function changed considerably after >5 years of nutrient additions to the soil, which resulted in a shift in microbial substrate use. For SOM decomposition with increased future nutrient availability under *in situ* conditions, more insights into the microbial community and its preferred substrates are needed.

6.2 Greenhouse gas production in degrading ice-rich permafrost deposits

The ice-rich permafrost deposits of Muostakh Island, the Buor Khaya Peninsula, and Bol'shoy Lyakhovsky are typical for NE Siberia and the sediment characteristics (%SOC, %N, C/N, $\delta^{13}C_{org}$) were all within the range of other permafrost deposits in the region (Schirrmeister *et al.*, 2011). It was hypothesized, that the climatic conditions during OM deposition affect the amount and quality of SOM and thus GHG production potentials after thaw. SOM decomposability therefore needs to be interpreted against the paleo-environmental background. In this work, it was shown that GHG production of age-diverse sediments from the MIS7–MIS1 was highly variable both within a sedimentary record as well as between the different study sites with no clear age or depth trend (Figure 43). The hypothesis could therefore only partially be confirmed for Weichselian glacial and Holocene interglacial permafrost deposits (without the active layer) from Muostakh Island and the Buor Khaya Peninsula. In both cases, higher CO_2 production was generally observed in glacial MIS3 deposits than in LGT and interglacial Holocene MIS1 deposits.

Direct measurements of CO_2 and CH_4 production potentials from degrading ice-rich permafrost in laboratory incubations are rare and require large sample amounts and long time series. Some studies have therefore investigated SOM quality in Yedoma and associated thermokarst deposits based on SOM degradation proxies, e.g. %SOC, C/N, stable isotopes, or lipid biomarkers with contradictory results. On the one hand, Strauss *et al.* (2015) report that Yedoma deposits have a lower higher-plant fatty-acid index compared to the associated thermokarst deposits, which suggests a higher degree of SOM degradation in Yedoma deposits. On the other hand, a lower carbon preference index (CPI) indicates that SOM in thermokarst deposits has undergone a higher degree of degradation than Yedoma SOM. The current work and others (e.g. Dutta *et al.*, 2006; Lee *et al.*, 2012; Knoblauch *et al.*, 2013) confirms that Yedoma deposits contain large amounts of relatively labile SOM, which can be quickly decomposed to GHG after thaw. In addition to SOM decomposition, leaching and decomposition of dissolved organic carbon (DOC) increase C losses from thawing Yedoma further (Drake *et al.*, 2015). Combined with the large areal extend of Yedoma, these regions pose a large potential C source in a warmer Arctic.

One way to analyze OM source and composition in more detail is sedimentary ancient DNA (sedaDNA), which can be used to reconstruct local plant communities. In the BK8 core, a total of 134 vascular plants and 20 bryophytes were identified through sedaDNA (Zimmermann *et al.*, 2017). *Salix*, Poaceae and Cyperaceae, whose roots are a main SOM source in tundra soils (Iversen *et al.*, 2015), are present throughout the core. The taxonomic richness was highest between 8.35–16 m bs, where also high CO_2 production was observed (Figure 35, Figure 36). This core section, which was dated to the MIS3 interstadial (54–30 ka BP, Schirrmeister *et al.*, 2017), was dominated by swamp and aquatic taxa (Zimmermann *et al.*, 2017). The widely observed occurrence of peaty layers and organic inclusions in MIS3 deposits (Schirrmeister *et al.*, 2011) and the presence of green algae and freshwater ostracods (Wetterich *et al.*, 2005,

2009) also point towards water-saturated environments, likely low-centered ice-wedge polygons, similar to modern polygonal landscapes in the study region. OM deposition in a moist anaerobic environment favored the accumulation of relatively undecomposed OM (de Klerk *et al.*, 2011), which explains the higher %SOC and higher CO_2 production potentials in MIS3 deposits. Further, high concentrations of branched glycerol dialkyl glycerol tetraether (br-GDGT), a microbial membrane compound, are indicative of an active past soil microbial community (Stapel *et al.*, 2016), which blossomed when the climate was relatively warm and wet. Overall, br-GDGT concentrations were highest at 10 m bs, 11.2 m bs, and 15 m bs (Stapel *et al.*, 2016), which corresponds to the same levels where the highest CO_2 production was observed. Decreasing abundance of swamp taxa and increasing abundance of terrestrial taxa at 8.8 m bs and >15 m bs (Zimmermann *et al.*, 2017), suggest that the shallow polygon pond intermittently dried out. This resulted in accelerated SOM decomposition under aerobic conditions prior to OM incorporation into permafrost, lower %SOC, and lower CO_2 production at these depths.

Sediments above the ice-wedge in the BK8 core showed similar %SOC, C/N, and $\delta^{13}C_{org}$ compared to the rest of the core, but SOM decomposability was consistently low in this section. This ~3 m long core section showed uniform ^{14}C ages of 11.4–10.1 ka BP (Schirrmeister *et al.*, 2017), which corresponds to the late glacial-early Holocene transition. After the LGM, temperatures in the Arctic quickly began to rise (Andreev *et al.*, 2011). Following a short period of cooling during the Younger Dryas (Renssen *et al.*, 2015), the warming trend quickly resumed, which resulted in active layer deepening and the remobilization and decomposition of large amounts of SOM between 11.7–11.1 ka BP (Tesi *et al.*, 2016). Similar conclusions are drawn for Holocene thermokarst deposits. One the one hand, they received fresh OM inputs, which explains their high %SOC (Strauss *et al.*, 2015). On the other hand, extensive thermokarst development during the early Holocene is also likely to have resulted in higher decomposition rates in thawed soils and the loss of labile SOM before the sediments were refrozen when climate conditions deteriorated after the Holocene climate optimum. If these sediments were to thaw again in the future, results from the current work suggest that the decomposability of the remaining SOC will be comparatively low. Therefore, it is concluded that climatic conditions can influence the vegetation composition on a regional level, but the local depositional environment as well as post-depositional processes are likely to control the amount and quality of the SOM that is presently incorporated into permafrost. SOM in MIS3 deposits accumulated mostly under moist conditions and was quickly frozen during IC formation (Schirrmeister *et al.*, 2011). SOM preserved in these deposits has therefore a high intrinsic quality. In contrast, deposits from the late glacial transition and early Holocene accumulated under drier conditions, labile compounds were lost prior to freezing, and only lower quality SOM remained.

For the Muostakh Island sequence, no such detailed palynological or microbial biomarker studies are yet available. The closest reference locations is the comprehensive permafrost record

at the Mamontovy Khayata section on the Bykovsky Peninsula (Andreev *et al.*, 2002a; Sher *et al.*, 2005). Sea level rise after the last glacial period, coastal erosion, and marine ingression of thermokarst depressions eventually separated Muostakh Island from the Bykovsky Peninsula (Romanovskii *et al.*, 2004; Grosse *et al.*, 2007). Today, the distance between the norther tip of Muostakh Island and the southern tip of the Bykovsky Peninsula is about 16 km (Figure 6). The distance between Muostakh Island and the Buor Khaya Peninsula is about 80 km. During the MIS4 and MIS3, fine-grained material accumulated on the large flat foreland plain of the Bykovsky Peninsula that was exposed at a time of lower sea level (Grosse *et al.*, 2007). It is therefore likely, that the SOM from the Bykovsky Peninsula, Muostakh Island, and the Buor Khaya Peninsula are of the same origin, which is supported by similar SOM decomposability. After 134 incubation days, the amount of SOM decomposition did not differ significantly (t-test, $p>0.05$) between MIS3 deposits from Muostakh Island (3.2 ± 1.6% of initial SOC aerobically and 0.7 ± 0.6% of initial SOC anaerobically) and the BK8 core (2.7 ± 1.1% of the initial SOC aerobically and 0.8 ± 0.3% of initial SOC anaerobically), which suggests that the IC deposits formed under similar environmental conditions.

A distinctive feature of the Muostakh sequence is the preservation of MIS2 deposits. Between ca 9–17 m asl, 8–9 m thick coarse-grained material was deposited in just a few thousand years between 20–16 ka BP (Meyer *et al.*, in prep). Interestingly, aerobic CO_2 production in MIS2 deposits from Muostakh Island were smaller than in MIS3 deposits, but slightly higher under anaerobic conditions (Figure 34). Pollen analysis suggest relatively cold and dry summer conditions during this stadial (Andreev *et al.*, 2002a, 2002b). Records from Kurungnakh, suggest very low pollen production and sparse vegetation cover on predominantly dry soils (Schirrmeister *et al.*, 2008; Wetterich *et al.*, 2008). Also, dung-inhabiting fungi spores suggest that large herds grazed in the area (Wetterich *et al.*, 2008). Grazing was an integral part of maintaining the steppe-tundra vegetation during the Late Pleistocene and the disappearance of large arctic mammals may have contributed to the shift to moss-tundra which currently dominates large areas in Siberia (Zimov *et al.*, 1995). In contemporary agriculture ecosystems, grazing has been shown to negatively affect SOM composition and stability (Wang *et al.*, 2015b). The limited amount of available data and spatially limited representation of MIS2 deposits, make it difficult to deduce conclusive answers.

Under aerobic conditions, the decomposability of MIS3 deposits from Bol'shoy Lyakhovsky in the Eastern Laptev Sea was nearly three times less (0.9 ± 0.5% of the initial SOC after 134 days) than what was observed for MUO12 and BK8 in the central Laptev Sea. Considerably lower temperatures and precipitation (Figure 9) characterize the modern climate on Bol'shoy Lyakhovsky. It is also likely that regional differences between the eastern and central Laptev Sea region would have affected the paleo-climate (Anderson & Lozhkin, 2001; Lozhkin & Anderson, 2011; Wetterich *et al.*, 2011, 2014). Variable summer temperatures, precipitation, thaw depth,

and vegetation composition could explain the differences in SOM quantity and quality in different locations. Interestingly, the differences in the amount of SOM that was decomposed were mostly due to differences in the initial CO_2 production rates. After 134 incubation days, the aerobic CO_2 production rates in Yedoma permafrost samples from Muostakh Island (2.3 ± 2.0 µg CO_2-C g^{-1} d^{-1}), Buor Khaya (1.6 ± 1.1 µg CO_2-C g^{-1} d^{-1}), and Bol'shoy Lyakhovsky (1.0 ± 0.6 µg CO_2-C g^{-1} d^{-1}) were all similar to each other (median 0.9 µg CO_2-C g^{-1} d^{-1}). These rates are within the range of other long-term production rates from Yedoma IC deposits in NE Siberia (Dutta *et al.*, 2006; Knoblauch *et al.*, 2013) and Alaska (Lee *et al.*, 2012). Initial GHG release from thawing permafrost will therefore likely depend on the geochemical SOM characteristics (Weiss *et al.*, 2016).

In a chronosequence (profile L7-07) close to the coring site of L14-02, Wetterich *et al.* (2014) describe continuous IC formation in the region during the MIS3, but with several meso-cycles of polygon development, evident by up to nine cryogenic horizons. This suggests that much of the cored polygon fillings from the L14-02 core, investigated in this work, accumulated under relatively wet conditions, with intermittent drier periods, especially in the upper core section (Wetterich *et al.*, 2014). For MUO12 and BK8 it was shown that SOM, which accumulated in wetter periods, was more decomposable than SOM, which accumulated under drier conditions. Similarly, the upper two samples of the L14-02 core produced less CO_2 (11–20 mg CO_2-C g^{-1} SOC aerobically, 4–6 mg CO_2-C g^{-1} SOC anaerobically) than the lowermost samples (23–45 mg CO_2-C g^{-1} SOC aerobically, 8–22 mg CO_2-C g^{-1} SOC anaerobically, Figure 39), but the overall sampling frequency of the L14-02 core was limited compared to BK8. MIS2 deposits, which were deposited under supposedly relatively dry conditions, were sampled from an outcrop. Contradictory to the hypothesis, the CO_2 production from these two samples (*BK1 and *BK2) was comparatively high compared to the L14-02 core (25–39 mg CO_2-C g^{-1} SOC aerobically, 1.4–2 mg CO_2-C g^{-1} SOC anaerobically after 134 incubation days). But the comparability of outcrop and core samples is limited. Core samples represent relatively undisturbed conditions. The bore hole temperature record shows little temperature variation at depths. Over the short monitoring period of only a few months, the permafrost temperature was ~-11 °C (Schwamborn & Wetterich, 2015), which is typical for terrestrial permafrost in Siberia (Drozdov *et al.*, 2005; Schirrmeister *et al.*, 2017). Outcrops on the other hand have already undergone significant warming. Although the upper thawed as well as the first few centimeter of frozen material was removed prior to outcrop sampling, the frozen material still has a temperature close to 0 °C, which may have already affected the microbial community. However, the outcrop sample corresponding to the MIS3 (L14-08 *BK8) also showed lower CO_2 production (23.4 ± 1.5 mg CO_2-C g^{-1} SOC aerobically, and 13.8 ± 0.4 mg CO_2-C g^{-1} SOC anaerobically after 134 incubation days). This apparent discrepancy could be a result of the before mentioned disturbance effect of outcrop samples compared to undisturbed core samples, or once again highlight the local heterogeneity, which affects the depositional environment and thus controls the amount and quality of the permafrost

SOM. The single investigated sample from the Yukagir IC (*BK7) showed the overall highest CO_2 production. However, the thickness of the Yugakir IC is only a few meters, while the Yedoma IC on Bol'shoy Lyakhovsky has an approximate thickness of 25 m (Schennen *et al.*, 2016). GHG from thawing Yedoma IC will therefore be more prominent.

All three investigated study sites are highly affected by coastal erosion, with erosion rates of 0.5–6.5 m a^{-1} (Günther *et al.*, 2013). Vonk *et al.* (2012) estimated that 66% of the SOC contained within the eroded material can be quickly decomposed and released back to the atmosphere before it is eventually reburied in the ocean. In the southern Laptev Sea, about 14 m of unfrozen redeposited terrestrial permafrost material accumulated (Overduin *et al.*, 2016). Data on GHG production from these submerged deposits are scarce (Tesi *et al.*, 2014), but thawed submarine and redeposited terrestrial permafrost material are not considered to be a major source of GHG from the Arctic shelf oceans (Overduin *et al.*, 2015). Also, the Yedoma-derived SOC deposited in Laptev Sea bottom sediments is relatively good preserved, which suggest little decomposition on land and during transport (Karlsson *et al.*, 2011). The estimated loss of SOC from thawed Yedoma by Vonk *et al.* (2012) seems therefore very high and is also considerably higher than what other studies suggest. In the current work, only 0.5–3% of the initial SOC was aerobically decomposed in Yedoma deposits within one thaw period of 134 days (anaerobically generally <1%). SOM decomposition dynamics are non-linear and turnover times of different SOC pools vary between a few months for the most labile compounds to several hundreds to thousands of years for stable and recalcitrant SOC compounds (Knoblauch *et al.*, 2013; Schädel *et al.*, 2014). In the current work, 50–80% of the total amount of CO_2 that was produced after 444 (L14) to 903 (BK8) incubation days, were already produced within the first few months of incubation. Assuming no new input of labile OM (e.g. from recent vegetation), decomposition rates are likely to remain low after the labile pool is depleted. A synthesis study of several incubations studies from high-latitude soils, including Yedoma-type deposits, estimate the size of the labile SOC pool to be generally <5% of the total SOC (Schädel *et al.*, 2014). For Yedoma deposits on Kurungnakh, Knoblauch *et al.* (2013) estimate the size of the labile pool to be even smaller (<2%). Thus, Knoblauch *et al.* (2013) report that only 15% of the SOC can be aerobcially decomposed to CO_2 over 100 years (assuming decompostion only occurs during four months per year, when the soil is not frozen). This would account for an additional C flux of 7 Pg from thawed permafrost to the atmopshere over 100 years (Knoblauch *et al.*, 2013). These numbers could be further reduced, considering, that a large proportion of passive SOC in deep mineral soils (up to 90% of the SOC) which is almost resistant to decomposition (Schädel *et al.*, 2014).

CH_4 production from deep permafrost deposits, or the lack thereof, is a highly controversial topic in permafrost sciences. In the current work, active methanogenesis was observed in most active layer samples and MIS5 Eemian lacustrine deposits. However, CH_4 production was generally several orders of magnitude lower than CO_2 production. In Yedoma deposits,

methanogenesis was only observed sporadically (5 out of 65 individual samples), which is consistent with other anaerobic Yedoma incubation studies (e.g. Knoblauch *et al.*, 2013; Lee *et al.*, 2012; Wagner *et al.*, 2007). Methanogens can cleave acetate to produce CH_4 and CO_2 (see section 0), which is the dominant methanogenic pathway in mineral permafrost-affected soils (Lee *et al.*, 2012). Chemical pore water and bulk sediment analyses showed that there are high concentrations of both free and SOM-bound acetate present in Yedoma deposits, indicating a high substrate potential for methanogenesis (Strauss *et al.*, 2015). For the BK8 site for example, SOM bound acetate concentrations of 20–30 mg L^{-1} are similar to active layer and Late Glacial-early Holocene concentrations (Stapel *et al.*, 2016), but CH_4 was produced only in the active layer. High acetate concentrations are also reported for the L14 cores (Stapel *et al.*, 2017), but no CH_4 production was observed during the 444-day incubation period, except in the active layer and lacustrine sediments. Increasing abundance of lacustrine chironomids suggest that the initial pond developed into a shallow lake, whose water depths eventually exceeded the maximum ice cover thickness (Ilyashuk *et al.*, 2006). After 444 incubation days, the Eemian lake deposits produced 3.0–262.7 µg CH_4-C g^{-1} SOC (0.4–9.3 µg CH_4-C g^{-1}). This is 18–24 times less than the production in the active layer, but highlights the importance of thermokarst lakes for CH_4 production. Thermokarst lakes have been a substantial source of CH_4 during the early Holocene (Zimov *et al.*, 1997; Walter *et al.*, 2007). But subsequent draining of many lakes during the Late Holocene (5 ka BP to present) resulted in net C-sequestration in refrozen taberal deposits (Walter Anthony *et al.*, 2014). Currently, the lake area in the Arctic is decreasing in the discontinuous permafrost zone, but increasing in the continuous permafrost zone (Smith *et al.*, 2005). Under future climate warming and renewed thermokarst activity, high levels of CH_4 production can therefore locally be expected, but are depended on favorable conditions (thawed soils, anaerobic conditions, methanogenic community present). The lacustrine sediments from the Krest-Yuryakh Suite on Bol'shoy Lyakhovsky could therefore give new insights into the long-term development of thermokarst-lake deposits in the Arctic and their role in the arctic C-cycle.

During thermokarst development, the downward progression of the thaw front would initially result in higher decomposition rates after fresh material is first made available by thaw, but CO_2 and CH_4 production rates quickly diminish with the depletion of the labile C pool (Kessler *et al.*, 2012), assuming no priming of native SOM through additional labile OM inputs. Decomposition rates immediately after thaw may further be limited by the inability of microbes to utilize the newly thawed substrate, which has been shown in a study by Ernakovich & Wallenstein (2015). They observed that permafrost microbes were not better equipped to decompose different substrates at low temperatures than active layer communities due to low functional diversity or activity. However, assuming that the lack of CH_4 production in Yedoma incubations is due to microbial rather than substrate limitations, the reproduction of ancient as well as the downward migration of recent methanogenic communities can theoretically lead to CH_4 production in these deposits.

7 Conclusion and outlook

This work advanced the understanding of GHG production potentials in thawing permafrost landscapes. The focus was twofold. First, the importance of different environmental parameters for SOM decomposition in near-surface soils was investigated. It was shown that seasonally and perennially frozen soils respond differently to freeze-thaw cycles, temperature increase, and higher labile OM availability. Decomposability was generally lower in deeper soil layers than in near-surface layers, however, permafrost SOM was more sensitive to temperature and responded stronger to labile OM additions than active layer material. The additional C release from successively thawing permafrost may therefore contribute substantially to future GHG production in tundra soils. However, the amount of C released, and whether C will be released as CO_2 or as CH_4 will largely depend on *in situ* thaw and hydrological conditions. CH_4 production in laboratory incubations was only observed after a long lag period of up to several months, possibly due to the overall low abundance of methanogenic microorganisms (Waldrop *et al.*, 2010) but, after methanogenesis was initiated, anaerobic decomposition processes soon dominated the relative climate forcing. However, it remains unclear if a viable methanogenic community can develop under *in situ* conditions or if they are outcompeted by other microbial groups.

The second focus was on the decomposability of deep permafrost SOM which formed under different climatic regimes. It could be shown, that glacial deposits often contained more labile SOC than interglacial deposits. But, strong regional differences in the decomposability of SOM from the same stratigraphic unit contort estimations of GHG production potentials. It is therefore unlikely that SOM decomposability can be generalized solely on the stratigraphic classification. CO_2 production in Yedoma IC deposits in the central Laptev Sea were nearly three times higher than in the eastern Laptev Sea region, which may be explained by regional climatic differences. The differences are further exacerbated by the influence of local depositional environments. Besides the active layer, considerable CH_4 production was only observed in Eemian lake deposits from Bol'shoy Lyakhovsky and only after several months of incubation. The depositional lake environment favored OM accumulation under anaerobic conditions and likely also froze a viable methanogenic community. Methanogenesis in Yedoma deposits was only sporadically observed (5 out of 65 individual samples), despite appropriate substrate (Stapel *et al.*, 2016, 2017).

Incubation studies are well suited to study individual processes and deconvolve the influence of different environmental drivers. However, results and conclusions drawn from soil incubations largely depend on laboratory conditions, which may differ from *in situ* conditions. The balance between pushing the system to observe warming-induced changes and choosing conditions that are relevant to the study site should be carefully considered. Long-term incubations provide a good first estimation of GHG production in thawing permafrost landscapes and are fundamental for modeling studies, but exclude complex soil-plant-atmosphere interactions. Especially the input of fresh OM from recent vegetation into the soil is often neglected. Further, more detailed chemical

analysis of SOM in permafrost-affected soils can help to better constrain the OM source as well as SOM decomposability after thaw and shed more light on SOM stabilization processes. A recent study by Gentsch *et al.* (2015) indicates that >50% of the total SOC in permafrost-affected soils in Siberia is protected from decomposition through mineral-organic associations.

Nevertheless, incubation data are useful as model input to study the bigger picture, extrapolate to less well studied regions, and project future scenarios. But, there are still several open questions that need further study to confidently project future warming-induced changes in northern ecosystems. The temperature sensitivity of anaerobic decomposition as well as the effect of labile OM input on anaerobic GHG production were not investigated in this work, but are needed to improve projections of circumpolar GHG production potentials in water-saturated compared to non-saturated soils. Also, the long-term formation of CH_4 from thawing permafrost-affected soils and sediments is one of the least understood processes. Based on only a handful of long-term (>1 year) anaerobic incubation studies, Schädel *et al.* (2016) concluded, that GHG production in permafrost-affected soils is dominated by CO_2. In the current work, however, CH_4 also contributed considerably to GHG in near-surface layers, suggesting that anaerobic decomposition processes and methanogenesis can play an important role in northern ecosystems. In recent years, the potential positive feedback between global warming and thawing of deep permafrost deposits has received more international attention. Especially improved chronostratigraphic correlation led to a better understanding of past landscape dynamics. However, the uneven distribution, sedimentary discordances, and sometimes poorly constrained ages hinder the understanding of spatial and temporal local and regional patterns. Some of these issues could be partially remedied by better accessibility to the Russian literature. Last, but not least, only GHG production was investigated, but not the plant-uptake of GHG and how this affects the C-balance of high-latitude ecosystems.

References

Abbott BW, Jones JB, Schuur EAG et al. (2016) Biomass offsets little or none of permafrost carbon release from soils, streams, and wildfire: An expert assessment. *Environmental Research Letters*, **11**, 34014.

Ainsworth EA, Long SP (2004) What have we learned from 15 years of free-air CO_2 enrichment (FACE)? A meta-analytic review of the responses of photosynthesis, canopy properties and plant production to rising CO_2. *New Phytologist*, **165**, 351–372.

Allison SD, Treseder KK (2011) Climate change feedbacks to microbial decomposition in boreal soils. *Fungal Ecology*, **4**, 362–374.

Anderson PM, Lozhkin AV (2001) The Stage 3 interstadial complex (Karginskii/middle Wisconsinan interval) of Beringia: variations in paleoenvironments and implications for paleoclimatic interpretations. *Quaternary Science Reviews*, **20**, 93–125.

Andreev AA, Schirrmeister L, Siegert C, Bobrov AA, Demske D, Seiffert M, Hubberten H-W (2002a) Paleoenvironmental changes in northeastern Siberia during the Late Quaternary - Evidence from pollen records of the Bykovsky Peninsula. *Polarforschung*, **70**, 13–25.

Andreev AA, Siegert C, Klimanov VA, Derevyagin AY, Shilova GN, Melles M (2002b) Late Pleistocene and Holocene vegetation and climate on the Taymyr Lowland, Northern Siberia. *Quaternary Research*, **57**, 138–150.

Andreev A, Grosse G, Schirrmeister L et al. (2004) Late Saalian and Eemian palaeoenvironmental history of the Bol'shoy Lyakhovsky Island (Laptev Sea region, Arctic Siberia). *Boreas*, **33**, 319–348.

Andreev AA, Grosse G, Schirrmeister L et al. (2009) Weichselian and Holocene palaeoenvironmental history of the Bol'shoy Lyakhovsky Island, New Siberian Archipelago, Arctic Siberia. *Boreas*, **38**, 72–110.

Andreev AA, Schirrmeister L, Tarasov PE et al. (2011) Vegetation and climate history in the Laptev Sea region (Arctic Siberia) during Late Quaternary inferred from pollen records. *Quaternary Science Reviews*, **30**, 2182–2199.

Anisimov OA, Nelson FE (1997) Permafrost zonation and climate change in the Northern Hemisphere: Results from transient general circulation models. *Climatic Change*, **35**, 241–258.

De Baets S, van de Weg MJ, Lewis R et al. (2016) Investigating the controls on soil organic matter decomposition in tussock tundra soil and permafrost after fire. *Soil Biology and Biochemistry*, **99**, 108–116.

Balogh J, Pintér K, Fóti S, Cserhalmi D, Papp M, Nagy Z (2011) Dependence of soil respiration on soil moisture, clay content, soil organic matter, and CO_2 uptake in dry grasslands. *Soil Biology and Biochemistry*, **43**, 1006–1013.

Bauch H., Mueller-Lupp T, Taldenkova E et al. (2001) Chronology of the Holocene transgression at the North Siberian margin. *Global and Planetary Change*, **31**, 125–139.

Bingeman CW, Varner JE, Martin WP (1953) The effect of the addition of organic materials on the decomposition of an organic soil. *Soil Science Society of America Journal*, **17**, 34.

Blagodatskaya E, Kuzyakov Y (2008) Mechanisms of real and apparent priming effects and their dependence on soil microbial biomass and community structure: critical review. *Biology and Fertility of Soils*, **45**, 115–131.

Blagodatskaya EV, Blagodatsky SA, Anderson T-H, Kuzyakov Y (2007) Priming effects in Chernozem induced by glucose and N in relation to microbial growth strategies. *Applied Soil Ecology*, **37**, 95–105.

van Bochove E, Pre´vost D, Pelletier F (2000) Effects of freeze–thaw and soil structure on nitrous oxide produced in a clay soil. *Soil Science Society of America Journal*, **64**, 1638.

Bockheim JG (2007) Importance of cryoturbation in redistributing organic carbon in permafrost-affected soils. *Soil Science Society of America Journal*, **71**, 1335.

Böhme L (2015) *Einfluss von Temperatur und Zugabe von frischem organischen Material auf den Kohlenstoffabbau in permafrostbeeinflussten Böden und Sedimenten*. Master Thesis, Universität Hamburg, 58 pp.

Boike J, Kattenstroth B, Abramova K et al. (2013) Baseline characteristics of climate, permafrost and land cover from a new permafrost observatory in the Lena River Delta, Siberia (1998–2011). *Biogeosciences*, **10**, 2105–2128.

Bolshiyanov D, Makarov A, Savelieva L (2015) Lena River delta formation during the Holocene. *Biogeosciences*, **12**, 579–593.

Bracho R, Natali S, Pegoraro E et al. (2016) Temperature sensitivity of organic matter decomposition of permafrost-region soils during laboratory incubations. *Soil Biology and Biochemistry*, **97**, 1–14.

Brown J, Ferrians Jr OJ, Heginbottom JA, Melnikov ES (1998) Circum-Arctic map of permafrost and ground-ice conditions. Boulder, CO: National Snow and Ice Data Center/World Data Center for Glaciology. *Digital media*.

Bulygina ON, Razuvaev VN (2012) *Daily temperature and precipitation data for 518 Russian meteorological stations*. Carbon Dioxide Information Analysis Center, Oak Ridge National Laboratory, U.S. Department of Energy, Oak Ridge, Tennessee (USA).

Campbell BJ, Polson SW, Hanson TE, Mack MC, Schuur EAG (2010) The effect of nutrient deposition on bacterial communities in Arctic tundra soil. *Environmental Microbiology*, **12**, 1842–1854.

Čapek P, Diáková K, Dickopp J-E et al. (2015) The effect of warming on the vulnerability of subducted organic carbon in arctic soils. *Soil Biology and Biochemistry*, **90**, 19–29.

Carroll JJ, Slupsky JD, Mather AE (1991) The solubility of carbon dioxide in water at low pressure. *Journal of Physical and Chemical Reference Data*, **20**, 1201.

CAVM Team (2003) *Circumpolar Arctic Vegetation Map (1:7,500,000 scale), Conservation of Arctic Flora and Fauna (CAFF) Map No. 1*. U.S. Fish and Wildlife Service, Anchorage, Alaska.

Chen R, Senbayram M, Blagodatsky S et al. (2014) Soil C and N availability determine the priming effect: Microbial N mining and stoichiometric decomposition theories. *Global Change Biology*, **20**, 2356–2367.

Cheshire M V., Chapman SJ (1996) Influence of the N and P status of plant material and of added N and P on the mineralization of C from ^{14}C-labelled ryegrass in soil. *Biology and Fertility of Soils*, **21**, 166–170.

Conant RT, Drijber RA, Haddix ML et al. (2008) Sensitivity of organic matter decomposition to warming varies with its quality. *Global Change Biology*, **14**, 868–877.

Davidson EA, Janssens IA (2006) Temperature sensitivity of soil carbon decomposition and feedbacks to climate change. *Nature*, **440**, 165–173.

Delisle G (2007) Near-surface permafrost degradation: How severe during the 21st century? *Geophysical Research Letters*, **34**, L09503.

Dorrepaal E, Toet S, van Logtestijn RSP, Swart E, van de Weg MJ, Callaghan T V., Aerts R (2009) Carbon respiration from subsurface peat accelerated by climate warming in the subarctic. *Nature*, **460**, 616–619.

Drake TW, Wickland KP, Spencer RGM, McKnight DM, Striegl RG (2015) Ancient low–molecular-weight organic acids in permafrost fuel rapid carbon dioxide production upon thaw. *Proceedings of the National Academy of Sciences*, **112**, 13946–13951.

Drozdov DS, Rivkin FM, Rachold V et al. (2005) Electronic atlas of the Russian Arctic coastal zone. *Geo-Marine Letters*, **25**, 81–88.

Dutta K, Schuur EAG, Neff JC, Zimov SA (2006) Potential carbon release from permafrost soils of Northeastern Siberia. *Global Change Biology*, **12**, 2336–2351.

Elberling B, Michelsen A, Schädel C et al. (2013) Long-term CO_2 production following permafrost thaw. *Nature Climate Change*, **3**, 890–894.

Ernakovich JG, Wallenstein MD (2015) Permafrost microbial community traits and functional diversity indicate low activity at in situ thaw temperatures. *Soil Biology and Biochemistry*, **87**, 78–89.

Euskirchen ES, Mcguire AD, Kicklighter DW et al. (2006) Importance of recent shifts in soil thermal dynamics on growing season length, productivity, and carbon sequestration in terrestrial high-latitude ecosystems. *Global Change Biology*, **12**, 731–750.

van Everdingen R (2005) Multi-language glossary of permafrost and related ground-ice terms.

Fan Z, Jastrow JD, Liang C, Matamala R, Miller RM (2013) Priming effects in boreal black spruce forest soils: Quantitative evaluation and sensitivity analysis. *PLoS ONE*, **8**, e77880.

FAO (2006) *Guidelines for soil description*, 4th edn. Food and Agriculture Organization of the United Nations, Rome.

Feng X, Nielsen LL, Simpson MJ (2007) Responses of soil organic matter and microorganisms to freeze–thaw cycles. *Soil Biology and Biochemistry*, **39**, 2027–2037.

Fontaine S, Mariotti A, Abbadie L (2003) The priming effect of organic matter: A question of microbial competition? *Soil Biology and Biochemistry*, **35**, 837–843.

Fontaine S, Bardoux G, Abbadie L, Mariotti A (2004) Carbon input to soil may decrease soil carbon content. *Ecology Letters*, **7**, 314–320.

Fontaine S, Barot S, Barré P, Bdioui N, Mary B, Rumpel C (2007) Stability of organic carbon in deep soil layers controlled by fresh carbon supply. *Nature*, **450**, 277–280.

Fontaine S, Henault C, Aamor A et al. (2011) Fungi mediate long term sequestration of carbon and nitrogen in soil through their priming effect. *Soil Biology and Biochemistry*, **43**, 86–96.

Froese DG, Westgate JA, Reyes A V., Enkin RJ, Preece SJ (2008) Ancient permafrost and a future, warmer Arctic. *Science*, **321**, 1648–1648.

Gentsch N, Mikutta R, Alves RJE et al. (2015) Storage and transformation of organic matter fractions in cryoturbated permafrost soils across the Siberian Arctic. *Biogeosciences*, **12**, 4525–4542.

Gerasimova M (2001) *Russian soil classification system.* (ed Arnold RW). VV Dokuchaev Soil Science Institute, Moscow (Russian Federation), 220 pp.

Gilichinsky D, Wagener S (1995) Microbial life in permafrost: A historical review. *Permafrost and Periglacial Processes*, **6**, 243–250.

Gillespie AW, Sanei H, Diochon A et al. (2014) Perennially and annually frozen soil carbon differ in their susceptibility to decomposition: Analysis of Subarctic earth hummocks by bioassay, XANES and pyrolysis. *Soil Biology and Biochemistry*, **68**, 106–116.

Gorham E (1991) Northern peatlands: Role in the carbon cycle and probable responses to climatic warming. *Ecological Applications*, **1**, 182–195.

Grigoriev MN (1993) Cryomorphogenesis in the Lena Delta. *Yakutsk: Permafrost Institute Press (in Russian)*.

Grigoriev MN, Overduin PP, Schirrmeister L, Wetterich S (2013) Scientific permafrost drilling campaign. In: *Russian-German cooperation SYSTEM LAPTEV SEA : The Expeditions Laptev Sea - Mamontov Klyk 2011 & Buor Khaya 2012*, 664th edn, Vol. 664 (eds Günther F, Overduin PP, Makarov AS, Grigoriev MN), pp. 75–86. Berichte der Polarforschung.

Grogan P, Michelsen A, Ambus P, Jonasson S (2004) Freeze–thaw regime effects on carbon and nitrogen dynamics in sub-arctic heath tundra mesocosms. *Soil Biology and Biochemistry*, **36**, 641–654.

Grosse G, Schirrmeister L, Siegert C, Kunitsky V V., Slagoda EA, Andreev AA, Dereviagyn AY (2007) Geological and geomorphological evolution of a sedimentary periglacial landscape in Northeast Siberia during the Late Quaternary. *Geomorphology*, **86**, 25–51.

Grosse G, Robinson JE, Bryant R et al. (2013) *Distribution of late Pleistocene ice-rich syngenetic permafrost of the Yedoma Suite in east and central Siberia, Russia*. 1-37 pp.

Günther F, Overduin PP, Sandakov a. V., Grosse G, Grigoriev MN (2013) Short- and long-term thermo-erosion of ice-rich permafrost coasts in the Laptev Sea region. *Biogeosciences*, **10**, 4297–4318.

Günther F, Overduin PP, Yakshina IA, Opel T, Baranskaya A V., Grigoriev MN (2015) Observing Muostakh disappear: Permafrost thaw subsidence and erosion of a ground-ice-rich island in response to arctic summer warming and sea ice reduction. *The Cryosphere*, **9**, 151–178.

Gupta V, Smemo KA, Yavitt JB, Fowle D, Branfireun B, Basiliko N (2013) Stable isotopes reveal widespread anaerobic methane oxidation across latitude and peatland type. *Environmental Science & Technology*, 130717064455005.

Hamdi S, Moyano F, Sall S, Bernoux M, Chevallier T (2013) Synthesis analysis of the temperature sensitivity of soil respiration from laboratory studies in relation to incubation methods and soil conditions. *Soil Biology and Biochemistry*, **58**, 115–126.

Harden JW, Koven CD, Ping C-L et al. (2012) Field information links permafrost carbon to physical vulnerabilities of thawing. *Geophysical Research Letters*, **39**, 1–6.

Hartley IP, Hopkins DW, Sommerkorn M, Wookey PA (2010) The response of organic matter mineralisation to nutrient and substrate additions in sub-arctic soils. *Soil Biology and Biochemistry*, **42**, 92–100.

Herrmann A, Witter E (2002) Sources of C and N contributing to the flush in mineralization upon freeze–thaw cycles in soils. *Soil Biology and Biochemistry*, **34**, 1495–1505.

Hobbie SE, Schimel JP, Trumbore SE, Randerson JR (2000) Controls over carbon storage and turnover in high-latitude soils. *Global Change Biology*, **6**, 196–210.

Hugelius G, Routh J, Kuhry P, Crill P (2012) Mapping the degree of decomposition and thaw remobilization potential of soil organic matter in discontinuous permafrost terrain. *Journal of Geophysical Research: Biogeosciences*, **117**, G02030.

Hugelius G, Strauss J, Zubrzycki S et al. (2014) Estimated stocks of circumpolar permafrost carbon with quantified uncertainty ranges and identified data gaps. *Biogeosciences*, **11**, 6573–6593.

Ilyashuk BP, Andreev AA, Bobrov AA, Tumskoy VE, Ilyashuk EA (2006) Interglacial history of a palaeo-lake and regional environment: A multi-proxy study of a permafrost deposit from Bol'shoy Lyakhovsky Island, Arctic Siberia. *Journal of Paleolimnology*, **35**, 855–872.

IUSS Working Group WRB (2014) *World Reference Base for Soil Resources 2014. International soil classification system for naming soils and creating legends for soil maps*. World Soil Resources Reports No. 106. FAO, Rome.

Iversen CM, Sloan VL, Sullivan PF et al. (2015) The unseen iceberg: Plant roots in arctic tundra. *New Phytologist*, **205**, 34–58.

Jastrow JD, Michael Miller R, Matamala R, Norby RJ, Boutton TW, Rice CW, Owensby CE (2005) Elevated atmospheric carbon dioxide increases soil carbon. *Global Change Biology*, **11**, 2057–2064.

Jones BM, Arp CD, Jorgenson MT, Hinkel KM, Schmutz JA, Flint PL (2009) Increase in the rate and uniformity of coastline erosion in Arctic Alaska. *Geophysical Research Letters*, **36**, n/a-n/a.

Jorgenson MT, Romanovsky V, Harden J et al. (2010) Resilience and vulnerability of permafrost to climate change. *Canadian Journal of Forest Research*, **40**, 1219–1236.

Kaiser C, Meyer H, Biasi C, Rusalimova O, Barsukov P, Richter A (2007) Conservation of soil organic matter through cryoturbation in arctic soils in Siberia. *Journal of Geophysical Research*, **112**, G02017.

Kanevskiy M, Shur Y, Fortier D, Jorgenson MT, Stephani E (2011) Cryostratigraphy of late Pleistocene syngenetic permafrost (yedoma) in northern Alaska, Itkillik River exposure. *Quaternary Research*, **75**, 584–596.

Karlsson ES, Charkin A, Dudarev O et al. (2011) Carbon isotopes and lipid biomarker investigation of sources, transport and degradation of terrestrial organic matter in the Buor-Khaya Bay, SE Laptev Sea. *Biogeosciences*, **8**, 1865–1879.

Kessler MA, Plug LJ, Walter Anthony KM (2012) Simulating the decadal- to millennial-scale dynamics of morphology and sequestered carbon mobilization of two thermokarst lakes in NW Alaska. *Journal of Geophysical Research: Biogeosciences*, **117**, G00M06.

Kienast F, Tarasov P, Schirrmeister L, Grosse G, Andreev AA (2008) Continental climate in the East Siberian Arctic during the last interglacial: Implications from palaeobotanical records. *Global and Planetary Change*, **60**, 535–562.

Kienast F, Wetterich S, Kuzmina S et al. (2011) Paleontological records indicate the occurrence of open woodlands in a dry inland climate at the present-day Arctic coast in western Beringia during the Last Interglacial. *Quaternary Science Reviews*, **30**, 2134–2159.

Kirschbaum MUF (1995) The temperature dependence of soil organic matter decomposition, and the effect of global warming on soil organic C storage. *Soil Biology and Biochemistry*, **27**, 753–760.

de Klerk P, Donner N, Karpov NS, Minke M, Joosten H (2011) Short-term dynamics of a low-centred ice-wedge polygon near Chokurdakh (NE Yakutia, NE Siberia) and climate change during the last ca 1250 years. *Quaternary Science Reviews*, **30**, 3013–3031.

Knoblauch C, Beer C, Sosnin A, Wagner D, Pfeiffer E-M (2013) Predicting long-term carbon mineralization and trace gas production from thawing permafrost of Northeast Siberia. *Global Change Biology*, **19**, 1160–1172.

Knoblauch C, Spott O, Evgrafova S, Kutzbach L, Pfeiffer E-M (2015) Regulation of methane production, oxidation, and emission by vascular plants and bryophytes in ponds of the northeast Siberian polygonal tundra. *Journal of Geophysical Research: Biogeosciences*, **120**, 2525–2541.

Knorr W, Prentice IC, House JI, Holland EA (2005) Long-term sensitivity of soil carbon turnover to warming. *Nature*, **433**, 298–301.

Kong AYY, Six J, Bryant DC, Denison RF, van Kessel C (2005) The relationship between carbon input, aggregation, and soil organic carbon stabilization in sustainable cropping systems. *Soil Science Society of America Journal*, **69**, 1078–1085.

Koven CD, Ringeval B, Friedlingstein P et al. (2011) Permafrost carbon-climate feedbacks accelerate global warming. *Proceedings of the National Academy of Sciences*, **108**, 14769–14774.

Kruse S, Wieczorek M, Jeltsch F, Herzschuh U (2016) Treeline dynamics in Siberia under changing climates as inferred from an individual-based model for Larix. *Ecological Modelling*, **338**, 101–121.

Kunitsky V, Schirrmeister L, Grosse G et al. (2000) Paleoclimate signals of ice-rich permafrost deposits. In: *Russian-German Cooperation SYSTEM LAPTEV SEA 2000: The Expedition Lena 1999*, 354th edn (eds Rachold V, Grigoriev MN), pp. 113–269. Berichte der Polarforschung.

Kutzbach L, Wagner D, Pfeiffer E-M (2004) Effect of microrelief and vegetation on methane emission from wet polygonal tundra, Lena Delta, Northern Siberia. *Biogeochemistry*, **69**, 341–362.

Kuzyakov Y (2010) Priming effects: Interactions between living and dead organic matter. *Soil Biology and Biochemistry*, **42**, 1363–1371.

Kuzyakov Y, Friedel J., Stahr K (2000) Review of mechanisms and quantification of priming effects. *Soil Biology and Biochemistry*, **32**, 1485–1498.

Larsen KS, Jonasson S, Michelsen A (2002) Repeated freeze–thaw cycles and their effects on biological processes in two arctic ecosystem types. *Applied Soil Ecology*, **21**, 187–195.

Lawrence DM, Slater AG (2005) A projection of severe near-surface permafrost degradation during the 21st century. *Geophysical Research Letters*, **32**, L24401.

Lee H, Schuur EAG, Inglett KS, Lavoie M, Chanton JP (2012) The rate of permafrost carbon release under aerobic and anaerobic conditions and its potential effects on climate. *Global Change Biology*, **18**, 515–527.

Lehner B, Döll P (2004) Development and validation of a global database of lakes, reservoirs and wetlands. *Journal of Hydrology*, **296**, 1–22.

Liang J, Li D, Shi Z et al. (2015) Methods for estimating temperature sensitivity of soil organic matter based on incubation data: A comparative evaluation. *Soil Biology and Biochemistry*, **80**, 127–135.

Liebner S, Harder J, Wagner D (2008) Bacterial diversity and community structure in polygonal tundra soils from Samoylov Island, Lena Delta, Siberia. *International Microbiology*, **11**, 195–202.

Lipson DA, Monson RK (1998) Plant-microbe competition for soil amino acids in the alpine tundra: Effects of freeze-thaw and dry-rewet events. *Oecologia*, **113**, 406–414.

Lipson DA, Zona D, Raab TK, Bozzolo F, Mauritz M, Oechel WC (2012) Water-table height and microtopography control biogeochemical cycling in an Arctic coastal tundra ecosystem. *Biogeosciences*, **9**, 577–591.

Lozhkin A V., Anderson PM (2011) Forest or no forest: Implications of the vegetation record for climatic stability in Western Beringia during oxygen isotope stage 3. *Quaternary Science Reviews*, **30**, 2160–2181.

Luo Y, Zhou X (2006) *Soil respiration and the environment*. Academic Press/Elsevier, San Diego, CA, USA, 328 pp.

von Lützow M, Kögel-Knabner I, Ludwig B et al. (2008) Stabilization mechanisms of organic matter in four temperate soils: Development and application of a conceptual model. *Journal of Plant Nutrition and Soil Science*, **171**, 111–124.

MacDougall AH, Knutti R (2016) Projecting the release of carbon from permafrost soils using a perturbed parameter ensemble modelling approach. *Biogeosciences*, **13**, 2123–2136.

MacDougall AH, Avis CA, Weaver AJ (2012) Significant contribution to climate warming from the permafrost carbon feedback. *Nature Geoscience*, **5**, 719–721.

Mack MC, Schuur EAG, Bret-Harte MS, Shaver GR, Chapin FS (2004) Ecosystem carbon storage in arctic tundra reduced by long-term nutrient fertilization. *Nature*, **431**, 440–443.

Mahecha MD, Reichstein M, Carvalhais N et al. (2010) Global convergence in the temperature sensitivity of respiration at ecosystem level. *Science*, **329**, 838–840.

Matzner E, Borken W (2008) Do freeze-thaw events enhance C and N losses from soils of different ecosystems? A review. *European Journal of Soil Science*, **59**, 274–284.

Megonigal JP, Hines ME, Visscher PT (2004) Anaerobic metabolism: Linkages to trace gases and aerobic processes. In: *Biogeochemistry*, Vol. 8 edn (eds Schlesinger WH, Holland HD, Turekian KK), pp. 317–424. Elsevier-Pergamon, Oxford, UK.

Meyer H, Opel T, Derevyagin AY et al. Late Quaternary palaeo-environmental history of Muostakh Island, Northern Siberia based on sedimentological and geocryological studies. (in prep).

Meyer H, Dereviagin A, Syromyatnikov I (2000) Paleoclimate signals of ice-rich permafrost deposits: Ground ice and water. In: *Russian-German Cooperation SYSTEM LAPTEV SEA 2000: The Expedition Lena 1999*, 354th edn (eds Rachold V, Grigoriev MN). Berichte der Polarforschung.

Meyer H, Dereviagin A, Siegert C, Schirrmeister L, Hubberten H-W (2002a) Palaeoclimate reconstruction on Big Lyakhovsky Island, north Siberia - Hydrogen and oxygen isotopes in ice wedges. *Permafrost and Periglacial Processes*, **13**, 91–105.

Meyer H, Derevyagin AY, Siegert C, Hubberten H-W (2002b) Paleoelimate studies on Bykovsky Peninsula, north Siberia - Hydrogen and oxygen isotopes in ground ice. *Polarforschung*, **70**, 37–51.

Meyer H, Opel T, Laepple T, Dereviagin AY, Hoffmann K, Werner M (2015a) Long-term winter warming trend in the Siberian Arctic during the mid- to late Holocene. *Nature Geoscience*, **8**, 122–125.

Meyer H, Opel T, Dereviagin A (2015b) Stratigraphic and sedimentological studies. In: *Russian-German Cooperation SYSTEM LAPTEV SEA: The expedition Lena 2012*, pp. 79–82. Berichte der Polarforschung.

Millero F, Huang F, Graham T, Pierrot D (2007) The dissociation of carbonic acid in NaCl solutions as a function of concentration and temperature. *Geochimica et Cosmochimica Acta*, **71**, 46–55.

Morgenstern A, Grosse G, Günther F, Fedorova I, Schirrmeister L (2011) Spatial analyses of thermokarst lakes and basins in Yedoma landscapes of the Lena Delta. *The Cryosphere*, **5**, 849–867.

Morgenstern A, Ulrich M, Günther F et al. (2013) Evolution of thermokarst in East Siberian ice-rich permafrost: A case study. *Geomorphology*, **201**, 363–379.

Morgenstern A, Grosse G, Arcos DR, Günther F, Overduin P, Schirrmeister L (2017) The role of thermal erosion in the degradation of Siberian ice-rich permafrost. *Journal of Geophysical Research: Earth Surface*, (in review).

Morozova D, Wagner D (2007) Stress response of methanogenic archaea from Siberian permafrost compared with methanogens from nonpermafrost habitats. *FEMS Microbiology Ecology*, **61**, 16–25.

Myers-Smith IH, Forbes BC, Wilmking M et al. (2011) Shrub expansion in tundra ecosystems: Dynamics, impacts and research priorities. *Environmental Research Letters*, **6**, 45509.

Myhre G, Shindell D, Breon F-M et al. (2013) Anthropogenic and natural radiative forcing. In: *Climate Change 2013 - The Physical Science Basis* (ed Intergovernmental Panel on Climate Change), pp. 659–740. Cambridge University Press, Cambridge.

Naidina OD, Bauch HA (2001) A Holocene pollen record from the Laptev Sea shelf, northern Yakutia. *Global and Planetary Change*, **31**, 141–153.

Natali SM, Schuur EAG, Rubin RL (2012) Increased plant productivity in Alaskan tundra as a result of experimental warming of soil and permafrost. *Journal of Ecology*, **100**, 488–498.

Oechel WC, Hastings SJ, Vourlrtis G, Jenkins M, Riechers G, Grulke N (1993) Recent change of Arctic tundra ecosystems from a net carbon dioxide sink to a source. *Nature*, **361**, 520–523.

Opel T (2015) Russian-German cooperation SYSTEM LAPTEV SEA: The expedition Lena 2012. *Berichte zur Polar- und Meeresforschung = Reports on polar and marine research*, **684**, 1–104.

Opel T, Wetterich S, Meyer H, Dereviagin AY, Fuchs MC, Schirrmeister L (2017) Ground-ice stable isotopes and cryostratigraphy reflect late Quaternary palaeoclimate in the Northeast Siberian Arctic (Oyogos Yar coast, Dmitry Laptev Strait). *Climate of the Past Discussions*, 1–37.

Osterkamp TE, Romanovsky VE (1999) Evidence for warming and thawing of discontinuous permafrost in Alaska. *Permafrost and Periglacial Processes*, **10**, 17–37.

Overduin PP, Liebner S, Knoblauch C et al. (2015) Methane oxidation following submarine permafrost degradation: Measurements from a central Laptev Sea shelf borehole. *Journal of Geophysical Research: Biogeosciences*, **120**, 1–14.

Overduin PP, Wetterich S, Günther F et al. (2016) Coastal dynamics and submarine permafrost in shallow water of the central Laptev Sea, East Siberia. *The Cryosphere*, **10**, 1449–1462.

Pfeiffer E-M, Wagner D, Kobabe S, Kutzbach L, Kurchatova A, Stoof G, Wille C (2002) Modern processes in permafrost affected soils. *Reports on Polar Research*, **426**, 21–41.

Pianka ER (1970) On r- and K-Selection. *The American Naturalist*, **104**, 592–597.

Pitul'ko VV, Pavlova EY, Kuz'mina SA, Nikol'skii PA, Basilyan AE, Tumskoi VE, Anisimov MA (2007) Natural-climatic changes in the Yana-Indigirka lowland during the terminal Kargino time and habitat of late Paleolithic man in northern part of East Siberia. *Doklady Earth Sciences*, **417**, 1256–1260.

Preuss I, Knoblauch C, Gebert J, Pfeiffer E-M (2013) Improved quantification of microbial CH_4 oxidation efficiency in arctic wetland soils using carbon isotope fractionation. *Biogeosciences*, **10**, 2539–2552.

Rachold V, Grigoriev MN, Are FE, Solomon S, Reimnitz E, Kassens H, Antonow M (2000) Coastal erosion vs riverine sediment discharge in the Arctic Shelf seas. *International Journal of Earth Sciences*, **89**, 450–460.

Reeburgh WS, Whalen SC, Alperin MJ (1993) The role of methylotrophy in the global methane budget. *Microbial growth on C1 compounds*, 1–14.

Renssen H, Mairesse A, Goosse H et al. (2015) Multiple causes of the Younger Dryas cold period. *Nature Geoscience*, **8**, 946–949.

Rey A, Jarvis P (2006) Modelling the effect of temperature on carbon mineralization rates across a network of European forest sites (FORCAST). *Global Change Biology*, **12**, 1894–1908.

Rivkina E, Gilichinsky D, Wagener S, Tiedje J, McGrath J (1998) Biogeochemical activity of anaerobic microorganisms from buried permafrost sediments. *Geomicrobiology Journal*, **15**, 187–193.

Romanovskii NN, Hubberten H-W, Gavrilov A V, Tumskoy VE, Tipenko GS, Grigoriev MN, Siegert C (2000) Thermokarst and land-ocean interactions, Laptev sea region, Russia. *Permafrost and Periglacial Processes*, **11**, 137–152.

Romanovskii NN, Hubberten H-W, Gavrilov A V., Tumskoy VE, Kholodov AL (2004) Permafrost of the east Siberian Arctic shelf and coastal lowlands. *Quaternary Science Reviews*, **23**, 1359–1369.

Schädel C, Schuur EAG, Bracho R et al. (2014) Circumpolar assessment of permafrost C quality and its vulnerability over time using long-term incubation data. *Global Change Biology*, **20**, 641–652.

Schädel C, Bader MK-F, Schuur EAG et al. (2016) Potential carbon emissions dominated by carbon dioxide from thawed permafrost soils. *Nature Climate Change*, **6**, 950–953.

Schaefer K, Zhang T, Bruhwiler L, Barrett AP (2011) Amount and timing of permafrost carbon release in response to climate warming. *Tellus B*, **63**, 165–180.

Schaefer K, Lantuit H, Romanovsky VE, Schuur EAG, Witt R (2014) The impact of the permafrost carbon feedback on global climate. *Environmental Research Letters*, **9**, 85003.

Schennen S, Tronicke J, Wetterich S, Allroggen N, Schwamborn G, Schirrmeister L (2016) 3D ground-penetrating radar imaging of ice complex deposits in northern East Siberia. *GEOPHYSICS*, **81**, WA195-WA202.

Schimel JP, Clein JS (1996) Microbial response to freeze-thaw cycles in tundra and taiga soils. *Soil Biology and Biochemistry*, **28**, 1061–1066.

Schirrmeister L, Siegert C, Kuznetsova T et al. (2002a) Paleoenvironmental and paleoclimatic records from permafrost deposits in the Arctic region of Northern Siberia. *Quaternary International*, **89**, 97–118.

Schirrmeister L, Oezen D, Geyh MA (2002b) ^{230}Th/U dating of frozen peat, Bol'shoy Lyakhovsky Island (Northern Siberia). *Quaternary Research*, **57**, 253–258.

Schirrmeister L, Grosse G, Schwamborn G et al. (2003) Late Quaternary history of the accumulation plain north of the Chekanovsky Ridge (Lena Delta, Russia): A multidisciplinary approach. *Polar Geography*, **27**, 277–319.

Schirrmeister L, Grosse G, Kunitsky V et al. (2008) Periglacial landscape evolution and environmental changes of Arctic lowland areas for the last 60000 years (western Laptev Sea coast, Cape Mamontov Klyk). *Polar Research*, **27**, 249–272.

Schirrmeister L, Kunitsky V, Grosse G et al. (2011) Sedimentary characteristics and origin of the Late Pleistocene Ice Complex on north-east Siberian Arctic coastal lowlands and islands – A review. *Quaternary International*, **241**, 3–25.

Schirrmeister L, Froese D, Tumskoy V, Grosse G, Wetterich S (2013) Yedoma: Late Pleistocene ice-rich syngenetic permafrost of Beringia. In: *Encyclopedia of Quaternary Science* (ed Elias SA), pp. 542–552. Elsevier, Amsterdam.

Schirrmeister L, Schwamborn G, Overduin PP et al. (2017) Yedoma Ice Complex of the Buor Khaya Peninsula (southern Laptev Sea). *Biogeosciences*, **14**, 1261–1283.

Schneider von Deimling T, Meinshausen M, Levermann A, Huber V, Frieler K, Lawrence DM, Brovkin V (2012) Estimating the near-surface permafrost-carbon feedback on global warming. *Biogeosciences*, **9**, 649–665.

Schneider von Deimling T, Grosse G, Strauss J et al. (2015) Observation-based modelling of permafrost carbon fluxes with accounting for deep carbon deposits and thermokarst activity. *Biogeosciences*, **12**, 3469–3488.

Schuur EAG, Bockheim J, Canadell JG et al. (2008) Vulnerability of permafrost carbon to climate change: Implications for the global carbon cycle. *BioScience*, **58**, 701.

Schuur EAG, Vogel JG, Crummer KG, Lee H, Sickman JO, Osterkamp TE (2009) The effect of permafrost thaw on old carbon release and net carbon exchange from tundra. *Nature*, **459**, 556–559.

Schuur EAG, McGuire AD, Schädel C et al. (2015) Climate change and the permafrost carbon feedback. *Nature*, **520**, 171–179.

Schwamborn G, Wetterich S (2015) *Russian-German cooperation CARBOPERM: Field campaigns to Bol'shoy Lyakhovsky Island in 2014*. Alfred Wegener Institute for Polar and Marine Research, Bremerhaven, 100 pp.

Schwamborn G, Rachold V, Grigoriev MN (2002) Late Quaternary sedimentation history of the Lena Delta. *Quaternary International*, **89**, 119–134.

Serreze MC, Walsh JE, Chapin III FS et al. (2000) Observational evidence of recent change in the northern high-latitude environment. *Climatic Change*, **46**, 159–207.

Shaver GR, Billings WD, Chapin III FS, Giblin AE, Nadelhoffer KJ, Oechel WC, Rastetter EB (1992) Global change and the carbon balance of Arctic ecosystems. *BioScience*, **42**, 433–441.

Sher AV, Kuzmina SA, Kuznetsova TV, Sulerzhitsky LD (2005) New insights into the Weichselian environment and climate of the East Siberian Arctic, derived from fossil insects, plants, and mammals. *Quaternary Science Reviews*, **24**, 533–569.

Shkatova VG (2011) The state of the Russian Quaternary stratigraphic base and main tasks for its improvement. In: *Proceedings of the 7th All-Russian Quaternary Conference* (eds Korsakova OP, Kol'ka VV), p. 326–328 [in Russian]. Geological Institute of the Kola Science Center, Apatity.

Siegert C, Schirrmeister L, Babiy O (2002) The sedimentological, mineralogical, and geochemical composition of late Pleistocene deposits from the Ice Complex on the Bykovsky Peninsula, northern Siberia. *Polarforschung*, **70**, 3–11.

Sistla SA, Asao S, Schimel JP (2012) Detecting microbial N-limitation in tussock tundra soil: Implications for Arctic soil organic carbon cycling. *Soil Biology and Biochemistry*, **55**, 78–84.

Smith LC, Sheng Y, MacDonald GM, Hinzman LD (2005) Disappearing arctic lakes. *Science*, **308**, 1429–1429.

Soulides DA, Allison FE (1961) Effect of drying and freezing soils on carbon dioxide production, available mineral nutrients, aggregation, and bacterial population. *Soil Science*, **91**, 291–298.

Stams AJM, de Bok FAM, Plugge CM, van Eekert MHA, Dolfing J, Schraa G (2006) Exocellular electron transfer in anaerobic microbial communities. *Environmental Microbiology*, **8**, 371–382.

Stapel JG, Schirrmeister L, Overduin PP, Wetterich S, Strauss J, Horsfield B, Mangelsdorf K (2016) Microbial lipid signatures and substrate potential of organic matter in permafrost deposits: Implications for future greenhouse gas production. *Journal of Geophysical Research: Biogeosciences*, **121**, 2652–2666.

Stapel JG, Schwamborn G, Schirrmeister L, Horsfield B, Mangelsdorf K (2017) Substrate potential of Eemian to Holocene permafrost organic matter for future microbial greenhouse gas production. *Biogeosciences Discussions*, 1–29.

Strauss J, Schirrmeister L, Grosse G, Wetterich S, Ulrich M, Herzschuh U, Hubberten H-W (2013) The deep permafrost carbon pool of the Yedoma region in Siberia and Alaska. *Geophysical Research Letters*, **40**, 6165–6170.

Strauss J, Schirrmeister L, Mangelsdorf K, Eichhorn L, Wetterich S, Herzschuh U (2015) Organic-matter quality of deep permafrost carbon – A study from Arctic Siberia. *Biogeosciences*, **12**, 2227–2245.

Strauss J, Laboor S, Fedorov AN et al. (2016) Database of Ice-Rich Yedoma Permafrost (IRYP).

Sundqvist HS, Kaufman DS, McKay NP et al. (2014) Arctic Holocene proxy climate database – new approaches to assessing geochronological accuracy and encoding climate variables. *Climate of the Past*, **10**, 1605–1631.

Tesi T, Semiletov I, Hugelius G, Dudarev O, Kuhry P, Gustafsson Ö (2014) Composition and fate of terrigenous organic matter along the Arctic land–ocean continuum in East Siberia: Insights from biomarkers and carbon isotopes. *Geochimica et Cosmochimica Acta*, **133**, 235–256.

Tesi T, Muschitiello F, Smittenberg RH et al. (2016) Massive remobilization of permafrost carbon during post-glacial warming. *Nature Communications*, **7**, 13653.

Tigges R (2014) *Organischer Kohlenstoffumsatz in eisreichen Permafrostböden- und sedimenten der Insel Muostakh, Laptew See, Nordost Sibirien*. Bachelor Thesis, Universität Hamburg, Hamburg, Germany, 46 pp.

Treat CC, Wollheim WM, Varner RK, Grandy AS, Talbot J, Frolking S (2014) Temperature and peat type control CO_2 and CH_4 production in Alaskan permafrost peats. *Global Change Biology*, **20**, 2674–2686.

Treat CC, Natali SM, Ernakovich J et al. (2015) A pan-Arctic synthesis of CH_4 and CO_2 production from anoxic soil incubations. *Global Change Biology*, **21**, 2787–2803.

Tumskoy VE (2012) Peculiarities of cryolithogenesis in northern Yakutia from the Middle Neopleistocene to the Holocene. *Kriosfera Zemli*, **16**, 12–21 [in Russian].

Ulrich M, Grosse G, Strauss J, Schirrmeister L (2014) Quantifying wedge-ice volumes in Yedoma and thermokarst Basin deposits. *Permafrost and Periglacial Processes*, **25**, 151–161.

Vishnivetskaya T, Kathariou S, McGrath J, Gilichinsky D, Tiedje JM (2000) Low-temperature recovery strategies for the isolation of bacteria from ancient permafrost sediments. *Extremophiles*, **4**, 165–173.

Vonk JE, Sánchez-García L, van Dongen BE et al. (2012) Activation of old carbon by erosion of coastal and subsea permafrost in Arctic Siberia. *Nature*, **489**, 137–140.

Wagner D, Gattinger A, Embacher A, Pfeiffer E-M, Schloter M, Lipski A (2007) Methanogenic activity and biomass in Holocene permafrost deposits of the Lena Delta, Siberian Arctic and its implication for the global methane budget. *Global Change Biology*, **13**, 1089–1099.

Waldrop MP, Wickland KP, White Iii R, Berhe AA, Harden JW, Romanovsky VE (2010) Molecular investigations into a globally important carbon pool: Permafrost-protected carbon in Alaskan soils. *Global Change Biology*, **16**, 2543–2554.

Walker HJ (1998) Arctic Deltas. *Journal of Coastal Research*, **14**, 719–738.

Walter KM, Zimov SA, Chanton JP, Verbyla D, Chapin FS (2006) Methane bubbling from Siberian thaw lakes as a positive feedback to climate warming. *Nature*, **443**, 71–75.

Walter KM, Edwards ME, Grosse G, Zimov SA, Chapin III FS (2007) Thermokarst lakes as a source of atmospheric CH_4 during the last deglaciation. *Science*, **318**, 633–636.

Walter Anthony KM, Zimov SA, Grosse G et al. (2014) A shift of thermokarst lakes from carbon sources to sinks during the Holocene epoch. *Nature*, **511**, 452–456.

Wang H, Boutton TW, Xu W, Hu G, Jiang P, Bai E (2015a) Quality of fresh organic matter affects priming of soil organic matter and substrate utilization patterns of microbes. *Scientific Reports*, **5**, 10102.

Wang C, He N, Zhang J, Lv Y, Wang L (2015b) Long-term grazing exclusion improves the composition and stability of soil organic matter in Inner Mongolian grasslands (ed Hui D). *PLOS ONE*, **10**, e0128837.

Walz J, Knoblauch C (2015) Böden und Landschaft der Großen Ljachow-Insel. In: Böden im Wandel (eds Knoblauch C, Fiencke C, Berger K). Hamburger Bodenkundliche Arbeiten, Band 77: 61-75.

Walz J, Knoblauch C, Böhme L, Pfeiffer E-M (2017) Regulation of soil organic matter decomposition in permafrost-affected Siberian tundra soils - Impact of oxygen availability, freezing and thawing, temperature, and labile organic matter. *Soil Biology and Biochemistry*, **110**, 34–43.

Weiss N, Blok D, Elberling B, Hugelius G, Jørgensen CJ, Siewert MB, Kuhry P (2016) Thermokarst dynamics and soil organic matter characteristics controlling initial carbon release from permafrost soils in the Siberian Yedoma region. *Sedimentary Geology*, **340**, 38–48.

Wetterich S, Schirrmeister L, Pietrzeniuk E (2005) Freshwater ostracodes in Quaternary permafrost deposits in the Siberian Arctic. *Journal of Paleolimnology*, **34**, 363–376.

Wetterich S, Kuzmina S, Andreev AA et al. (2008) Palaeoenvironmental dynamics inferred from late Quaternary permafrost deposits on Kurungnakh Island, Lena Delta, Northeast Siberia, Russia. *Quaternary Science Reviews*, **27**, 1523–1540.

Wetterich S, Schirrmeister L, Andreev AA, Pudenz M, Plessen B, Meyer H, Kunitsky V V. (2009) Eemian and Late Glacial/Holocene palaeoenvironmental records from permafrost sequences at the Dmitry Laptev Strait (NE Siberia, Russia). *Palaeogeography, Palaeoclimatology, Palaeoecology*, **279**, 73–95.

Wetterich S, Rudaya N, Tumskoy V, Andreev AA, Opel T, Schirrmeister L, Meyer H (2011) Last Glacial Maximum records in permafrost of the East Siberian Arctic. *Quaternary Science Reviews*, **30**, 3139–3151.

Wetterich S, Tumskoy V, Rudaya N et al. (2014) Ice Complex formation in arctic East Siberia during the MIS3 Interstadial. *Quaternary Science Reviews*, **84**, 39–55.

Wetterich S, Tumskoy V, Rudaya N et al. (2016) Ice Complex permafrost of MIS5 age in the Dmitry Laptev Strait coastal region (East Siberian Arctic). *Quaternary Science Reviews*, **147**, 298–311.

Whalen SC, Reeburgh WS (2000) Methane oxidation, production, and emission at contrasting sites in a boreal bog. *Geomicrobiology Journal*, **17**, 237–251.

Wild B, Schnecker J, Alves RJE et al. (2014) Input of easily available organic C and N stimulates microbial decomposition of soil organic matter in arctic permafrost soil. *Soil Biology and Biochemistry*, **75**, 143–151.

Wild B, Gentsch N, Čapek P et al. (2016) Plant-derived compounds stimulate the decomposition of organic matter in arctic permafrost soils. *Scientific Reports*, **6**, 25607.

Winterfeld M, Schirrmeister L, Grigoriev MN, Kunitsky V V., Andreev A, Murray A, Overduin PP (2011) Coastal permafrost landscape development since the Late Pleistocene in the western Laptev Sea, Siberia. *Boreas*, **40**, 697–713.

Yamamoto S, Alcauskas JB, Crozier TE (1976) Solubility of methane in distilled water and seawater. *Journal of Chemical & Engineering Data*, **21**, 78–80.

Zhang T, Barry RG, Knowles K, Heginbottom JA, Brown J (2008) Statistics and characteristics of permafrost and ground-ice distribution in the Northern Hemisphere. *Polar Geography*, **31**, 47–68.

Zimmermann HH, Raschke E, Epp LS et al. (2017) Sedimentary ancient DNA and pollen reveal the composition of plant organic matter in Late Quaternary permafrost sediments of the Buor Khaya Peninsula (north-eastern Siberia). *Biogeosciences*, **14**, 575–596.

Zimov SA, Chuprynin VI, Oreshko AP, Chapin III FS, Reynolds JF, Chapin MC (1995) Steppe-tundra transition: A herbivore-driven biome shift at the end of the Pleistocene. *The American Naturalist*, **146**, 765–794.

Zimov SA, Voropaev Y V., Semiletov IP et al. (1997) North Siberian lakes: A methane source fueled by Pleistocene carbon. *Science*, **277**, 800–802.

Zimov SA, Davydov SP, Zimova GM, Davydova AI, Schuur EAG, Dutta K, Chapin III FS (2006) Permafrost carbon: Stock and decomposability of a globally significant carbon pool. *Geophysical Research Letters*, **33**, L20502.

Zubrzycki S (2012) Drilling frozen soils in Siberia. *Polarforschung*, **81**, 151–153.

Zubrzycki S, Kutzbach L, Grosse G, Desyatkin A, Pfeiffer E-M (2013) Organic carbon and total nitrogen stocks in soils of the Lena River Delta. *Biogeosciences*, **10**, 3507–3524.

Zubrzycki S, Kutzbach L, Pfeiffer E-M (2014) Permafrost-affected soils and their carbon pools with a focus on the Russian Arctic. *Solid Earth*, **5**, 595–609.

Acknowledgements

My sincerest gratitude goes to my supervisors, Prof. Dr. Eva-Maria Pfeiffer and Dr. Christian Knoblauch. They encouraged me to take my first tentative steps in permafrost science, guided me throughout my years at the Institute of Soil Science, shared their vast knowledge with me during our many discussions, and helped me to develop my scientific skill set.

During the field campaigns, I could profit immensely from Christian's and Prof. Dr. Lars Kutzbach's expertise about soil processes in the Lena River Delta and Dr. Sebastian Wetterich's and Dr. Georg Schwamborn's (both AWI Potsdam) detailed explanations about the paleo-environmental history of NE Siberia. Afterwards, Dr. Lutz Schirrmeister (also AWI Potsdam) and Dr. Thomas Opel (AWI Potsdam, University of Sussex) serenely continued to describe and clarify small but intricate differences between sedimentary units and thus helped to understand the regional landscape development. Also thanks to all other participants, which made the expeditions a most educational and pleasurable experience. In particular, Norman Rüggen, Tim Eckhardt, Mercedes "Nana" Molina Gámez, and Stephan Schennen (Universität Potsdam) for their untiring support during sampling. The expeditions were also a success thanks to the logistical and technical support from Russian and German partners, in particular Mikhail N. Grigoriev (Permafrost Institute, Yakutsk), Dr. Irena Fedorova and Alexander Makarov (both AARI, St. Petersburg), Antonina Chetverova (St. Petersburg State University), and Waldemar Schneider and Günter "Molo" Stoof (both AWI Potsdam).

In the home laboratory, Birgit Schwinge and Birgit Grabellus gave me a hand and thus made sure I could get all my samples processed and managed my several thousand gas measurements at the gas chromatograph. During my last year, while I was increasingly concerned with writing, I could depend on Ronja Tigges to keep the experiments running.

Continuous support also came from family and friends, who patiently listened to my mumblings about the SOC, SOM, CO_2, Kuchchugui, thermokarst, priming, and so on. Discussions about these topics with people, who were not as submerged in a topic as I was, helped to restructure my thoughts when I could no longer see the wood for the trees.

The School of Integrated Climate System Sciences (SICSS) also shaped my time as a doctoral candidate by encouraging active discussion between students and lecturers from different disciplines and partaking in additional educational opportunities.

This work was supported by the German Ministry of Education and Research (CarboPerm-Project, BMBF Grant No. 03G0836A) and the cluster of excellence 'Integrated Climate System Analysis and Prediction' (CliSAP) under grant DFG EXC 177.